Methane Oxidation over, and Sulfur Interactions with, Pd/Pt Bimetallic Catalysts

A Dissertation

Presented to

The Faculty of Department of Chemical and Biomolecular Engineering

University of Houston

In Partial Fulfillment

Of the Requirements for the Degree

Doctor of Philosophy

in Chemical Engineering

by

Monique Shauntá Wilburn

December 2016

Methane Oxidation over, and Sulfur Interactions with, Pd/Pt Bimetallic Catalysts

_____

Monique Shauntá Wilburn

Approved:

_____

Chair of the Committee
Dr. Jeffrey Rimer, Associate Professor
Chemical and Biomolecular Engineering

Committee Members:

_____

Dr. William Epling, Professor
University of Virginia Chemical Engineering

_____

Dr. Michael Harold, Professor
Chemical and Biomolecular Engineering

_____

Dr. James Meen, Research Associate Professor
Chemistry

_____

Dr. Tracy Benson, Associate Professor
Lamar University Chemical Engineering

_____

Dr. Suresh K. Khator, Associate
Dean, Cullen College of Engineering

_____

Dr. Michael Harold, Professor and Chair,
Chemical and Biomolecular Engineering

Acknowledgements

I would like to extend my sincere appreciation and gratitude to my Ph.D. advisor, Dr. Bill Epling. As if taking a chance on a part-time Ph.D. student was not enough, Dr. Epling was always flexible and accommodating of my NASA obligations while still managing to hold me accountable for my development as an academic researcher. In addition to Dr. Epling being patient as I transitioned from an aerospace engineer into a chemical engineer, he also helped me develop realistic expectations for research progress. Dr. Epling was always willing to share his knowledge and challenge me to ensure that I thoroughly understood experimental findings and what required further study. Even more importantly, Dr. Epling gave me the freedom to flush out new ideas and investigate unique experimental findings thoroughly. He also helped me develop better probing skills to find the causes for themes in the data. I believe that these aspects were essential for me to develop better investigative research skills and a sense of when it is time to move on to study another aspect. On a personal note, Dr. Epling also helped me mature in regards to having patience with others as well as myself. He also took the time to remind me that I have to periodically set aside time to thoroughly evaluate who I really want to be and what I really want to accomplish later in life. Overall, I believe that working for Dr. Epling helped me become a better researcher as well as gain a better appreciation for the level of effort and expertise required for becoming a respected academic researcher.

I would like extend my sincere gratitude to Dr. Eric Dimpault-Darcy for encouraging me to pursue a graduate degree and for his never-ending support and encouragement throughout my NASA and academic careers. In addition to providing me

with a strong example of a professional chemical engineer and researcher, he also stressed the importance of integrity, development of technical expertise, advocating for my team and ideas, and finding my niche in my field. Dr. Darcy always challenged me to work harder, work smarter, defend my technical positions, make education a lifelong journey, and most importantly not to underestimate my potential or capabilities as an engineer. For my personal development, Dr. Darcy has shown me how to keep my composure in the most challenging situations, remain humble even when high levels of success are attained, put family first while still striving to pursue career goals, and the importance of taking time to further develop myself as well as mentor others.

I would like to thank my committee members, Dr. James Meen, Dr. Tracy Benson, Dr. Michael Harold, and Dr. Jeffrey Rimer, for agreeing to be part of my defense committee. I would like to extend a special thanks to Dr. Harold and Dr. Rimer for their support and advice during my Ph.D. studies. I would like to acknowledge Mike Hoke and Jack Watson from Matheson Tri-Gas for helpful discussions on purification columns and Joseph Matlock from Bronkhorst USA for helpful suggestions on controlling low-flow rate water injection systems. I would also like to acknowledge the National Aeronautics and Space Administration for the allowance of a flexible work schedule while conducting my academic research studies.

I would like to thank Dr. Tayebeh Hamzehlouyan and Dr. Justin Dodson for helpful discussions regarding the SO_2 sorption studies and CO pulse-injection chemisorption techniques respectively. Also, I would like to thank Dr. Ousmane Diallo, Dr. Tayebeh Hamzehlouyan, and Dr. Justin Dodson for their encouragement throughout my academic research career. I would like to thank my first set of lab mates: Dr. Yong

Liu for always making me feel welcomed, John Pierce for helping me get up to speed in the lab and for his encouragement, and Dr. Li Zhang and Melanie Hazlett for their helpful suggestions on catalysis synthesis when I first joined the lab. I would also like to thank my lab mate Dr. Vencon Easterling as well as “my kids” Francesco Piubello, Yasser Jangjou, Anh Vu, and Kyle Karinshak for ensuring that my overall graduate lab experience was everything but dull or uneventful.

Last but surely not least, I would like to extend my gratitude to my family. I would like to thank my little brother, Carl Wilburn II, for always having my back, being a loyal confidant, and providing unconditional love, support, and understanding. I would also like to thank my sister, LaTasha Jeneen Wilburn, for always reminding me that there are things in life which are more important than my career goals and encouraging me to strive for those things as well. I would like to thank my mother, Deaconess Josephine Rochelle Wilburn, for stressing the importance of having grace in all situations, treating people with manners regardless of how they treat you, having a strong spiritual faith even when a positive outcome does not seem possible, and never forgetting where I came from no matter what level of achievement I attain. I would like to thank my father, Deacon Carl Wilburn I, for ensuring that I knew the importance of a strong work ethic, honoring my commitments, maintaining a positive spirit and outlook in the most challenging times because how I behaved during these times would define my character, and ensuring that all decisions are led by faith and prayer. I am eternally grateful to my Granddad, Walter Wilburn, for making me believe at an early age that I could actually graduate from college and work at NASA one day and to my Grandma, Margaret Wilburn, for instilling in me not only the importance of believing in myself and dreaming but also protecting

my dreams and spirit from naysayers as I move through my life journey. Glory to God who provided me with the perseverance required to complete the work herein.

Methane Oxidation over, and Sulfur Interactions with, Pd/Pt Bimetallic Catalysts

An Abstract

of a

Dissertation

Presented to

The Faculty of Department of Chemical and Biomolecular Engineering

University of Houston

In Partial Fulfillment

Of the Requirements for the Degree

Doctor of Philosophy

in Chemical Engineering

by

Monique Shauntá Wilburn

December 2016

Abstract

Using $Pt/Pd/Al_2O_3$ catalysts, the effect of Pt/Pd ratio, and H_2O and SO_2 exposure on complete CH_4 oxidation (combustion) was studied. Small substitutions of Pt moles for Pd moles resulted in an increased CH_4 oxidation activity in comparison to monometallic Pd. Greater substitutions led to decreased activity. In terms of sulfur poisoning, DRIFTS and TPD studies show that SO_2 sorption characteristics depend on both precious metal crystallite particle size and Pd:Pt mole ratio. Catalysts with a small particle size or high Pd content tended to form more aluminum sulfate species, which decomposed at high-temperature. Large particle size or low-Pd content catalysts tended to form more low-temperature decomposing and desorbing species, such as molecular SO_2 and aluminum surface sulfite. It was found that the amount of SO_2 adsorbed and later desorbed during TPD decreased with increasing particle size or Pt content in the bimetallic $Pd\text{-}Pt/Al_2O_3$ catalysts.

To decouple particle size and mole ratio aspects during CH_4 oxidation experiments, catalysts with various metal compositions but similar particle sizes were compared. CO and SO_2 adsorption DRIFTS studies were used to identify sites impacted by SO_2 exposure and evaluate the Pd:Pt mole ratio effect on sulfur surface species formation. Temperature-programmed oxidation, desorption, and reduction processes were used to evaluate sulfur species decomposition and performance regeneration effectiveness. At low temperatures, Pd-based catalysts with little to no Pt substitution tended to form aluminum sulfate species, which could be removed at high temperatures to recover catalytic activity, but Pd-based catalysts with higher Pt substitution were less

effective at sulfate formation at low temperatures. In this case, molecular SO_2 and aluminum surface sulfite species inhibited the CH_4 oxidation reaction over a broader temperature range. In general, the effectiveness of SO_2 regeneration methods decreased with increasing Pt content. For bimetallic catalysts containing more Pt moles than Pd moles, sulfur decays CH_4 oxidation activity to a lesser degree than the high-temperature regeneration methods due to the associated sintering effects. In terms of H_2O impact, although the CH_4 oxidation reaction was inhibited in the presence of H_2O for catalysts containing Pd, only low-Pd content catalysts decayed due to H_2O exposure.

Table of Contents

List of Figures

List of Tables

Chapter 1 Introduction and Background

1.1 Introduction

Since meeting the legislation regarding vehicle exhaust emissions is becoming more challenging, and there is growing concern over energy independence, alternative fuels are being investigated. Natural gas is one such, and is typically viewed as a lower emission producing fuel in comparison to gasoline and diesel [Abbasi et al., 2012]. Natural gas primarily consists of methane (CH_4), other hydrocarbons like ethane and propane [Abbasi et al., 2012; Varde and Bohr, 1993; Trimm and Lee, 1995], and trace sulfur species [Abbasi et al., 2012]. In comparison to combustion in diesel vehicles, lean-burn natural gas engine combustion can result in lower CO_2, CO, NO_x, and soot emissions. On the other hand, if incomplete CH_4 combustion occurs, the remaining CH_4 can be emitted in the vehicle exhaust [Abbasi et al., 2012].

Natural gas vehicle exhaust temperatures are typically between 300 to 550 °C [Abbasi et al., 2012; Stodolsky and Santini, 1992]. Heavier hydrocarbons, like propane and ethane, can be completely converted in oxygen-rich conditions in this temperature range [Trimm and Lee, 1995]. As a result, the primary component of natural gas engine emissions is uncombusted CH_4 [Stodolsky and Santini, 1992], while ethane and propane are only present in small amounts [Varde and Bohr, 1993].

Taking into account the high level of CH_4 emissions, Stodolsky and Santini found that natural gas vehicles, over longer-term uses (~100 year period), could still result in lower CO_2-equivalent emissions when compared to gasoline fueled vehicles [Stodolosky and Santini, 1992]. Since CH_4 is a strong greenhouse gas, incomplete conversion of CH_4

is not desirable for environmental reasons, and improvements in catalytic aftertreatment systems for natural gas vehicles have not been thoroughly investigated [Abbasi et al., 2012].

Due to the high specific catalytic activity associated with noble metals, catalysts which utilize platinum (Pt), palladium (Pd), or a combination of the two have been used for CH_4, ethane, and propane combustion [Abbasi et al., 2012; Demoulin et al., 2008]. Although much work has been published on CH_4 oxidation using Pd and Pt catalysts, less has been published in regards to the use of Pd:Pt bimetallic catalysts in regards to their deactivation characteristics [Yamamoto and Uchida, 1998] or variations in activity due to other hydrocarbons being present in natural gas [Demoulin et al., 2008] or CO_2 being present in the natural gas engine exhaust. With the goal of designing and characterizing a Pd:Pt catalyst which is best suited for use in a natural gas vehicle aftertreatment system, the focus of this research effort was placed on understanding how alumina-supported Pd:Pt catalysts perform during simulated natural gas engine aftertreatment system oxidation and deactivate due to aging or poisoning effects. In comparison to carbon monoxide, ethane, and propane, CH_4 is the most prominent and most difficult to oxidize constituent in natural gas engine exhaust. For this reason, this research effort placed sole emphasis on CH_4 oxidation. The contents of this work will discuss the literature findings which drove the focus of the research area, a summary of the research conducted, conclusions, and suggestions for future work.

1.2 Emissions

Studies like that originating from Engine, Fuel, and Emissions Engineering Inc. and the Gas Technology Institute show that the particulate matter emissions from natural gas engine vehicles are less than that of diesel engine vehicles [Weaver et al., 2000]. In regards to the NO_x emission levels for buses, it was found that the emissions for natural gas engines was generally lower than that of diesel engines. However, in a few instances, the NO_x emissions from natural gas engine buses were equal to or greater than that of diesel. It is suspected that the inconsistency in the measured NO_x emission levels was due to some vehicles having an improper air to fuel ratio setting [Weaver et al., 2000]. Similarly, the National Renewable Energy Laboratory and Southwest Research Institute conducted experiments to assess the emission characteristics of two Cummins L10-240G natural gas engines and determine how the emissions could change as a function of the fuel/air ratio. Both engine experiments resulted in similar total hydrocarbon (THC), non-CH_4 hydrocarbons, and particulate matter emissions. However, the NO_x and CO emissions were significantly reduced with a lower fuel/air ratio. It was concluded that CO and NO_x emissions could be controlled by adjusting the engine's fuel/air ratio setting [Sharp et al., 1993]. In a study by Hupperich and Dürnholtz, it was found that too lean of a mixture can cause NO_x emission values to increase and too rich of a mixture can cause the hydrocarbon and CO emission values to greatly increase [Hupperich and Dürnholtzl, 1996].

Hupperich and Dürnholtz conducted emission experiments on passenger cars, light-duty trucks, and heavy-duty trucks which utilized diesel, gasoline, or natural gas for fuel. Using the U.S. Federal Test Procedure (FTP) 75, it was found that the NO_x and CO

emissions are greatly reduced for natural gas compared to gasoline. The NO_x and PM emissions are greatly reduced while the CO emission values increased for natural gas compared to diesel. However, the THC emission values increased when using natural gas [Hupperich and Dürnholtzl, 1996]. Ishii et al. found that the FTP experiments with 6-cyclinder vehicle engines produced THC, NO_x, and CO emissions which were 60%, 30%, and 20% less respectively for natural gas in comparison to gasoline [Ishii et al., 1994].

Subramanian et al. used Pd/Al_2O_3 catalysts and simulated natural gas vehicle exhaust to assess how the air/fuel ratio, catalyst space velocity, and trace SO_2 each affect conversion at 550 °C. The simulated exhaust consisted of CH_4, NO, and CO. When using high air/fuel ratios, it was found that low space velocities were necessary in order to completely oxidize CH_4 and avoid additional formation of CO. In contrast, low air/fuel ratios were required to achieve any conversion of NO, which was independent of space velocity. When SO_2 was added to the feed gas, CH_4 conversion was reduced [Subramanian et al., 1993].

Varde and Bohr tested 4-cyclinder vehicle engines and used Pt-Rh-Pd based catalytic converters. A standard emissions cart was used to measure NO_x, CO, and THC in the engine exhaust. CH_4 accounted for most of the THCs in the engine exhaust, and NO accounted for most of the NO_x in the engine exhaust. When a lower air/fuel ratio was used, 90 to 98% conversion was achieved for CO and NO_x. The catalytic converters were able to remove the ethane and propane portion of the THCs, but CH_4 conversion was limited [Varde and Bohr, 1993].

Hesterberg et al. conducted a literature review to compare emissions data collected from vehicle engines which utilize diesel or natural gas fuels. When no

aftertreatment system was used, natural gas-fueled buses emitted higher THC levels than diesel-fueled buses. Diesel-fueled buses emitted more particulate matter. When comparing the effectiveness of oxidation catalysts and three-way catalytic converters for natural gas engine exhaust aftertreatment, both systems reduced the CO emissions by over 60%. Between the two catalyst types, the oxidation catalyst reduced more particulate matter. The three-way catalyst provided a greater reduction of the THC, NO_x, and NO_2 emissions [Hesterberg et al., 2008].

1.3 Catalyst coatings

Noble metals supported on metal oxide supports are considered the best oxidation catalysts for low-temperature complete CH_4 oxidation, and Pd is known to be most active [Gélin and Primet, 2002; Zwinkels et al., 1993]. Due to costs associated with noble metals, metal oxide and perovskite-type oxide catalysts are being assessed as potential substitutes for noble metal catalysts [Xiang et al., 2013]. Metal oxide catalysts are less active in comparison to noble metal catalysts like Pd for CH_4 oxidation [Trimm and Lee, 1995; Gélin and Primet, 2002]. For complete ethane oxidation, metal oxide catalysts initially show similar activity to that of Pd but a reduction in activity was observed for subsequent experiments [Demoulin et al., 2008; Tahir and Koh, 1997]. Typically, when perovskite-type oxide catalysts were used, high temperatures (500 to 600 °C) were required for complete CH_4 conversion [Xiang et al., 2013; Tahir and Koh, 1997; Wu and Luo, 2011; Kucharczyk and Zabrzeski, 2008; Wang et al., 2011; Petrović et al., 2005; Miller et al., 2000; Giebeler et al., 2007]. Some perovskites were able to achieve complete conversion of propane at temperatures similar to that with Pd. While Pd

catalysts only displayed a loss in activity after exposure to H_2O, the perovskite catalysts displayed a reduction in activity due to both H_2O and CO_2 exposure [Klvana et al., 2001].

Although found to be resistant to sulfur poisoning, little research has been performed on complete CH_4 oxidation with a Pt-based catalyst. Pd-based catalysts have demonstrated mechanical instability and significant activity losses during use [Abbasi et al., 2012]. When Pt and Pd were used in bimetallic catalysts, catalytic activity increases as long as smaller Pt amounts are used [Yamamoto and Uchida, 1998; Kinnunen et al., 2012; Skoglundh et al., 1991; Lapisardi et al., 2007; Lapisardi et al., 2006]. Similarly, when large amounts of H_2O are present [Lapisardi et al., 2007; Lapisardi et al., 2006] or long durations of time on stream exist, Pd catalysts showed better catalytic activity when small Pt amounts were substituted for Pd [Yamamoto and Uchida, 1998; Kinnunen et al., 2012]. Other research studies showed, that for alumina supported catalysts with a combination of Pt and Pd, higher activity over time on stream in comparison to monometallic Pt and Pd alumina supported catalysts [Yamamoto and Uchida, 1998; Lapisardi et al., 2007], especially when small amounts of Pt were substituted for Pd in Pd/Al_2O_3 catalysts [Kinnunen et al., 2012].

1.4 Activity and kinetics for complete CH_4 oxidation

In O_2-rich environments, metal surfaces are more likely to become oxidized or be covered with chemisorbed O_2 than CH_4 because these surfaces uptake O_2 more effectively than CH_4. In the case of Pt, the metal surface is generally covered with chemisorbed O_2 inhibiting the CH_4 oxidation reaction [Burch, 1999]. When O_2 coverage is reduced to ~50%, maximum CH_4 conversion can be achieved [Burch, 1996]. Burch et

al. postulated that this result is due to ease at which the C-H bond in CH_4 can be activated. At 50% O_2 coverage, partially oxidized Pt surfaces have chemisorbed oxygen ions neighboring free metal sites. The proximity of these sites can promote CH_4 dissociative adsorption and light-off the oxidation reaction [Burch, 1999].

For Pd surfaces in O_2-rich environments, O_2 also chemisorbs on Pd, but then it dissociates. Upon dissociation, the oxygen is then free to react with Pd and form PdO, which is stable, even during O_2 environment changes [Burch, 1999] as long as the temperature is kept below 650 °C [Farrauto, 1992]. As the temperature is increased to ~800 to 850 °C, not only does the PdO decompose, returning to metallic Pd, but also the metallic Pd particles tend to agglomerate. When the temperature is reduced, some redispersion and reoxidation can occur, but in this case, at least two distinct oxidized Pd species, PdO and PdO_x are formed [Farrauto, 1992]. It is suspected that PdO_x species such as PdO_2 and Pd_2O_3 are not stable at low temperatures, so PdO is primarily present at the temperatures utilized for lean-burn natural gas engine exhaust [McCarty, 1995]. Since O_2 chemisorbs more easily than CH_4 at these temperatures and PdO forms with ease [Burch, 1999], it has been proposed that CH_4 oxidation activity is highly dependent on 1) CH_4 interacting with accessible metallic Pd sites and 2) PdO sites subtracting H atoms from CH_4 [Fujimoto et al., 1998; Chin et al., 2013]. Researchers have proposed that as PdO sites are reduced or decompose to form metallic Pd, activity during low-temperature O_2-rich CH_4 oxidation declines [Farrauto, 1995].

A simplified depiction of the overall reaction for complete CH_4 oxidation is as follows,

$$CH_4 + 2O_2 = CO_2 + 2H_2O. \quad (1)$$

Whether CH_4 is completely oxidized strongly depends on the ratio of O_2 to CH_4 used. Under stoichiometric or O_2-rich conditions, complete oxidation of CH_4 is typical and CO_2 and H_2O form [Trimm and Lee, 1995; Burch and Loader, 1994; Cullis and Willatt, 1983; Mouaddib et al., 1992]. CO_2 [Burch et al., 1995] and H_2O are also typically part of the natural-gas engine exhaust [Yamamoto and Uchida, 1998], and thus researchers have investigated the relationship between the complete CH_4 oxidation reaction rate and the CH_4, O_2, CO_2, and H_2O concentrations. Results show the reaction rate to be first order with respect to CH_4 and no dependence on O_2 [Abbasi et al., 2012; Otto, 1989; Cullis and Willatt, 1983; Niwa et al., 1983; Trimm and Lee, 1995; P. Gélin and M. Primet, 2002]. Although Yao found similar results for Pd wires, a dependency on O_2 was observed during oxidation experiments using Pt wires [Yao, 1980]. Zhu et al. conducted experiments using palladium foils. They found no O_2 dependence in the 510 to 600 °C temperature range, and in the 285-350 °C range a slight dependence on O_2 was observed [Zhu et al., 2005]. It should be noted that a dependence on O_2 was only observed for non-supported Pd and Pt catalysts.

When CH_4 oxidation experiments were conducted on Pd foils between 285 to 350 °C, a significant dependence on H_2O was observed [Zhu et al., 2005]. Hayes et al. conducted experiments on ~4.3 to 6.3 wt. % Pd/Al_2O_3 monoliths and found that the CH_4 oxidation reaction is inhibited by water formed during the oxidation reaction [Hayes et al., 2001]. Giezen et al. performed CH_4 oxidation experiments over Pd/Al_2O_3 catalysts [Giezen et al., 1999] and also concluded that the H_2O formed as a reaction product inhibited the reaction. Similarly, for experiments with Pt-Pd/Al_2O_3, both feed and product H_2O inhibition was observed [Abbasi et al., 2012]. However, Abbasi et al. conducted

experiments on Pt/Al_2O_3 catalysts and only observed a dependency on H_2O when H_2O vapor was added to the feed gas and did not observe a dependency on H_2O formed as a reaction product. Cullis and Willatt observed the same, the amount of H_2O formed as a reaction product did not have an effect on the reaction rate during experiments with Pd/Al_2O_3 and Pt/Al_2O_3 catalysts [Cullis and Willatt, 1984].

At temperatures less than 450 °C, Burch et al. found that Pd/Al_2O_3 catalysts were sensitive to CO_2 and H_2O addition during CH_4 oxidation. H_2O inhibition masked CO_2 inhibition when both were present in the feed [Burch et al., 1995]. In a set of propane oxidation kinetics using Pd/Al_2O_3, when H_2O vapor was injected into the feed stream, a reduction in oxidation rate was observed. However, no reduction was observed when CO_2 was introduced into the stream [van de Beld et al., 1995].

1.5 Deactivation

Becker et al. concluded that Pt/Al_2O_3 catalysts suffer from O_2 poisoning during CH_4 oxidation under O_2-rich conditions [Becker et al., 2009]. Carlsson et al. found similar results for oxidation of CH_4 and propane over Pt/Al_2O_3 catalysts in O_2-rich conditions [Becker et al., 2009; Carlsson et al., 2004]. In the case of propane oxidation, Carlsson et al. also found that the activity could be restored when lean-O_2 conditions were imposed periodically [Carlsson et al., 2004]. Yamamoto and Uchida conducted CH_4 oxidation experiments at 400 °C. H_2O vapor was included in the feed gas, and catalyst samples with various combinations of Pt and Pd on alumina were used. The catalyst samples which displayed the highest activity with time on stream contained 40% Pt and 60% Pd on a mass density basis [Yamamoto and Uchida, 1998].

Kinnunen et al. found that Pd-Pt/Al_2O_3 catalysts with higher amounts of Pt have lower activities during CH_4 oxidation in comparison to samples with higher amounts of Pd [Kinnunen et al., 2012]. Lapisardi et al. assessed the catalytic activity of Pt/Al_2O_3, Pd/Al_2O_3, and Pd-Pt/Al_2O_3 catalysts during CH_4 oxidation. All catalyst samples possessed a total metal loading of ~2 wt. %. When a dry feed gas was used, the $Pd_{0.93}Pt_{0.07}/Al_2O_3$ and $Pd_{0.65}Pt_{0.35}/Al_2O_3$ displayed activities similar to that of Pd/Al_2O_3. As the amount of Pt in the Pd-Pt/Al_2O_3 samples was increased, the samples became less active and displayed activities similar to that of Pt/Al_2O_3 catalysts. The aged $Pd_{0.93}Pt_{0.07}/Al_2O_3$ and $Pd_{0.65}Pt_{0.35}/Al_2O_3$ displayed higher activities than Pd/Al_2O_3 [Lapisardi et al., 2007]. When H_2O vapor was included in the feed gas, the aged Pd/Al_2O_3, $Pd_{0.93}Pt_{0.07}/Al_2O_3$, and $Pd_{0.55}Pt_{0.45}/Al_2O_3$ samples were more active than the fresh samples. The aged Pt and Pd-Pt/Al_2O_3 samples with higher amounts of Pt were less active than the fresh catalysts. Overall, Lapisardi et al. found that addition of Pt to Pd/Al_2O_3 catalysts provided a benefit to initial activity and activity over time on stream when the ratio of Pt to Pd was less than 0.5 [Lapisardi et al., 2006].

Electron micrographs of fresh $Pd_{0.65}Pt_{0.35}/Al_2O_3$ samples displayed evidence of very small particles in Pt-rich regions and large particles in Pd-rich regions. After these catalyst samples were aged in steam at 600 °C, only large particles were observed. For this reason, it was concluded that catalysts which utilize any Pt are likely to sinter when exposed to steam at high temperatures [Lapisardi et al., 2007]. Nonetheless, when large amounts of H_2O are added to the feed stream, $Pd_{0.93}Pt_{0.07}/Al_2O_3$, $Pd_{0.65}Pt_{0.35}/Al_2O_3$, and $Pd_{0.55}Pt_{0.45}/Al_2O_3$ displayed a less significant reduction in catalytic activity in comparison with monometallic Pd/Al_2O_3 catalysts [Lapisardi et al., 2006].

Lampert et al. conducted CH_4, ethane, and propane oxidation experiments on fresh and steam aged Pd/Al_2O_3 catalysts. When approximately 1 ppm SO_2 was added to the feed, the activity of the catalysts was reduced in all cases. The temperatures at which 50% conversion was achieved increased in the following order: fresh catalyst for CH_4 oxidation < steam aged catalyst for propane oxidation < steam aged catalyst for ethane oxidation < steam aged catalyst for CH_4 oxidation. Based on these results, Lampert et al. concluded that steam aging did not protect the catalysts from further deactivation upon exposure to the feed gas containing SO_2 [Lampert et al., 1997].

Mowery et al. conducted oxidation experiments in simulated lean-burn natural gas engine exhaust with fresh and engine-aged Pd/Al_2O_3 catalysts. When a dry feed was used, fresh and engine-aged catalysts displayed similar levels of catalytic activity. When a wet feed gas stream was utilized, a significant reduction in activity was observed for engine-aged catalysts, and characterization studies showed that the decay was likely due to sulfates. In addition to permanent activity loss associated with water exposure, water inhibition was observed during wet feed experiments. Although inhibition and decay were also observed when SO_2 was injected into the feed, the activity loss was partially recoverable at 460 °C and completely recoverable at 520 °C. When water and SO_2 were present, the activity loss occurred more rapidly and was less recoverable [Mowery et al., 1999]. The researchers suspected that water facilitated SO_x migration from the alumina support to the PdO, resulting in increased deactivation [Mowery et al., 1999], so further characterization studies were performed to investigate this aspect [Mowery and McCormick, 2001].

As shown in Figure 1.1, Mowery et al. proposed that in dry conditions SO_2 adsorbs on PdO and alumina. In the case of PdO, SO_2 is oxidized to SO_3 which will either spillover to the support or be further oxidized to form palladium sulfate [$PdSO_4$]. However, PdO does not become sulfated at a fast rate or to a large extent because the alumina support scavenges SO_2 and SO_3, resulting in the SO_x species being displaced from PdO to the support. When water is present, the alumina sites become occupied with water thereby reducing the amount of SO_2 uptake that can occur. As a result, a higher level of sulfation is likely due to 1) more SO_3 formation on PdO, 2) less SO_3 spilling over to the alumina so more $PdSO_4$ forming, and 3) the SO_3 which does manage to migrate to alumina forms alumina sulfate species [$(Al_2(SO_4)_3$] [Mowery and McCormick, 2001].

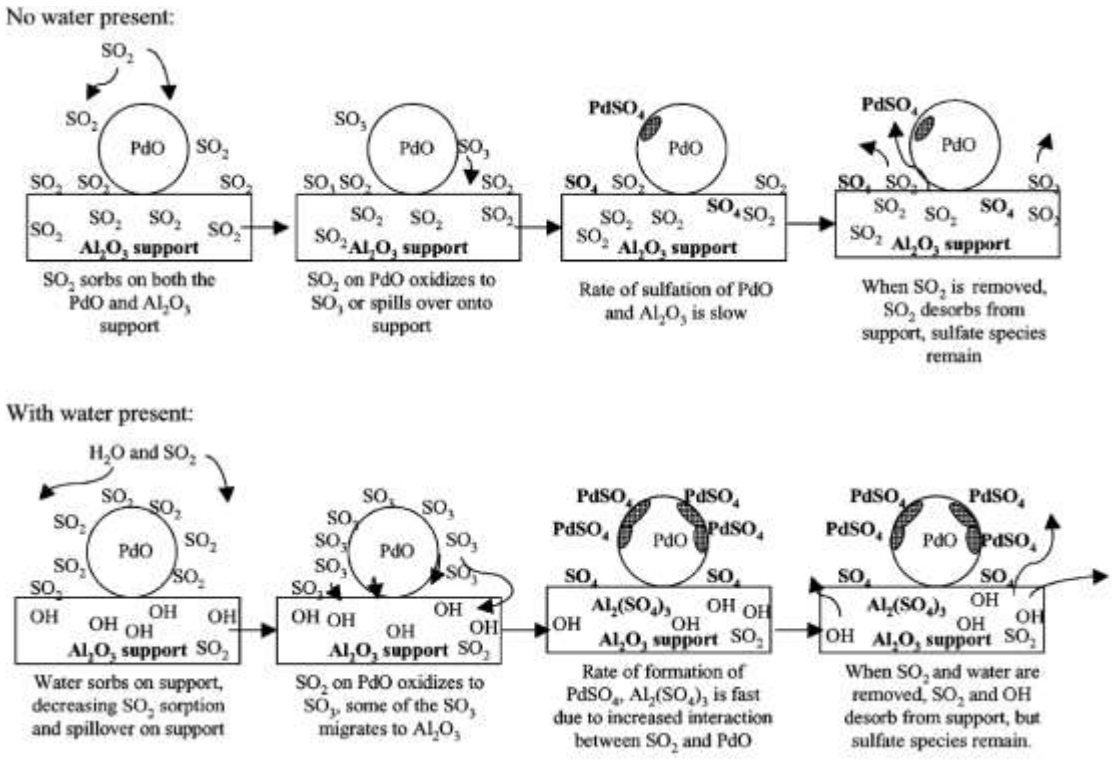

Figure 1.1: Proposed sulfation mechanism of Pd/Al_2O_3 [Mowery and McCormick, 2001]

Lapisardi et al. assessed the catalytic activity of Pt/Al_2O_3, Pd/Al_2O_3, and $Pd\text{-}Pt/Al_2O_3$ catalyst samples during CH_4 oxidation with addition of H_2S. The Pd/Al_2O_3, $Pd_{0.93}Pt_{0.07}/Al_2O_3$, and $Pd_{0.65}Pt_{0.35}/Al_2O_3$ samples displayed a sharp and rapid decay in activity upon exposure to H_2S. On the other hand, the Pt/Al_2O_3 and $Pd_{0.06}Pt_{0.94}/Al_2O_3$ catalysts displayed a gradual decline in activity over time [Lapisardi et al., 2007]. Lampert et al. performed CH_4 oxidation experiments on the following Pd/Al_2O_3 catalysts: steam aged, steam and oil aged, aged by exposure to engine outlet conditions, and steam aged with exposure to SO_2 or SO_3. The steam aged catalysts displayed the highest activity during CH_4 oxidation. All other catalysts samples displayed similar levels of lower activity. Based on these results, the authors concluded that the presence of sulfur alone was enough to deactivate the catalysts regardless of whether other potential poisons were contained in the engine inlet or oil feed sources [Lampert et al., 1997].

1.6 Research objectives

With a newfound abundance of economically recoverable natural gas, its use as a vehicle fuel seems opportunistic. In comparison to combustion in diesel vehicles, vehicular combustion of natural gas can result in lower emissions of CO_2, CO, NO_x, and soot. On the other hand, if incomplete conversion of CH_4 occurs, the remaining CH_4 can be emitted in the vehicle exhaust. In regards to abatement of CH_4, a strong greenhouse gas, improvements in catalytic aftertreatment systems for natural gas vehicles has not been thoroughly investigated.

Due to the high specific catalytic activity associated with noble metals, catalysts which utilize sulfur-resistant Pt, high-activity Pd, or a combination of the two have been used for CH_4 oxidation. Although much work has been published on CH_4 oxidation using

Pd and Pt catalysts, less has been published in regards to the use of Pd:Pt bimetallic catalysts and deactivation characteristics. Natural gas vehicle exhaust at the high end has temperatures between 300 and 550 °C, and contains water and trace amounts of sulfur. Since aftertreatment systems for natural gas vehicles must simultaneously display high catalytic activity at low temperatures as well as tolerance to water and sulfur, I set out to evaluate how the substitution of Pt for Pd would affect catalytic activity after exposure to water, high temperatures, or sulfur. Ten Pd-Pt/Al_2O_3 powder catalysts were prepared using the following molar compositions: $Pd_{1.0}Pt_{0.0}/Al_2O_3$, $Pd_{0.9}Pt_{0.1}/Al_2O_3$, $Pd_{0.7}Pt_{0.3}/Al_2O_3$, $Pd_{0.5}Pt_{0.5}/Al_2O_3$, $Pd_{0.3}Pt_{0.7}/Al_2O_3$, $Pd_{0.2}Pt_{0.8}/Al_2O_3$, $Pd_{0.15}Pt_{0.85}/Al_2O_3$, $Pd_{0.1}Pt_{0.9}/Al_2O_3$, $Pd_{0.05}Pt_{0.95}/Al_2O_3$, and $Pd_{0.0}Pt_{1.0}/Al_2O_3$. The contents of this dissertation will provide a summary of the research conducted to this end.

This dissertation contains the following chapters and content. Chapter 2 describes the experimental methods and equipment utilized in performing this work. Chapter 3 details the experiments necessary to characterize the impact of trace sulfur exposure on the CH_4 oxidation reaction. CH_4 oxidation experiments were conducted on each catalyst to assess catalytic activity prior to and after saturation exposure to ~ 30 ppm SO_2. Three simultaneously processes are involved with CH_4 oxidation with SO_2 treated catalysts: CH_4 oxidation, SO_2 oxidation, and SO_2 desorption. It was necessary to study each of these processes independently in order to obtain a complete understanding of the results discussed in Chapter 3. Chapter 4 discusses the experiments conducted to determine the kinetic reaction rate equation associated with complete CH_4 oxidation with Pd:Pt catalysts. A MATLAB script was developed to fit experimental kinetic parameters to the data obtained. The resultant kinetic parameters were used as inputs to the MATLAB-

based reactor model, which was developed in order to predict catalytic performance during CH_4 oxidation for each catalyst. Chapter 5 details the experiments required to understand how H_2O and high-temperature exposure, each a potential deactivation source, affect catalytic activity of CH_4 oxidation catalysts. Fresh catalyst samples were exposed to high temperatures, 650 and 900 °C, in an effort to sinter the samples. For a second set of fresh catalysts, CH_4 oxidation experiments were conducted in the presence of ~1.8 vol. % H_2O. CH_4 oxidation and CO chemisorption experiments were conducted on each catalyst to assess catalytic activity and precious metal crystallite particle size prior to and after exposure to each of the potential deactivation conditions.

In an effort to understand why the sulfur release characteristics of bimetallic catalysts varied with Pd:Pt mole ratio during CH_4 oxidation with SO_2-treated catalysts, I set out to decouple the CH_4 oxidation reaction from the sulfur characteristics by conducting temperature-programmed desorption (TPD) studies on SO_2-treated catalysts. I found that the Pd:Pt mole ratio and precious metal particle size are both key to understanding SO_2 adsorption and desorption characteristics. To gain a better understanding of what affects sulfur release characteristics in bimetallic catalysts, I worked to decouple the Pd:Pt mole ratio and particle size contributions as discussed in Chapters 6 and 7 respectively. To determine how Pd-Pt mole ratio affects sulfur release, TPD profiles of various mole ratio catalysts with similar particle sizes were compared. To determine how particle size affects sulfur release of mono and bimetallic catalysts, Pd, Pt, and high-Pd content catalyst TPDs were compared to TPDs of catalysts with the same mole ratio but differing in particle size. Diffuse Reflectance Infrared Fourier Transform Spectroscopy (DRIFTS) studies were performed to characterize metal chemical states via

CO adsorption studies and to identify how molecular SO_2, surface sulfite and sulfates, and bulk sulfate species are formed on the catalyst during SO_2 exposure as a function of mole ratio and particle size. Chapter 8 details the conclusions and recommended future work for these studies.

Chapter 2 Experimental Methods

To perform the experiments discussed herein two reactor systems, one water bubbler, and one pulse-injection valve were utilized. The CH_4 oxidation, SO_2 adsorption, and SO_2 TPD experiments were performed with a powder reactor system and a MKS MultiGas 2030 FTIR gas analyzer. When hydrothermal aging or water injection was required, the water bubbler was coupled with the powder reactor system set-up. For the CO chemisorption studies, the Valco Vici pulse-injection valve was paired with the powder reactor system. For catalyst surface studies, the CO chemisorption, SO_2 adsorption, and SO_2 TPD characterization studies were performed using the DRIFTS reactor system, with a Harrick Scientific Praying Mantis reaction cell.

2.1 Powder Reactor System

2.1.1 Gas supply

The main carrier gas for the powder reactor system was N_2, which was supplied via the laboratory ONSITE nitrogen generator. Upon exiting the nitrogen generator, the N_2 passed through Matheson Tri-Gas PUR-GAS Inline Purifiers: a triple (oxygen, moisture, and hydrocarbon) trap, a triple indicating trap to show when the trap is consumed, and another triple trap. These traps were placed in this order to 1) reduce the amount of trace contaminants in the carrier gas, 2) further reduce the trace species concentration and have some indication of when traps needs to be replaced, and 3) provide some control of trace species if the traps become saturated. Due to the sensitivity of SO_x to interactions with water and oxygen and the potential for precious metal sites to

uptake water instead of CO during CO chemisorption, it was pertinent to provide measures for avoiding inadvertent influences on the data.

Other gases were introduced via gas cylinders, which were procured from Praxair Gas. The gas name, type, and concentration are listed in Table 2.1.

Table 2.1: Gas cylinder information

Gas Name	Type	~Concentration [%]
O_2	Pure	100.0
SO_2	N_2 balanced	0.1
CH_4	N_2 balanced	4.0
H_2	Pure	100.0
CO	N_2 balanced	10.0

In order to minimize trace moisture in the reactor feed gas stream, Matheson Tri-Gas PUR-GAS Inline Moisture Traps were installed on the CH_4 and O_2 lines. In order to minimize moisture and oxygen in the H_2 feed gas stream, Matheson Tri-Gas PUR-GAS Inline Triple Traps were installed on the H_2 feed lines. These provisions were made to reduce the likelihood of inaccurate particle size measurements, inadvertent water inhibition during CH_4 oxidation, water interactions with SO_2 during SO_2 adsorption studies in the presence of O_2, and incomplete reduction during H_2 pretreatment processes.

Bronkhorst and MKS mass flow controllers were used to control the feed gas flowrates. Three-way valves were used to route the gas flow through the bypass line or catalyst bed and into the overhead vent or MKS MultiGas FTIR 2030 gas analyzer, which

is described below. All stainless steel tubing, valves, and fittings used for the reactor system shown in Figure 2.1 were procured from Swagelok.

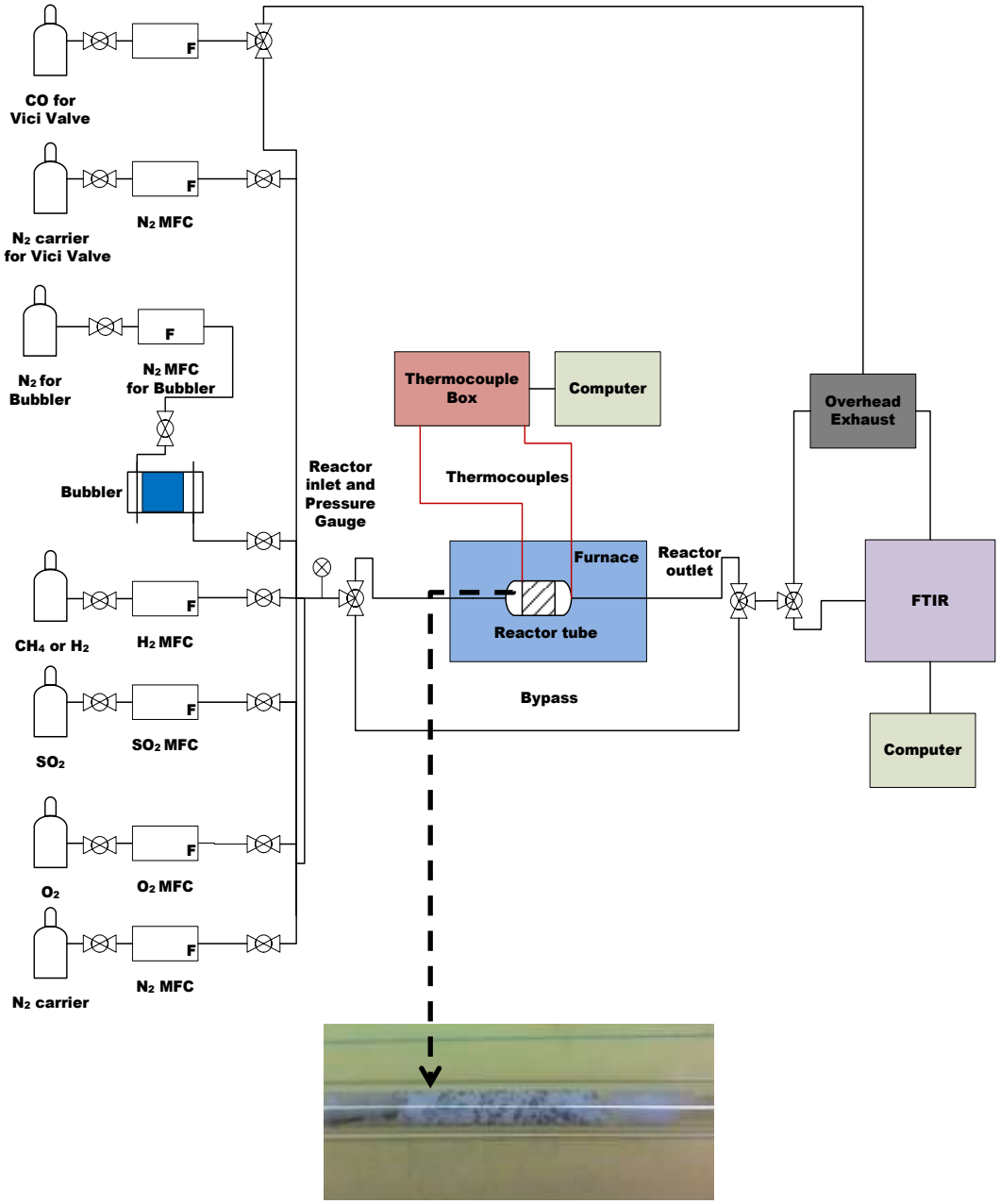

Figure 2.1: MKS FTIR Reactor System

2.1.2 Reactor system and data acquisition

Each catalyst bed consisted of active catalyst and inert beads. To achieve an equivalent monolith space velocity of 50,000 hr^{-1}, 200 ml/min total flowrate and 29.3 mg of active catalyst sample was used. The active catalyst sample mass,

$$m_{active\ powder\ catalyst} = \frac{\dot{V}\rho_{monolith}}{SV_{monolith}}, \quad (1)$$

where m is the active mass of the powder catalyst sample, $\dot{V}$ is the volumetric flowrate, $\rho_{monolith}$ is the monolith loading, and $SV_{monolith}$ is the monolith space velocity. Silica beads were mixed with each catalyst to dilute the catalyst bed in an effort to prevent dense packing and hot spots within the catalyst bed. A dilution ratio of 1:8 for active to inert mass was used. The active and inert catalyst particles were sieved to achieve a mesh size range of 250 to 420 μm. Each resulting catalyst sample was installed in a 4 mm diameter quartz tube. Quartz wool was placed at each end of the catalyst bed in order to secure the bed particles, maintain the catalyst bed position in the quartz tube, and maintain the catalyst bed length of 20 mm.

Omega heating tapes and variacs were used to apply and set the heat input to the lines. The manifold and reactor system lines were maintained at 150 °C to 180 °C in order to prevent water and sulfur species from depositing on the lines. Tetraglas insulation tape from Darco Southern was used to insulate the lines in an effort to minimize heat loss to the surrounding environment and minimize the potential for accidental contact burns. A Thermoscientific Linderg/Blue tube furnace was used to set and control the temperature supplied to the catalyst bed. Type K thermocouples were placed at the inlet and outlet of the catalyst bed in order to measure the inlet and outlet gas temperatures. These temperature measurements were acquired utilizing National

Instruments Field Point hardware and LabView software and stored in a Microsoft Excel file. As adsorption and oxidation studies were performed, the MKS gas analyzer, described below, was utilized to monitor gas concentrations.

2.1.3 Pulse injection

A Valco Vici pulse-injection valve was used to supply 10 µL doses of CO to catalyst samples at regular intervals. First, the valve position was set to route flow from port 1 to port 6, as shown in Figure 2a. CO was flown through port 1 and into the injection loop whereas N_2 carrier gas was flown into port 4. When the sample loop was filled, the valve was turned to route flow from port 1 to port 2. CO from the injection loop was pushed into the reactor manifold by the N_2 carrier gas, as shown in Figure 2.2b.

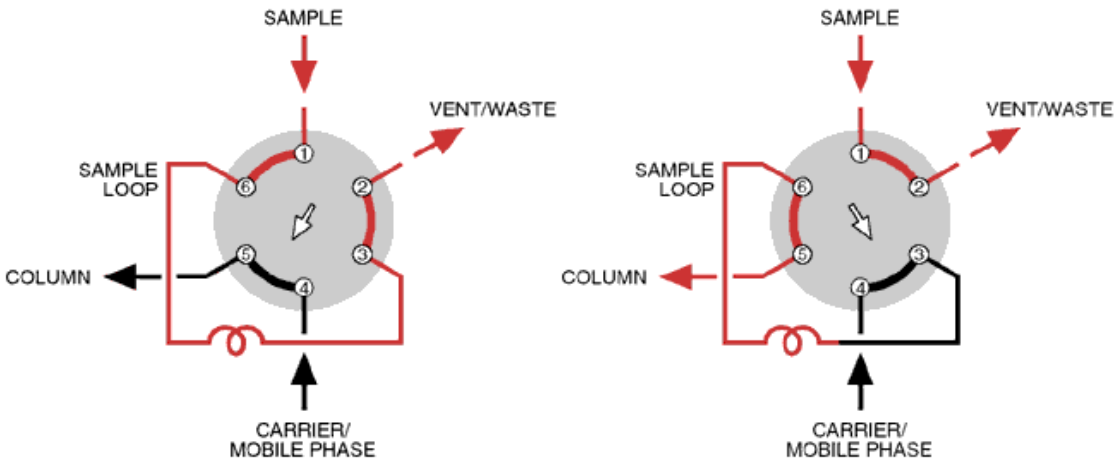

Figure 2.2: Valco Vici Pulse-Injection Valve (a) Filling injection loop with CO and (b) CO Injection [Valco Instruments]

The sample loop filling and injection sequence was repeated periodically to allow the catalyst sample to gradually uptake CO. When the injection pulse-signature ceased to

change with each additional CO pulse injection, the sample was considered saturated. After saturation was achieved, the total volume of CO adsorbed was used to determine the sample dispersion and particle size. The CO injection pulse was measured using an MKS MultiGas FTIR 2030 to be described below.

2.1.4 Water injection

During wet CH_4 oxidation studies and hydrothermal aging of catalysts, a water bubbler was used to generate and inject water vapor into the reactor manifold, achieving an overall concentration of ~1.8 vol. % H_2O. A W.A. Hammond drying column was procured from Cole-Parmer and repurposed to serve as a water bubbler. All desiccant and other sorbent media was removed from the column. The water bubbler consisted of a column, a sealing lid/gasket, inlet and outlet ports, glass beads, and deionized water. 2 mm glass beads were filled halfway up the column height to facilitate contact between the injected gas and water in an effort to achieve saturation. Deionized water was poured into the column until three quarters of the bubbler height had been achieved to allow sufficient headspace for water vapor to exit the column without water condensate exiting as well.

To generate water vapor, N_2 was bubbled through the bottom of water bubbler as shown in Figure 2.3. As the N_2 bubbled through the beads and water, the gas absorbed some of the water. The resultant moistened-N_2 was routed to the reactor manifold, and was maintained at 150 °C to ensure the water vapor did not condense in the lines. Variacs and Omega heating tapes were used to set and apply the heat input to the lines. The line heating losses were minimized via Tetraglas insulation tape.

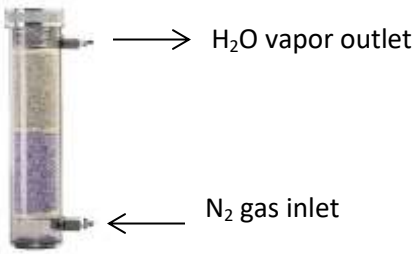

Courtesy of Cole-Parmer

Figure 2.3: After removing contents from drying column, the container was repurposed for water bubbler use.

2.1.5 Gas analysis and data acquisition

An MKS MultiGas 2030 FTIR Spectrometer gas analyzer can be used for automotive diesel, catalysis, and stack emission concentration measurement applications. For the work discussed herein, the MKS analyzer system was used to measure the gas concentrations at the outlet of the catalyst bed or bypass line. The MKS analyzer system is shown in Figure 2.4. The main external interfaces of the analyzer consist of VCR fittings for gas injection for analysis and ejection post-analysis, a standard power cord to route power from the facility to the analyzer, an Ethernet data cable to transmit data from the instrument to the MKS software installed on a laboratory desktop computer, a Swagelok quick-disconnect port, and a liquid-N_2 fill port. Purge gas was supplied to the quick-disconnect port and regulated at 15 psig to ensure that the MKS analyzer was always operating in a non-condensing environment for hardware longevity. During spectra acquisition, the liquid-N_2 was used to cool the mercury-cadmium telluride (MCT) detector.

The MKS analyzer system is capable of detecting and differentiating multicomponent gas mixture components that are IR sensitive with accuracy in some cases to the ppb to ppm range. In order to accomplish this, the system consists of a 2102

Process FTIR Spectrometer (Figure 2.5a), high-optical-throughput sampling cell (Figure 2.5b), analysis software, and quantitative spectral library.

Figure 2.4: MKS MultiGas 2030 FTIR

2.5a

2.5b

Figure 2.5: MKS MultiGas 2030 FTIR components (a) 2102 Process FTIR Spectrometer and (b) gas cell [MKS Instruments, 2007]

The main internal components consist of the 2102 Process FTIR Spectrometer and sample gas cell. The 2102 Process FTIR Spectrometer was specifically designed to monitor environmental and process gas streams similar to that encountered with engine exhaust emissions and emissions abatement experiments. The spectrometer, utilizing a 0.25 mm x 0.25 mm element MCT detector, can achieve spectral resolutions up to 0.5 cm^{-1} with minimal noise to support IR spectral analysis. The spectrometer is connected to an MKS-patented 200 mL gas cell. The gas cell, which has a 5.11 m pathlength, contains VCR ports described above, a gas line heater, mirrors, ZnSe windows, and Kalrez O-rings. The gas line heater ensures that the temperature is maintained as the gas sample enters the gas cell. The mirrors provide sufficient aberration-correction to maximize

optical-throughput during spectral acquisition. Kalrez O-rings and ZnSe windows were utilized because they are compatible with sulfur species and support periodic cleaning respectively [MKS Instruments, 2007].

Prior to performing each experiment with the powder reactor system, 200 ml/min of N_2 was flown through the reactor system until the MKS FTIR spectra ceased to change. Sixteen scans of background spectra were then collected and were automatically subtracted from spectra collected during the experiments for a particular sample. All spectra were collected and processed utilizing the MKS MG2000 software, which was installed on a laboratory desktop computer. The MKS software analyzed the spectral data in real-time and real-time concentrations were output based on their spectral library.

2.2 Diffuse Reflectance Infrared Fourier Transform Spectroscopy (DRIFTS) Reactor System

2.2.1 Gas supply

All gas cylinders were procured from Praxair Gas. The gas name, type, and concentration are listed in Table 2.2. The main carrier gas, He, was flown through a Matheson Tri-Gas PUR-GAS Moisture trap to reduce the trace moisture in the carrier gas. This provision was necessary to reduce the likelihood of inadvertent water uptake instead of CO by precious metal sites during CO chemisorption or water interactions with SO_2 during SO_2 adsorption. As shown in Figure 2.6, the He carrier gas helped dilute and carry the other gases through the reactor manifold. Prior to entering the manifold, MKS mass flow controllers were used to control the reactant gas flowrates. Three-way valves

were used to route the gas flow into the Harrick Scientific Praying Mantis DRIFTS cell or into the overhead vent. All stainless steel tubing, valves, and fittings were procured from Swagelok.

Table 2.2: DRIFTS Gas cylinder information

Gas Name	Type	~Concentration [%]
He	Pure	100.0
O_2	Pure	100.0
H_2	Pure	100.0
CO	He balanced	0.5
SO_2	N_2 balanced	0.1

2.2.2 Reactor system, analysis, and data acquisition

For the work discussed herein, the DRIFTS reactor system was used to characterize surface species on powder catalyst samples in a controlled temperature environment. In order to accomplish this, the DRIFTS reactor system utilizes a ThermoScientific Nicolet 6700 Spectrometer, OMNIC software with associated laboratory desktop computer, a Harrick Scientific Praying Mantis Accessory (Figure 2.7a) coupled with an associated Praying Mantis High-Temperature Reaction Chamber (Figure 2.7b), Watlow EZ-Zone temperature profile programming software, and auxiliary gas equipment shown in Figure 2.6.

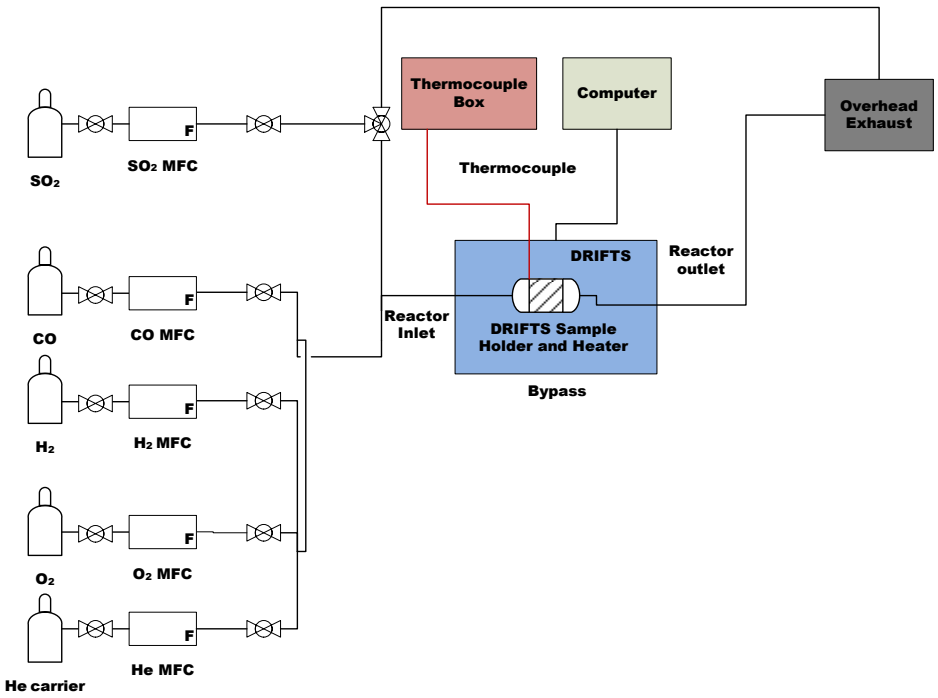

Figure 2.6: DRIFTS reactor system

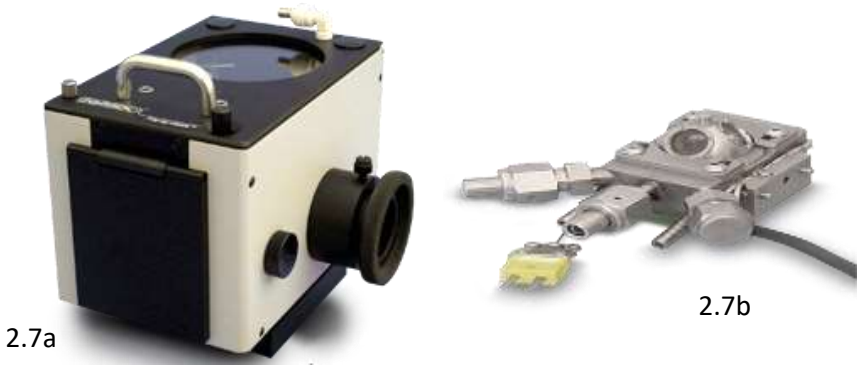

Figure 2.7: DRIFTS Auxiliary Components (a) Praying Mantis Accessory and (b) High-Temperature Reaction Chamber [Harrick Scientific Products]

Similar to the MKS spectrometer, the ThermoScientific Nicolet 6700

Spectrometer utilizes a MCT detector and is cooled with liquid N_2 during experiments.

The spectrometer and OMNIC software collect and store spectra over a 4000 to 650 cm^{-1}

wavelength range. All DRIFTS were collected with 64 scans and a resolution of 4 cm^{-1}. Background spectra were collected in 50 ml/min of He only at the experimental temperature. The background spectrum corresponding to each experimental temperature was subtracted from all spectra collected during the following experiments for that catalyst.

The Harrick Scientific Praying Mantis Accessory mates to the spectrometer and contains two 90° off-axis ellipsoid mirrors which can be adjusted to support efficient diffuse reflectance illumination and collection [Harrick Scientific Products]. The High-Temperature Reaction Chamber, which is installed in the Praying Mantis Accessory housing, consists of the following: two ports to route cooling water in and out of the chamber base via a water pump, four ZnSe windows, three gas inlet/outlet ports, and a temperature controller with an associated Type K thermocouple.

Two of the three inlet/outlet ports were used to route gas flow through the Praying Mantis cell and into the overhead vent. The third port, which supports chamber evacuation, was capped and not utilized during these experiments. The Watlow EZ-Zone software was used to set the temperature of the Praying Mantis heater. The Praying Mantis temperature controller and thermocouple were used to heat and control the cell temperature via a feedback loop.

Undiluted catalyst samples of ~40 mg were pressed into the sample holder of the DRIFTS Harrick Scientific Praying Mantis High-Temperature Reaction Chamber Cell. A total flow stream of 50 ml/min was directed through the DRIFTS reactor sample holder continuously during experiments. The manifold and reactor system lines were heated to 150 °C and were purged with 50 ml/min of He overnight prior to any experiments in

order to reduce any trace moisture in the lines. During experiments, the manifold and reactor system lines were maintained at 150 °C in order to prevent water and sulfur species from depositing on the lines. Omega heating tapes and variacs were used to heat and set the heat input to the lines. Tetraglas insulation tape was used to insulate the lines in an effort to minimize heat loss to the surroundings [Harrick manuals and datasheets].

2.3 Safety

Bulwark flame resistant lab coats and polycarbonate safety glasses were utilized during all laboratory operations. Nitrile gloves and 3M Particulate Respirators with Nuisance Level Organic Vapor Relief were used during catalysts synthesis and sample preparation. 3M Organic Vapor and Acid Gas cartridges were used with a 3M 5000 series respirator during gas cylinder installation or removal, tubing modifications, and MFC installation or removal, for items which came in contact with sulfur species. To prevent toxic gases from being emitted into the lab atmosphere, all reactor exhaust gases were continuously routed to an overhead vent. To limit potential for accidental exposure to trace sulfur acid which could form during sulfur studies, a Pyrex collector was used to collect any condensate. During H_2 reduction of sulfur treated catalysts, H_2S forms. In this case, the reactor exhaust gases were continuously routed through a 277 mg Shell Gas Sulfur Trap sorbent media bed, then was bubbled through a Pyrex collector containing a 200 ml Methyl diethanolamine (MDEA) bath, and was finally routed to an overhead vent. Butyl gloves were used when handling the Pyrex containers. A CO monitor with an alarm function was placed near the CO feed lines and CO pulse-injection valve. A Beacon Gas Monitor was procured from Praxair to monitor the laboratory environment and alarm upon exceeding limits set for CH_4, NH_3, or SO_2 gases.

Chapter 3 Sulfur Deactivation and Regeneration of Mono- and Bimetallic Pd-Pt Methane Oxidation Catalysts

Note: The material in this chapter has been submitted for publication. Therefore the introduction and experimental methodology may appear redundant with other sections. Reference and figure numbers were changed for dissertation consistency.

3.1 Introduction

Natural gas contains methane, other hydrocarbons, such as ethane and propane [Abbasi et al., 2012; Varde and Bohr, 1993; Trimm and Lee, 1995], and trace level species including sulfur species [Gélin and Primet, 2002]. In comparison with diesel engines, natural gas engine combustion produces lower CO_2, CO, NO_x, and soot emissions. One concern is of course the associated methane emissions and methane's greenhouse gas potential. A typical approach to mitigate such emissions would be the installation of an exhaust stream oxidation catalyst. Over such catalysts, under lean-burn conditions heavier hydrocarbons can be completely oxidized at low temperatures [Trimm and Lee, 1995] but high temperatures are necessary for complete methane conversion [Gélin and Primet, 2002]. However, lean-burn natural gas engine exhaust temperatures are relatively low [Demoulin et al., 2008], resulting in methane slip. Furthermore, those trace sulfur species deactivate methane oxidation catalysts resulting in reduced catalytic

activity with time-on-stream and thus increased levels of unconverted methane in natural gas engine exhaust [Lapisardi et al., 2007].

There has been a substantial amount of CH_4 oxidation research published, with a comprehensive review of these by Gélin and Primet [Gélin and Primet, 2002]. Specific challenges discussed in their review article include the required CH_4 oxidation temperature resulting in thermal sintering, the low CH_4 concentrations in the exhaust, H_2O inhibition, and degradation via sulfur poisoning. Studies have shown that for O_2:CH_4 molar ratios exceeding 2, i.e., lean-burn operation conditions, PdO-based catalysts are significantly more active than Pt-based catalysts [Gélin and Primet, 2002]. Interestingly, under rich conditions, i.e., when there are stoichiometric or sub-stoichiometric amounts of O_2 relative to CH_4, Pt has been found to be more active[Burch and Loader, 1994]. Substituting small Pt amounts for Pd, i.e. bimetallics, provides some sintering resistance and increased catalytic activity [Lapisardi et al., 2007,Yamamoto and Uchida, 1998,Kinnunen et al., 2012,Skoglundh et al., 1991,Lapisardi et al., 2006,Ohtsuka, 2011,Castellazzi, 2010,Persson et al., 2006,Corro et al., 2010], with improved resilience with time on stream [Yamamoto and Uchida, 1998,Kinnunen et al., 2012,Persson et al., 2006,Corro et al., 2010] in comparison to monometallic Pd catalysts. Thus there are known benefits of bimetallic systems for CH_4 oxidation.

In terms of sulfur poisoning/deactivation, it is well known that Pd-based catalysts are quite susceptible to sulfur. In one example, CH_4 oxidation on fresh and steam aged Pd/Al_2O_3 catalysts was evaluated. When 1 ppm SO_2 was added to the feed, the activity declined similarly for both catalysts [Lampert et al., 1997]. In contrast to the abrupt decay in Pd-based catalyst activity upon SO_2 exposure [Lampert et al., 1997], Lapisardi et al.

found that CH_4 oxidation activity gradually declined for Pt/Al_2O_3 catalysts when exposed to H_2S [Lapisardi et al., 2007]. Ottinger and coworkers studied sulfur regeneration of a Pd-based CH_4 oxidation catalyst via high temperature exposure as well as via a reductive treatment. They found that for the thermal regeneration, temperatures greater than 500 °C were required to regain some activity, whereas the reductive treatment provided better regeneration efficiency [Ottinger et al., 2015]. Similarly, Arosio et al. [Arosio et al., 2006] showed that, for Pd-based catalysts, higher temperatures (>750 °C) were required for sulfur regeneration in the presence of simulated lean-CH_4 oxidation conditions, but switching from this lean atmosphere to one which was CH_4-rich resulted in much lower temperatures required to recover activity.

Although bimetallic Pt/Pd catalysts show resistance to sintering and improved activity, researchers found that these bimetallic benefits only held true in the absence of sulfur [Lapisardi et al., 2007]. Interestingly, SO_2 poisoning of a Pt/Pd bimetallic sample resulted in decreased activity, but a pre-reduction prior to SO_2 exposure had significantly less impact [Corro et al., 2010]. Since aluminum surface and bulk sulfates are stable up to 650 °C [Waqif et al., 1991] and 800 °C to 920 °C [Saur et al., 1986] respectively, it is likely that sulfur species will compromise activity to some extent until these species can be decomposed at high temperatures. Although some researchers reported that aluminum sulfates are quite resistant to reduction [Saur et al., 1986], others found that aluminum sulfates, which thermally decompose above 800 °C, can be reduced in H_2 at 600 °C [Waqif et al., 1991].

In this study three approaches based on gas environment were evaluated for CH_4 oxidation activity regeneration, which should correlate to sulfur species decomposition.

Here we focused on evaluating model sulfur regeneration methods as a function of Pd:Pt mole ratio.

3.2 Experimental methods

3.2.1 Catalyst preparation and reactor experimental set-up

The precursors, $Pd(NO_3)$ and $Pt(NH_3)_4(NO_3)_2$, and Puralox γ-Al_2O_3, were procured from Sigma-Aldrich. Using the incipient wetness impregnation method, the following Pd-Pt/Al_2O_3 powder catalysts were prepared: $Pd_{1.0}Pt_{0.0}/Al_2O_3$, $Pd_{0.9}Pt_{0.1}/Al_2O_3$, $Pd_{0.7}Pt_{0.3}/Al_2O_3$, $Pd_{0.3}Pt_{0.7}/Al_2O_3$, and $Pd_{0.0}Pt_{1.0}/Al_2O_3$. All catalysts contained the same total number of precious metal (PM) moles used to synthesize a 1 wt. % Pd/Al_2O_3 catalyst. After drying overnight, all samples were calcined in air at 550 °C.

For all reactor pretreatment and experimental conditions, 29.3 mg of active catalyst was used with a 200 mL/min flow, to achieve a space velocity of 50,000 hr^{-1}. The active catalyst mass was diluted with inert silica beads to prevent dense packing and hot spots within the catalyst bed. Each sample was installed in a 4 mm diameter quartz tube. Quartz wool was placed at both catalyst bed ends to secure the bed particles, maintain the catalyst bed position in the quartz tube, and maintain the 20 mm catalyst bed length. Prior to experiments, each catalyst underwent an oxidation pretreatment with 10 vol. % O_2 in N_2 at 500 °C for 1 hour. Each catalyst sample was then pretreated with 2000 ppm CH_4 and 10 vol. % O_2 in N_2 until CH_4 conversion stabilized. Catalysts having been prepared through this protocol are referred to as fresh catalyst samples.

Bronkhorst and MKS mass flow controllers were used to control the inlet gas flowrates. For all reactor experiments, the gas concentrations at the catalyst bed outlet were measured using an MKS MultiGas 2030 FTIR Spectrometer gas analyzer. A

Thermoscientific Lindberg/Blue tube furnace was used to set and control the temperature supplied to the catalyst bed. Type K thermocouples were placed at the catalyst bed inlet and outlet to measure the inlet and outlet gas temperatures.

All catalytic activity assessments used the same reference temperature-programmed oxidation (TPO) protocol: 2000 ppm CH_4 and 10 vol. % O_2 in N_2 with a 5 °C/min temperature ramp rate. Following the pretreatment under reactants, each sample underwent a reference TPO to obtain a baseline of its fresh catalytic activity. After each regeneration procedure, the reference TPO was performed again in an effort to compare the initial catalytic activity to that observed following regeneration.

Each sample was exposed to 30 ppm SO_2 and 10 vol. % O_2 in N_2 at 100 °C. After SO_2 saturation was achieved, the reactor was purged with N_2 at 100 °C to reduce the residual SO_2 in the reactor system lines and remove weakly adsorbed SO_2 from the sample.

3.2.2 Sulfur regeneration

After the SO_2 exposure, each catalyst sample underwent one of the following regeneration methods.

1. Selected samples underwent the reference TPO protocol. CH_4 oxidation and SO_2 desorption were monitored during the temperature ramp. The SO_2 release characteristics helped define experimental conditions for SO_2 DRIFTS studies, to be discussed below.
2. After the selected samples were saturated with SO_2, a temperature-programmed desorption (TPD) was then performed in an effort to desorb and decompose sulfur species. The TPD was performed in a flow stream of N_2 only using the following

protocol: a ramp rate of 10 °C/minute to 900 °C followed by a hold at 900 °C for an additional 15 minutes.

3. After SO_2 exposure, a temperature-programmed reduction (TPR) was performed with designated samples at 600 °C in a 5 vol. % H_2 in N_2 flow stream for 30 minutes in an attempt to reduce sulfate species. Following reduction, the reactor was purged with N_2 prior to the reoxidizing the sample in 10 vol. % O_2 in N_2 at 600 °C for 30 minutes.

3.2.3 Thermal degradation effects

After the catalyst CH_4 conversion stabilized, the sample temperature was increased in pure N_2 using the following furnace protocol: a ramp rate of 10 °C/minute to 650 °C followed by a hold at 650 °C for an additional 15 minutes. After cooling the sample, a reference TPO was performed to assess changes in performance due to the 650 °C exposure. The above protocol was repeated for a 900 °C exposure.

Precious metal particle sizes were measured after these high temperature exposures. After the TPO reference protocol, the samples were reduced at 400 °C under a 5 vol. % H_2 in N_2 flow stream. Following reduction, the reactor was cooled to 35 °C. Using a Valco pulse injection valve, 10 μL of CO were injected in regular intervals. When the injection pulse-signature was consistently repeated, the sample was assumed saturated. After saturation was achieved, the total volume of CO adsorbed was used to determine the sample PM dispersion and corresponding particle size. These data were used to assess whether the high temperatures required for TPD and TPR regeneration had any negative effect on CH_4 oxidation activity.

3.2.4 Diffuse reflectance infrared Fourier transform spectroscopy (DRIFTS) characterization

In preparation for the DRIFTS experiments, each catalyst was aged in a 1.8 vol. % H_2O and 10 vol. % O_2 in N_2 flow stream for 8 hours at 700 °C to achieve a PM particle size similar to that used in the reactor experiments. After the aging period, the reactor was purged with N_2 at 700 °C for 30 minutes to minimize the residual H_2O and O_2 content within the catalyst bed and reactor system lines. After aging in the reactor, catalysts were then transferred to the Harrick Scientific Praying Mantis DRIFTS cell. Background spectra were gathered in 50 ml/min of He only at 35 °C, 100 °C, and 300 °C. The background spectra were subtracted from their corresponding spectra obtained at each temperature during the following experiments.

Prior to experiments, each catalyst underwent an oxidation treatment at 100 °C with 10 vol. % O_2 in He for 5 minutes. The catalyst was then reduced at 400 °C with 5 vol. % H_2 in He for 30 minutes. After reduction, the catalyst was maintained at 400 °C for an additional 30 minutes while the cell was purged with He to minimize the residual H_2 content within the DRIFTS cell and system lines. The catalyst was then cooled to 35 °C and exposed to 1 vol. % CO and 10 vol. % N_2 in He until CO saturation. For all DRIFTS experiments, saturation was determined by a lack of change in the collected DRIFTS spectra.

The system was purged with He prior to increasing the sample temperature to 100 °C. Each catalyst was then exposed to 100 ppm SO_2 and 10 vol. % N_2 in He at 100 °C. After the catalyst was saturated at 100 °C, the plotted SO_2 adsorption spectrum was obtained. The system was purged with He prior to decreasing the catalyst temperature to

35 °C. CO adsorption was repeated and spectra collected upon CO saturation at 35 °C. The system was then purged with He again prior to increasing the sample temperature to 300 °C. The SO_2 desorption spectrum was obtained after the DRIFTS spectra ceased to change at 300 °C. The desorption temperature, 300 °C, was selected based on sulfur release during TPD experiments discussed below. Again the system was purged with He prior to decreasing the catalyst temperature to 35 °C. CO adsorption was repeated and spectra collected upon CO saturation at 35 °C. CO adsorption spectra were collected prior to and after the SO_2 sorption DRIFTS experiments in an effort to determine the types of sites impacted by SO_2 adsorption.

3.3 Results and discussion

3.3.1 Baseline catalytic activity

Prior to sulfur exposure, the samples underwent a reference TPO to obtain a measure of the fresh catalytic activity. The ignition profiles obtained during this experiment are compared in Figure 3.1. Substituting some Pt into the formulation, 0.9 Pd-0.1 Pt, resulted in increased activity in comparison to monometallic Pd. Greater substitutions led to decreased activity, with the monometallic Pt sample the poorest tested. Lapisardi et al. observed similar trends for 2 wt. % Pd:Pt/Al_2O_3 catalysts [Lapisardi et al., 2007].

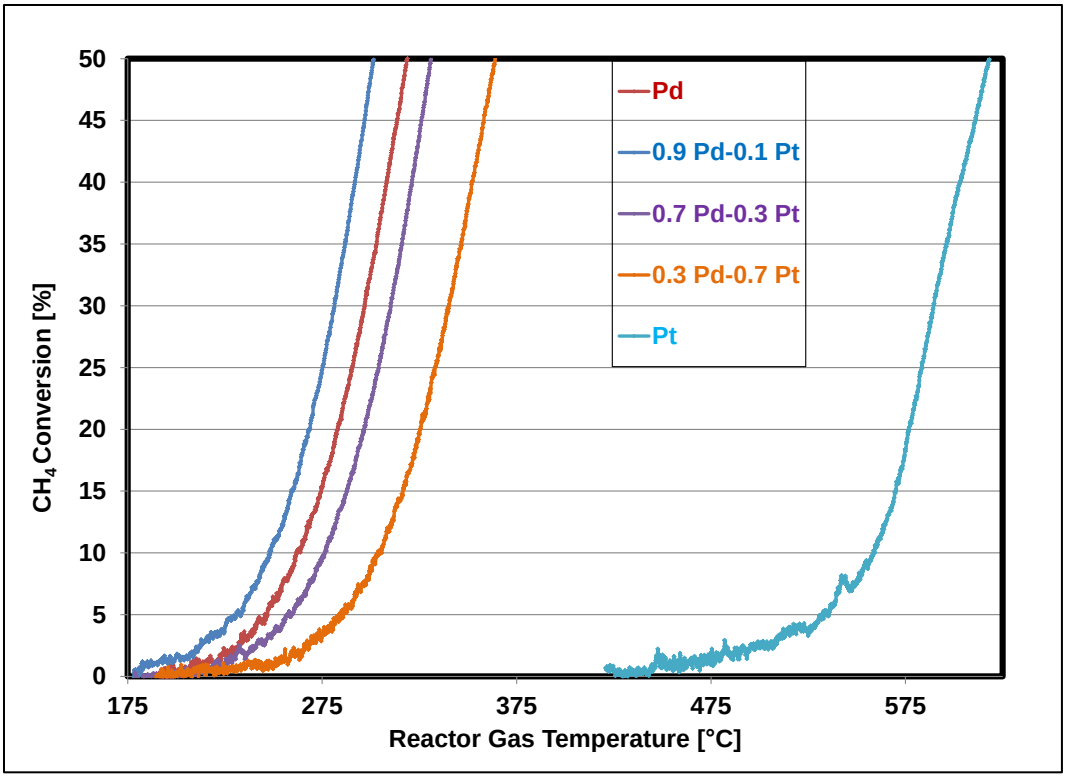

Figure 3.1: CH_4 TPO over the fresh catalysts in flowing 2000 ppm CH_4 and 10 vol. % O_2 in N_2, with a ramp rate of 5 °C/min.

3.3.2 Sulfur impact on catalytic activity

After SO_2 exposure, the same TPO experiment was performed to assess how SO_2 impacted catalytic activity. The ignition curves for the fresh and SO_2-exposed monometallic samples are compared in Figure 3.2a. SO_2 exposure inhibited the CH_4 oxidation reaction for monometallic Pd, but monometallic Pt was unaffected by this SO_2 treatment. Using T_{50} (the temperature where 50% CH_4 conversion was attained) as a metric, the changes in catalytic activities of the SO_2-exposed monometallic and bimetallic catalysts are compared in Figure 3.2b.

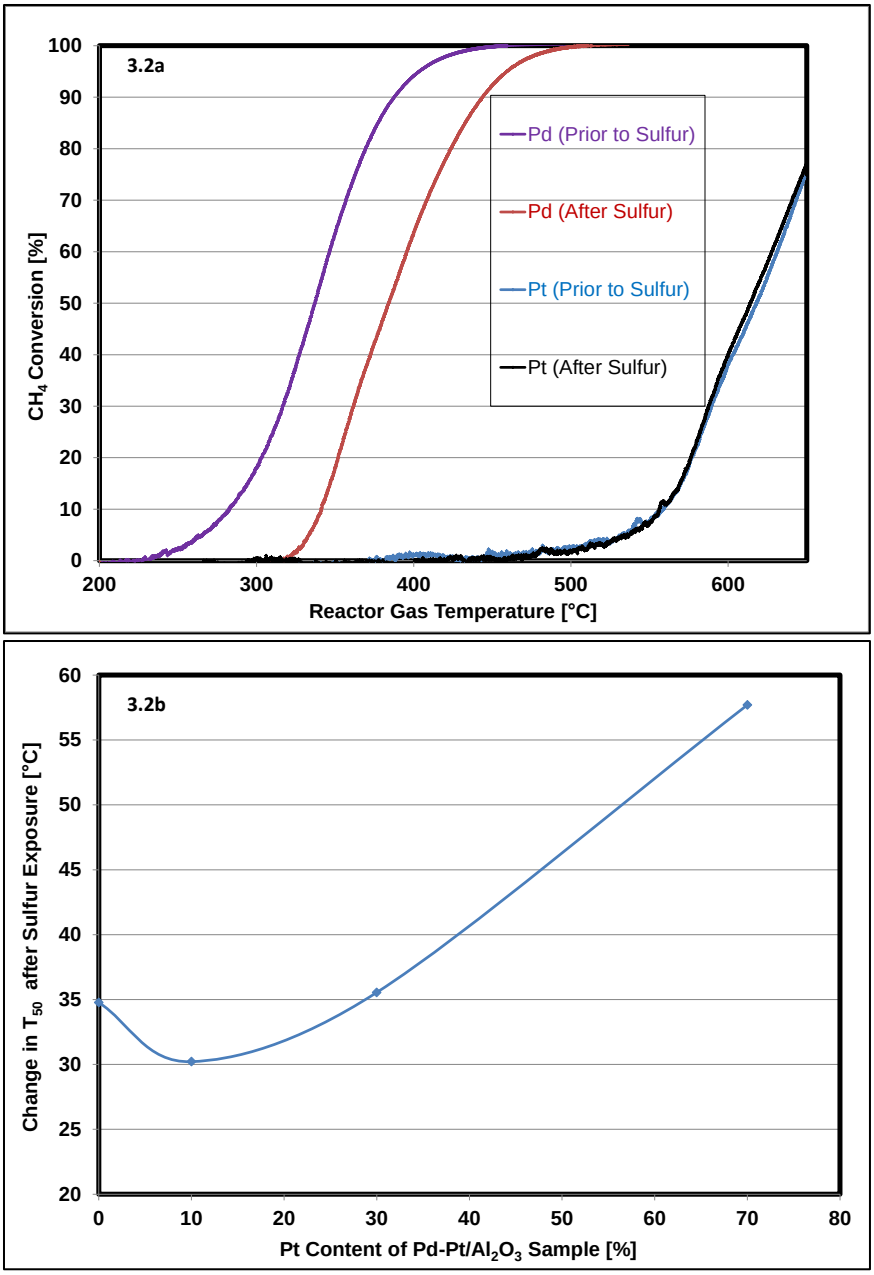

Figure 3.2: CH_4 TPO in flowing 2000 ppm CH_4 and 10 vol. % O_2 in N_2, with a ramp rate of 5 °C/min. a) CH_4 conversion for fresh and SO_2-exposed monometallic catalysts; (b) the change in T_{50} after sulfur exposure for catalysts.

In comparison to monometallic Pd, sulfur inhibition decreased upon substituting 10% Pt into the sample, 0.9 Pd-0.1 Pt. Recalling that monometallic Pt was SO_2 resistant, it was suspected that increased substitution into Pd catalysts would result in decreased sulfur

inhibition during CH_4 oxidation. Instead, similar to that observed for fresh CH_4 oxidation activity, further increases in Pt substitution led to reduced benefit, to the extent that with 70% Pt, the loss in activity with SO_2 exposure was the greatest.

In overlaying the measured sulfur desorption concentrations with the conversion plots (Figure 3.3), the onset of methane oxidation was observed after a SO_2 desorption feature. Note, no SO_3 or H_2SO_4 was observed. Both the sulfur release and inhibition extents appeared to vary with Pd:Pt mole ratio.

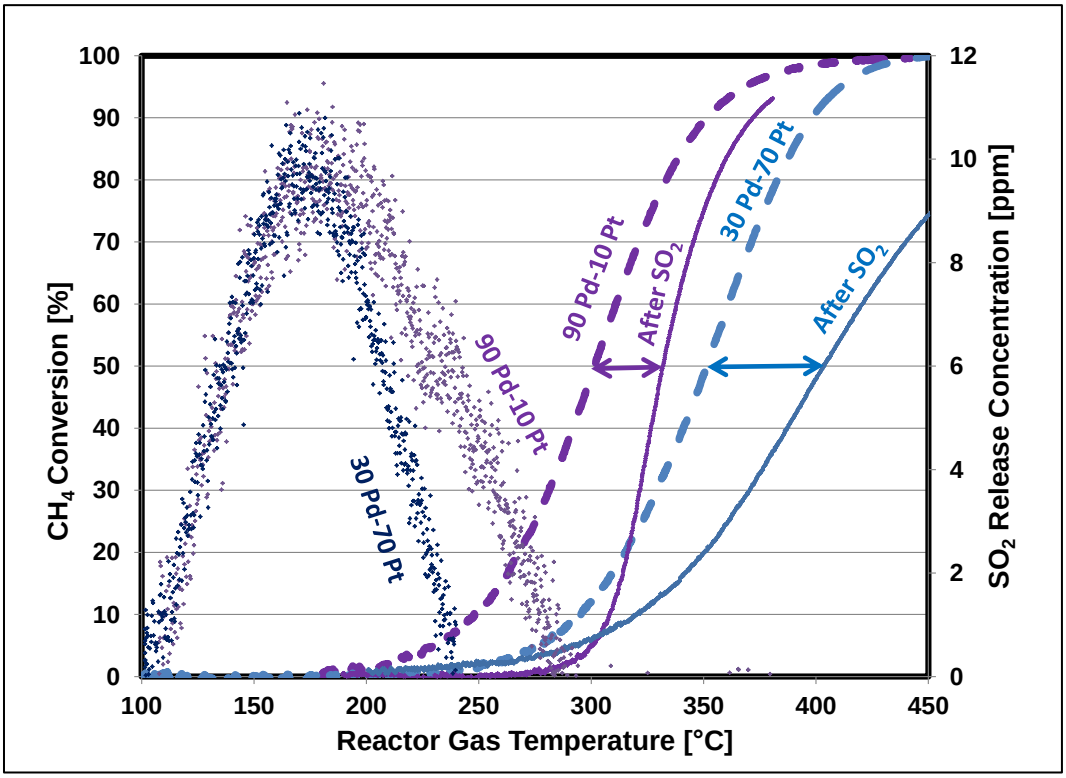

Figure 3.3: SO_2 release and inhibition during TPO over the 0.9 Pd-0.1 Pt and 0.3 Pd-0.7 Pt samples in flowing 2000 ppm CH_4 and 10 vol. % O_2 in N_2, with a ramp rate of 5 °C/min.

3.3.3 DRIFTS studies

DRIFTS were used to characterize how the sulfur release and CH_4 oxidation inhibition varied with mole ratio. Although monometallic Pd was more active than Pt for

complete CH_4 oxidation, the CH_4 oxidation reaction was inhibited at low temperatures after exposing the monometallic Pd sample to SO_2, unlike Pt. The 0.3 Pd-0.7 Pt sample was less active and less resistant to sulfur poisoning in comparison to the other characterized bimetallic samples. For these reasons, monometallic Pd and Pt as well as bimetallic 0.3 Pd-0.7 Pt were selected for study using DRIFTS. CO DRIFTS studies were performed to determine how sulfur exposure impacts the PM sites. The SO_2 DRIFTS studies were performed to help identify the sulfur species types formed during adsorption at 100 °C and which were stable up to 300 °C, the temperature at which SO_2 release at low temperature ended, as shown in Figure 3.3.

3.3.3.1 CO adsorption

After catalysts were saturated with CO at 35 °C, DRIFTS spectra were collected. Prior to SO_2 exposure, the Pd spectrum contained intense peaks at 2088 cm^{-1} and 1996 cm^{-1} as well as a lower intensity peak at 1936 cm^{-1} (Figure 3.4a). The 2088 cm^{-1} and 1996 cm^{-1} peaks were assigned to CO linearly adsorbed on metallic Pd (Pd^0-CO) [Rades et al., 1996,Zhang et al., 2014,Bensalem et al., 1996,Martinez-Arias et al., 2004] and CO bridged across two metallic Pd atoms [Zhang et al., 2014,Martinez-Arias et al., 2004] respectively. The lower intensity peak corresponds to CO bridged across two partially oxidized Pd atoms (Pd^+-CO) [Saur et al., 1986,Zhang et al., 2014,Toshima et al., 2001]. After SO_2 exposure, the peaks at 1996 cm^{-1} and 1936 cm^{-1} disappeared while the peak at 2088 cm^{-1} shifted to 2102 cm^{-1} and was significantly reduced in intensity. After low-temperature desorbing sulfur species were removed via TPD to 300 °C, the sample was cooled to 35 °C and exposed to CO while spectra were collected.

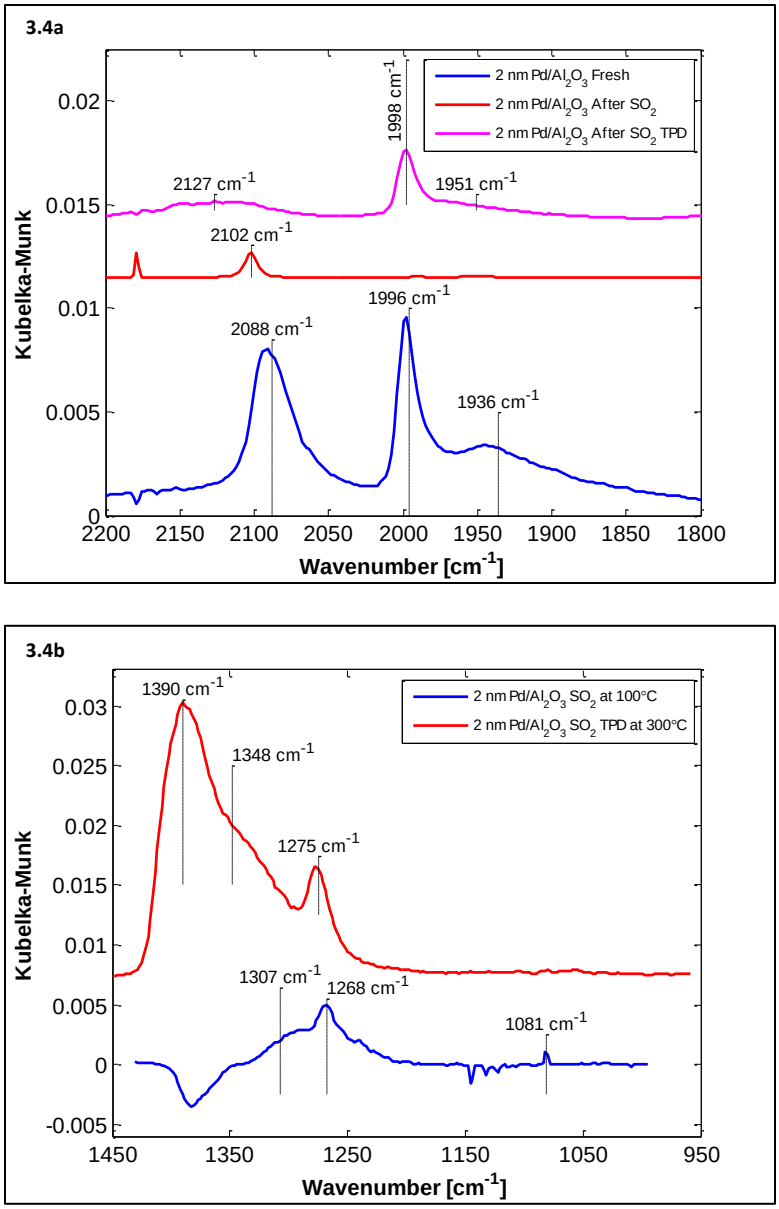

Figure 3.4: DRIFTS spectra obtained from a Pd/Al_2O_3 catalyst (a) after CO saturation at 35 °C before and after SO_2 exposure, as well as after the TPD to 300 °C; (b) after SO_2 saturation at 100 °C and TPD to 300 °C.

The peaks corresponding to CO adsorbed in a bridged manner across two metallic Pd atoms, 1998 cm^{-1}, and two partially oxidized Pd atoms, 1951 cm^{-1}, reappeared. The peak at 2102 cm^{-1} stretched resulting in a peak position at 2127 cm^{-1}, corresponding to CO linearly adsorbed on partially oxidized Pd (Pd^{2+}-CO). The changes in CO adsorption

spectra upon sulfur exposure and after sulfur desorption up to 300 °C provide evidence that the Pd sites were covered with sulfur species during adsorption but some were re-available after the TPD to 300 °C. Though still associated with CO linearly bound adsorption sites, the peak shift to 2127 cm^{-1} shows that some reduced Pd sites were partially reoxidized, probably via the alumina support, as the sample temperature was increased to 300 °C.

Prior to SO_2 exposure, CO adsorption spectra collected from 0.3 Pd-0.7 Pt contained peaks at 2090 cm^{-1} and 1988 cm^{-1} (Figure 3.5a). Not shown here for brevity, CO adsorption spectra collected from hydrothermally aged bimetallic samples with at least 30 mol% displayed peaks at 2090 cm^{-1} and ~1995 cm^{-1}, which correspond to CO linearly and bridged adsorption on metallic Pd sites. Due to the similarities in spectra, peaks from the 0.3 Pd-0.7 Pt sample were assigned to linear and bridged CO adsorption on metallic Pd respectively. In spite of the sample being bimetallic, no Pt features were observed, so we inferred that Pd atoms completely covered the Pt atoms [Waqif et al., 1991].

After SO_2 exposure, the peak at 1988 cm^{-1} disappeared while the peak at 2090 cm^{-1} shifted to 2098 cm^{-1} and was significantly reduced in intensity (Figure 3.5b). Following the TPD to 300 °C, CO adsorption spectra were obtained after CO saturation. The peaks corresponding to CO adsorbed linearly, 2095 cm^{-1}, and bridged, 1981 cm^{-1}, on metallic Pd were once again detectable. A new peak evolved at 1912 cm^{-1} corresponding to CO bridged across partially oxidized Pd (Pd_2^+-CO) atoms [Zhang et al., 2014, Bensalem et al., 1996]. This new peak provides evidence that some metallic Pd sites were again partially reoxidized during the temperature ramp to 300 °C. Due to the low peak

intensities observed in the final 0.3 Pd-0.7 Pt CO spectra, we inferred that the Pd sites were still partially covered with sulfur species even after increasing the sample temperature to 300 °C.

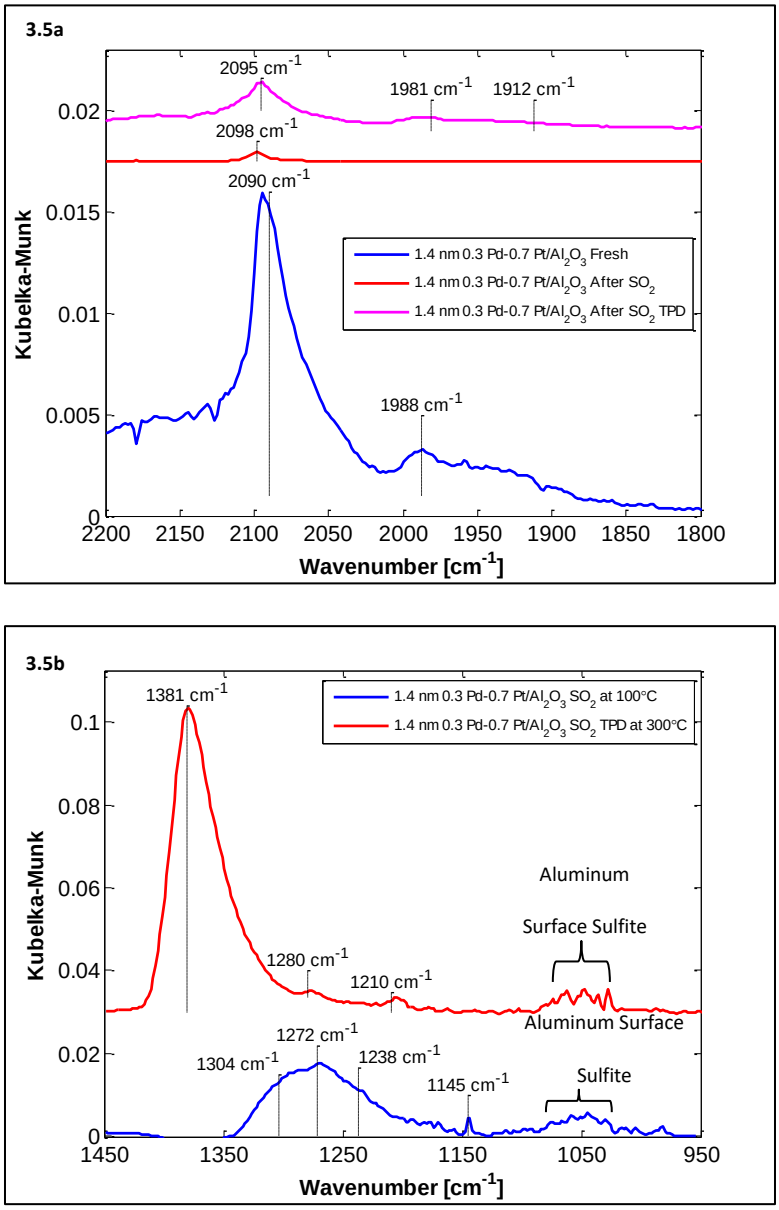

Figure 3.5: DRIFTS spectra obtained from a 0.3 Pd-0.7 Pt/Al_2O_3 catalyst (a) after CO saturation at 35 °C before and after SO_2 exposure, as well as after the TPD to 300 °C; (b) after SO_2 saturation at 100 °C and TPD to 300 °C.

Before being exposed to SO_2, the spectrum obtained after exposing the monometallic Pt sample to CO (Figure 3.6a) contained a peak at 2094 cm^{-1} and a broad band from 1908 to 1830 cm^{-1}.

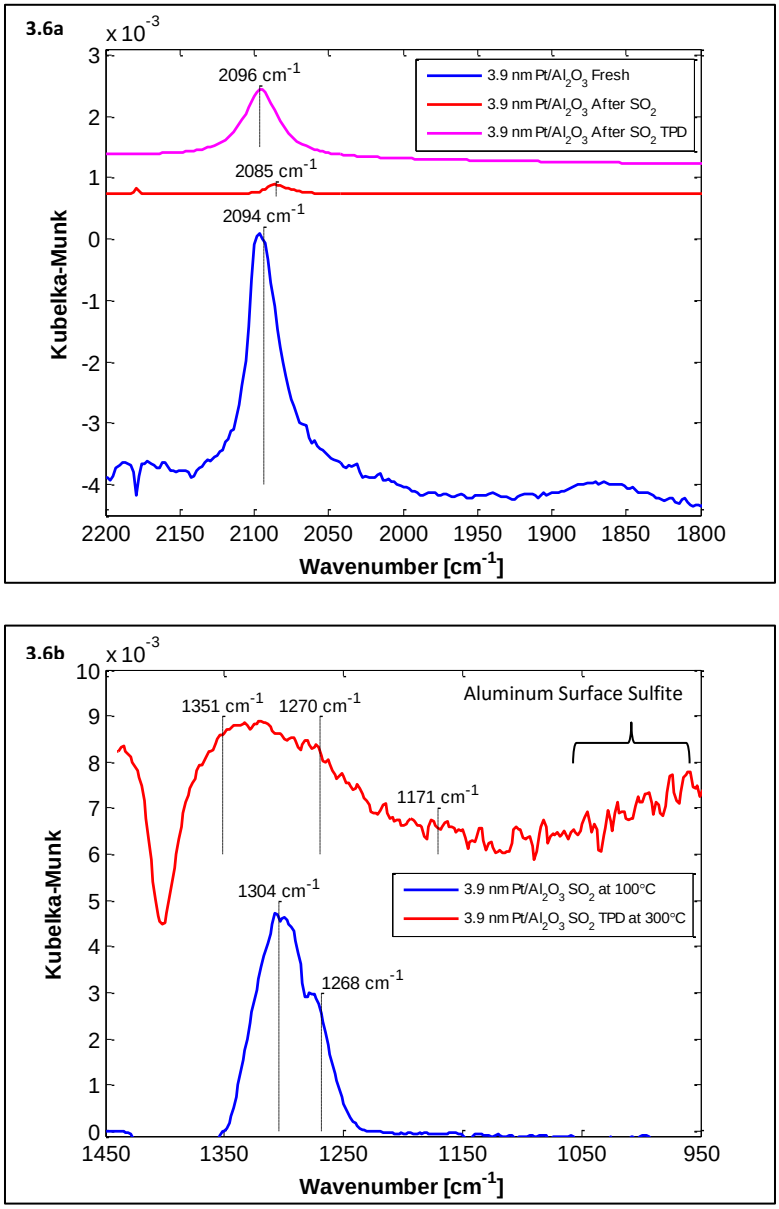

Figure 3.6: DRIFTS spectra obtained from a Pt/Al_2O_3 catalyst (a) after CO saturation at 35 °C before and after SO_2 exposure, as well as after the TPD to 300 °C; (b) after SO_2 saturation at 100 °C and TPD to 300 °C.

The bands at 2094 cm^{-1} and from 1908 to 1830 cm^{-1} were assigned to CO adsorbed on Pt sites in linearly [Saur et al., 1986,Rades et al., 1996] and bridged modes [Zhang et al., 2014,Bensalem et al., 1996,Martinez-Arias et al., 2004] respectively. Following SO_2 exposure, the CO adsorption spectrum for Pt no longer contained the broad band from 1908 to 1830 cm^{-1} (Figure 3.6b). The peak at 2094 cm^{-1} also shifted to 2085 cm^{-1} and was reduced in intensity. Although there was a slight peak shift, the peak at 2085 cm^{-1} we still assign to CO linearly adsorbed on Pt sites. Following TPD to 300 °C, CO adsorption spectra were obtained again after CO saturation. The peaks corresponding to CO linearly adsorbed on Pt sites, 2096 cm^{-1}, reappeared, but no peaks associated with bridged CO adsorbed across Pt sites were observed. The CO spectral changes upon SO_2 exposure and after the TPD to 300 °C provides evidence that the metallic Pt sites that typically adsorb CO in a linearly manner, were covered with SO_2 until removed at 300 °C. The Pt sites that typically adsorb CO in a bridged manner, were not detected in the CO adsorption spectra even after 300 °C exposure. We inferred that these sites still contained sulfur species which only decompose at temperatures greater than 300 °C.

3.3.3.2 SO_2 adsorption and desorption

During the CH_4 TPO with samples that had been exposed to SO_2, there were differences on a mole ratio basis in the amount of sulfur species released and the temperature span over which desorption occurred. To investigate these differences, representative DRIFTS spectra were collected from Pd, 0.3 Pd-0.7 Pt, and Pt catalysts (Figures 3.4b, 3.5b, and 3.6b) after SO_2 exposure at 100 °C and TPD up to 300 °C. When catalysts supported on alumina are exposed to SO_2 below 200 °C, aluminum surface

sulfite species [$Al_2(SO_3)_3$] form, then molecular SO_2 chemisorbs and physisorbs on the aluminum surface and hydroxyl groups respectively [Datta et al., 1985]. During 100 °C SO_2 exposure, the spectrum obtained from the Pd sample (Figure 3.5b) displayed peaks at 1307 cm^{-1}, 1266 cm^{-1}, and 1081 cm^{-1}. The peaks at 1307 cm^{-1} and 1266 cm^{-1} were assigned to physisorbed [Datta et al., 1985,Mitchell et al., 1996] and chemisorbed molecular SO_2 [Datta et al., 1985] respectively. The low intensity peak at 1081 cm^{-1} corresponds to alumina surface sulfite species [Chang, 1978,Yu and Shaw, 1998]. Upon increasing the monometallic Pd sample temperature to 300 °C, the band at 1081 cm^{-1} disappeared while the peaks at 1307 cm^{-1} and 1266 cm^{-1} shifted to 1348 cm^{-1} and 1275 cm^{-1}. The peaks at 1348 cm^{-1} and 1275 cm^{-1} were assigned to bulk aluminum sulfates [Mowery and McCormick, 2001,Bounechada et al., 2013]. The new peak, which evolved at 1390 cm^{-1}, was assigned to aluminum surface sulfate species [Chang, 1978,Piéplu et al., 2013,Nam and Gavalas, 1989]. The disappearance of aluminum surface sulfites coupled with aluminum sulfate formation demonstrates that the Pd sample was capable of oxidizing some molecular SO_2 and aluminum surface sulfite species to form aluminum sulfates, but no palladium sulfates [$PdSO_4$] were observed, during the temperature ramp up to 300 °C.

After SO_2 saturation at 100 °C, the spectra obtained from the 0.3 Pd-0.7 Pt sample (Figure 3.5b) contained peaks at 1304 cm^{-1}, 1272 cm^{-1}, 1238 cm^{-1}, 1145 cm^{-1}, and a broad band from 1080 to 1030 cm^{-1}. This broad band was assigned to aluminum surface sulfite species [Chang, 1978,Yu and Shaw, 1998]. The peak at 1238 cm^{-1} corresponds to $PdSO_4$ [Mowery and McCormick, 2001]. The peaks at 1304 cm^{-1} and 1145 cm^{-1} as well as 1272 cm^{-1} were assigned to physisorbed [Datta et al., 1985,Mitchell et al., 1996] and

chemisorbed molecular SO_2 [Datta et al., 1985] respectively. Upon increasing the 0.3 Pd-0.7 Pt sample temperature to 300 °C, the bands at 1304 cm^{-1} and 1145 cm^{-1} disappeared due to physisorbed molecular SO_2 desorption. The peak at 1272 cm^{-1} shifted to 1280 cm^{-1}, which was assigned to bulk aluminum sulfate [Bounechada et al., 2013]. The peak associated with $PdSO_4$ disappeared while a new peak evolved at 1210 cm^{-1}. Since the peak at 1210 cm^{-1} corresponds to aluminum surface sulfate species [Chang, 1978,Piéplu et al., 2013,Nam and Gavalas, 1989], we deduced that the sulfates on Pd, $PdSO_4$, spilled over to the alumina support during the temperature ramp. Another new peak corresponding to aluminum surface sulfates evolved at 1381 cm^{-1} while the broad band from 1080 cm^{-1} to 1030 cm^{-1} stayed intact. These data confirm that the 0.3 Pd-0.7 Pt sample was not capable of completely oxidizing or decomposing aluminum surface sulfite species during the temperature ramp up to 300 °C but did decompose $PdSO_4$ during the temperature ramp. Note, no $PdSO_4$ was observed when characterizing the monometallic Pd sample, suggesting that Pt influences its formation.

During Pt's exposure to SO_2, physisorbed, 1304 cm^{-1}, and chemisorbed, 1268 cm^{-1}, molecular SO_2 [Datta et al., 1985] formed. After increasing the sample temperature to 300 °C, aluminum surface sulfite species formed, resulting in a wide band from ~1100 cm^{-1} to ~950 cm^{-1} [Datta et al., 1985]. The peak at 1268 cm^{-1} shifted to 1270 cm^{-1}, while new peaks at 1351 cm^{-1} and 1171cm^{-1} appeared. The peaks at 1351 cm^{-1} and 1171 cm^{-1} were assigned to aluminum surface and bulk sulfates respectively [Mowery and McCormick, 2001]. The DRIFTS data show that Pt does not begin to oxidize sulfur species until the temperature was increased from 100 °C to 300 °C, and chemisorbed molecular SO_2 species, 1270 cm^{-1}, were still stable on Pt at 300 °C.

3.3.4 Sulfur regeneration methods

There were significant differences in the extent of sulfur inhibition on the CH_4 oxidation reaction as well as the sulfur release characteristics during the reactor TPO and DRIFTS TPD between the samples. In order to evaluate how the atmosphere (inert, oxidizing, and reducing) might induce sulfur species decomposition and therefore CH_4 oxidation recovery, TPD, TPO and TPR methods were compared.

3.3.4.1 TPO regeneration

Since SO_2 was released during the CH_4 TPO from SO_2-exposed samples (Figure 3.3), we suspected that some activity was recovered due to this sulfur removal. To assess the effectiveness of the TPO in removing sulfur species and recovering activity, a subsequent reference TPO was performed. No samples, besides the Pt whose activity was unaffected by sulfur exposure, recovered their original activity after TPO regeneration. After the sulfur was released, Pd recovered the most activity (Table 3.1) but originally lost the most activity in comparison to the other samples. The 0.9 Pd-0.1 Pt sample lost the least activity overall and recovered slightly less activity than Pd after TPO regeneration. The 0.3 Pd-0.7 Pt sample lost the most activity overall and recovered the least activity when compared to the Pd and 0.9 Pd-0.1 Pt samples. These results show that TPO regeneration was most effective for monometallic Pd. With Pt substitution, the TPO regeneration method became less effective in recovering lost activity.

Table 3.1: Change in T_{50} values due to TPO regeneration in flowing 2000 ppm CH_4 and 10 vol. % O_2 in N_2.

Pd Mole %	Pt Mole %	ΔT_{50} Between Fresh and TPO Regenerated Catalysts	ΔT_{50} Between SO_2 Treated and TPO Regenerated Catalysts
100	0	18.3	-16.4
90	10	14.5	-15.7
30	70	48.0	-9.7

As shown in Figure 3.4a, only aluminum sulfates were present on the monometallic Pd catalyst after increasing the sample temperature to 300 °C, whereas the 0.3 Pd-0.7 Pt and Pt sample still contained some aluminum surface sulfite species (Figures 3.5a and 3.6a). It is possible that these species, or their oxidation, competed with CH_4 oxidation above 300 °C. Therefore, for the 0.3 Pd-0.7 Pt sample, this competition resulted in sulfur inhibiting the CH_4 oxidation reaction over a larger temperature span. In the case of Pt, the CH_4 oxidation reaction does not begin until approximately 450 °C, so we postulate that the sulfite species have already been oxidized or decomposed by 450 °C such that there are no other reactions or species competing with CH_4 oxidation in this case. We speculate that the sulfites must be associated with the precious metal sites, and since alumina-based, are located at the precious metal/support interface [Burch et al., 1998]. With their oxidation to sulfates, and the ability of the sulfate to "spillover" or migrate along or into alumina, the activity can then be regained [Li et al., 2013].

Some SO_2 was released during the TPO, and some activity was recovered per subsequent TPO data review. However, sulfate species are stable up to temperatures

greater than that used for the reference TPO. Therefore, other regeneration methods, TPD and TPR, were assessed to determine whether more activity could be recovered with partial or complete sulfate decomposition.

3.3.4.2 TPD Regeneration

Since aluminum surface and bulk sulfates were still present on the catalysts after the low-temperature desorbing species were released (Figures 3.4b, 3.5b, and 3.6b), a TPD was performed to see if activity could improve upon decomposing species stable up to ~900 °C [Saur et al., 1986]. Since monometallics are known to sinter and it is understood that bimetallics have some sinter resistance, TPDs were only performed on the three bimetallic samples to minimize the potential for sintering effects impacting these results. After TPD, the SO_2 exposed 0.9 Pd-0.1 Pt recovered more activity in comparison to the other bimetallic samples (Table 3.2). The 0.7 Pd-0.3 Pt sample recovered some activity after TPD, as shown in Figure 3.7, whereas 0.3 Pd-0.7 Pt sample lost even more activity. In an effort to understand why the TPD had a worse effect on the 0.3 Pd-0.7 Pt sample than the SO_2 exposure, a separate sintering experiment was performed with fresh bimetallic samples, i.e., samples not exposed to SO_2.

Table 3.2: Change in T_{50} values after TPD regeneration in flowing N_2 to 900 °C.

Pd Mole %	Pt Mole %	ΔT_{50} Between Fresh and TPD Regenerated Catalysts	ΔT_{50} Between SO_2 Treated and TPD Regenerated Catalysts
90	10	11.1	-22.4
70	30	34.2	-7.8
30	70	112.1	54.4

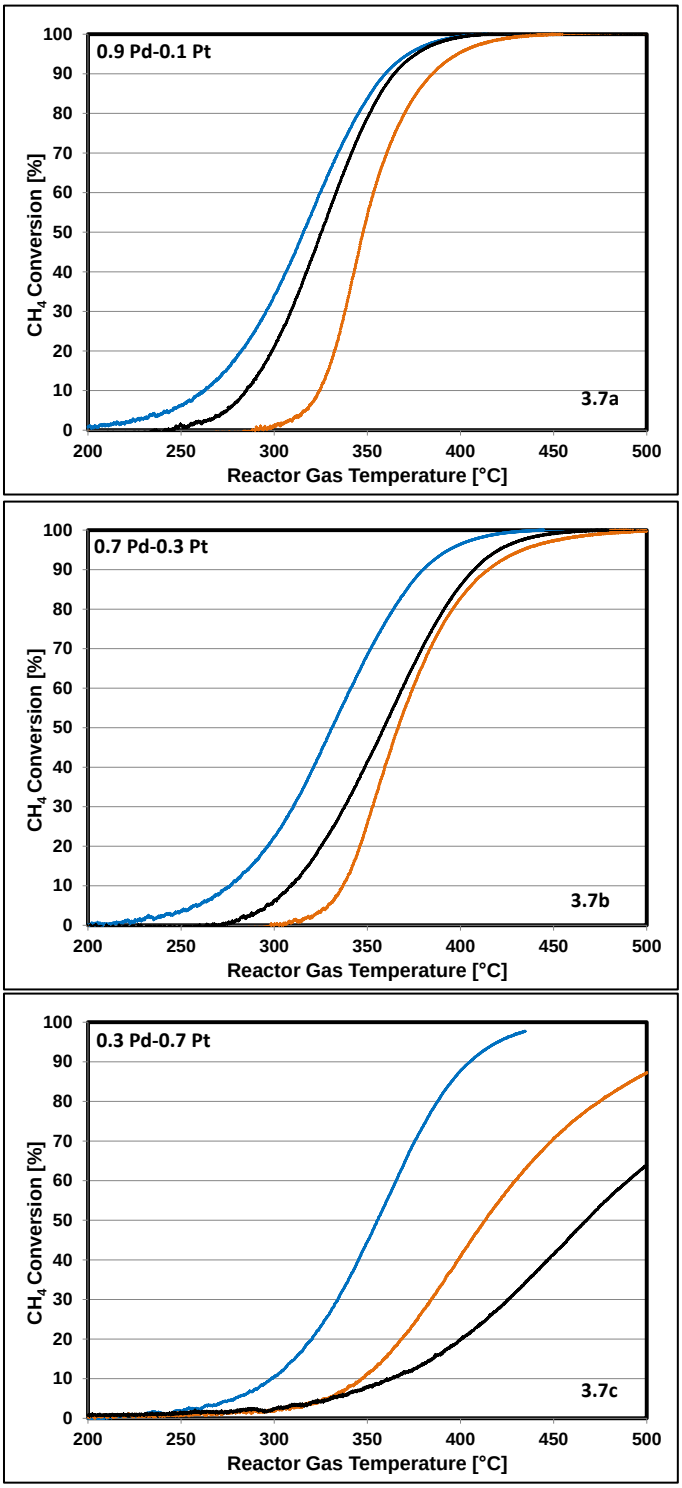

Figure 3.7: Assessment of sulfur TPD regeneration effectiveness, flowing 2000 ppm CH_4 and 10 vol. % O_2 in N_2, with a ramp rate of 5 °C/min. Catalyst color legend defined as blue (fresh), orange (SO_2-treated), and black (after TPD).

After 900 °C exposure, each sample underwent a reference TPO and CO chemisorption experiment. The 0.9 Pd-0.1 Pt sample slightly decayed due to the 900 °C exposure (Table 3.3). For the 0.3 Pd-0.7 Pt sample, the activity was greatly reduced after the 900 °C exposure, to a similar extent as that observed after the TPD after SO_2 exposure. In assessing the 900 °C exposure effects on particle size (Table 3.3), the 0.9 Pd-0.1 Pt and 0.7 Pd-0.3 Pt sample particle sizes approximately doubled whereas the 0.3 Pd-0.7 Pt sample more than quadrupled. Although all samples sintered due to the 900 °C exposure, the TPD regeneration helped improve activity of 0.9 Pd-0.1 Pt relative to the SO_2-exposed sample performance. As more Pt was substituted for Pd, less benefit from the TPD regeneration was observed. We concluded that as more Pt was substituted into the Pd catalyst, the more the sintering effects impacted the activity in comparison to the sulfur exposure.

Table 3.3: Change in T_{50} and particle sizes after exposure to 650 °C and 900 °C in flowing N_2.

Pd Mole %	Pt Mole %	ΔT_{50} After 650 °C Exposure	ΔT_{50} After 900 °C Exposure	Factor Increase in PM Particle Size After 900 °C Exposure
90	10	-7.0	0.8	2.2
70	30	22.4	29.3	1.9
30	70	105.6	153.2	4.4

3.3.4.3 TPR Regeneration

The CH_4 oxidation reaction was most inhibited over the SO_2-exposed 0.3 Pd-0.7 Pt sample, which lost even more activity after TPD regeneration due to the significant amount of sintering at 900 °C. Since research has shown that some aluminum sulfates can be reduced in H_2 at 600 °C [Waqif et al., 1991], we evaluated TPR to 600 °C as a regeneration method, with sintering impacts hopefully minimized. The CH_4 oxidation activity for the SO_2-exposed Pt was unaffected by the TPR (Figure 3.8).

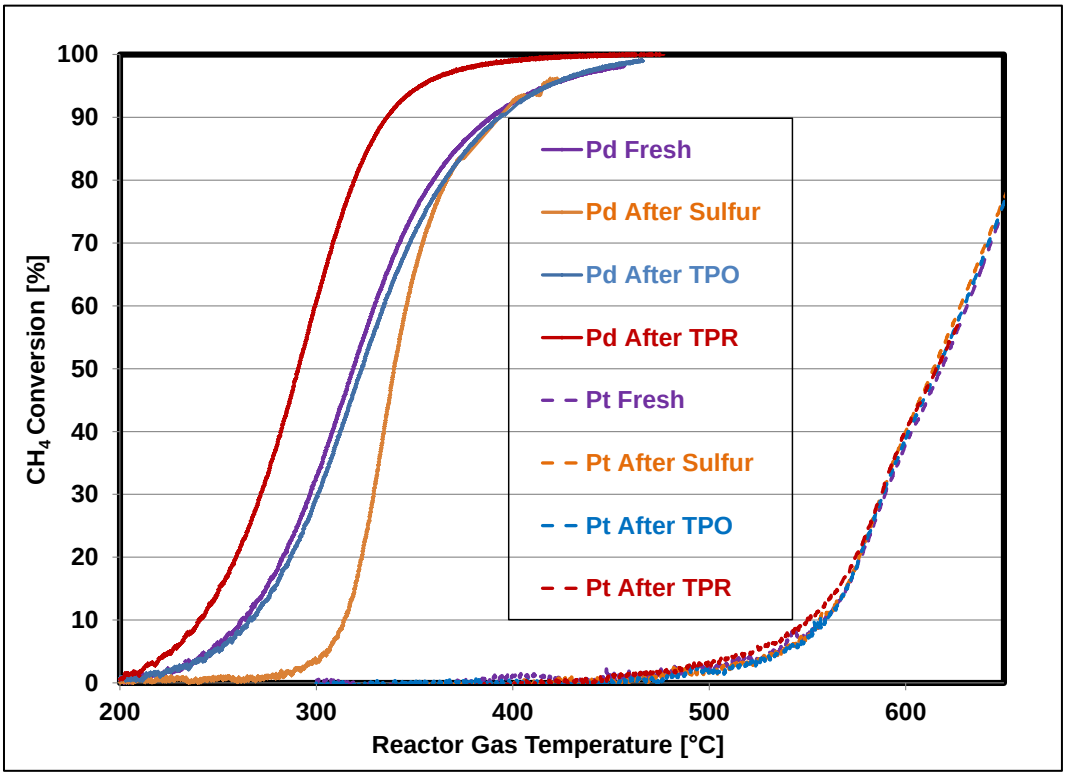

Figure 3.8: Comparison of fresh, SO_2-treated, and SO_2 regenerated monometallic catalysts, flowing 2000 ppm CH_4 and 10 vol. % O_2 in N_2, with a ramp rate of 5 °C/min.

The SO_2-exposed Pd and 0.9 Pd-0.1 Pt samples not only recovered the activity lost due to sulfur exposure, but also exceeded their fresh catalyst activity (Figure 3.9a).

Cullis and Willatt [Cullis and Willatt, 1983] found that Pd-based catalysts achieve maximum CH_4 oxidation activity when the catalyst is first reduced then allowed to adsorb O_2 to oxidize the Pd particles to some extent prior to undergoing the CH_4 oxidation reaction. Since the TPR method reduces the sulfates and Pd particles, we concluded that the reduction process 1) removes sulfur species thereby recovering catalytic activity and 2) when followed by a reoxidation process, forms a more highly active oxide on the Pd and 0.9 Pd-0.1 Pt catalysts. In contrast, the SO_2-exposed 0.3 Pd-0.7 Pt activity decayed further after TPR (Figure 3.9b). This decay was even greater than that observed after TPD regeneration.

Again to investigate the 0.3 Pd-0.7 Pt decay, fresh samples were exposed to 650 °C, a temperature similar to that used for the TPR protocol. A reference TPO was performed to determine whether any activity loss occurred due to the 650 °C exposure. As shown in Table 3.3, the 0.9 Pd-0.1 Pt activity improved slightly after the 650 °C exposure. However, as more Pt was substituted for Pd in the bimetallic catalysts, activity was lost. Recalling the sintering observed at 900 °C (Table 3.3), the PM particles in the 0.3 Pd-0.7 Pt sample grew twice as much as that of the other bimetallic particles upon 900 °C exposure. Müller et al. found that smaller Pd particles are more easily oxidized to form PdO in comparison to larger Pd particles [Müller et al., 1997], so sintering Pd particles coupled with a reduction process could make reoxidizing the large Pd particles more challenging.

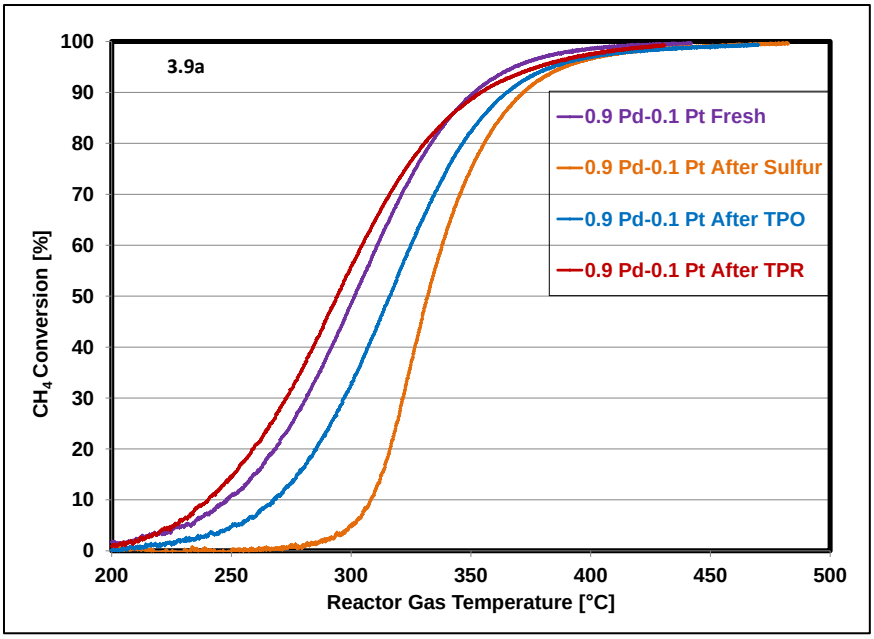

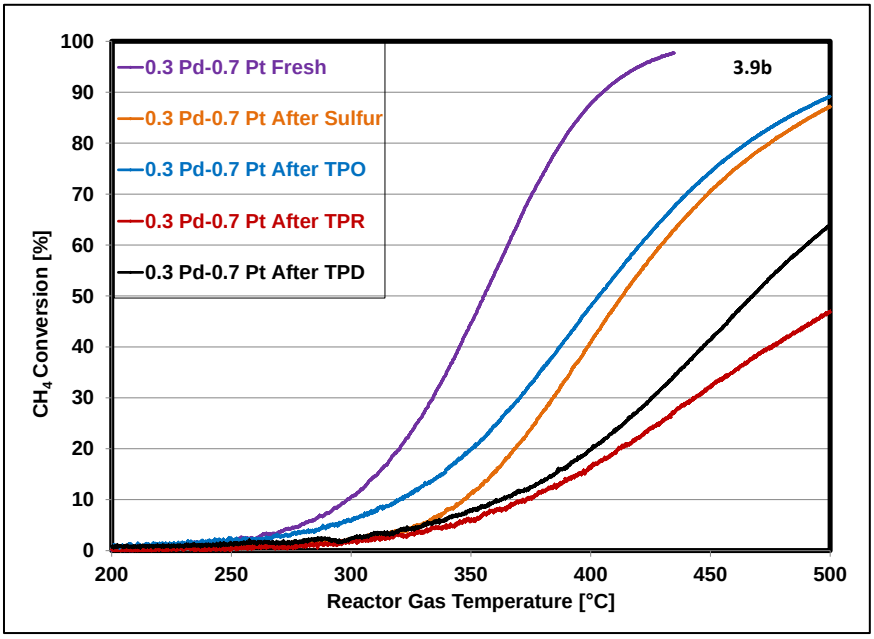

Figure 3.9: Comparison of fresh, SO_2-treated, and SO_2 regenerated catalysts, flowing 2000 ppm CH_4 and 10 vol. % O_2 in N_2, with a ramp rate of 5 °C/min.(a) 0.9 Pd-0.1 Pt/Al_2O_3 (b) 0.3 Pd-0.7 Pt/Al_2O_3.

3.3.5 Interpretation of regeneration results

During SO_2 exposure at 100 °C, sulfur species covered Pd sites (Figure 3.4a) resulting in less available sites to participate in the CH_4 oxidation reaction (Figure 3.2a

and 3.2b). Since Pd is effective at oxidizing these sulfur species to form sulfates below 300 °C (Figure 3.4b), CH_4 oxidation on SO_2-exposed Pd catalysts will be inhibited at low temperatures until sulfur species have been desorbed or oxidized to form sulfates that can spillover to the support, thereby freeing up the Pd. Any remaining inhibition is due to aluminum sulfates, which require high temperatures or reduction for decomposition (Figure 3.8). Since the precious metal site is the active site, the sulfates that are impacting performance are likely in close proximity to the precious metal sites, maybe at the interface between them and the alumina support [Wilson et al., 1999; Jones et al., 2003]. In contrast, the 0.3 Pd-0.7 Pt did not completely oxidize aluminum sulfite species (Figure 3.5b) below 300 °C to form aluminum sulfates. And we speculate that these sulfite species are at the alumina/metal interface and thus do influence/inhibit the oxidation reaction. Although $PdSO_4$, which formed at 100 °C, decomposed below 300 °C, the sulfite decomposition or oxidation was slow enough that inhibition still existed at/above 300 °C, until all sulfites are oxidized to form sulfates or decompose on 0.3 Pd-0.7 Pt. Similarly, no sulfites or sulfates are formed at 100 °C with monometallic Pt (Figure 3.6b) and complete aluminum sulfite oxidation at 300 °C was not observed (Figure 3.6b). In this case, it is unlikely that the sulfite oxidation reaction inhibits the CH_4 oxidation reaction because even fresh Pt did not begin to oxidize CH_4 until higher temperatures (Figure 3.1). As more Pt was added, less sulfite decomposition or oxidation occurred. We postulate that this delayed sulfite decomposition or sulfate formation also results in an increased temperature at which active sites can be regenerated via sulfur desorption, sulfate migration, or sulfate spillover.

As shown in Figure 3.1, initially Pt substitution for Pd (0.9 Pd-0.1 Pt) resulted in increased CH_4 oxidation activity. Additional Pt substitution for Pd resulted in incremental reductions in activity. Recalling that the 0.9 Pd-0.1 Pt sample slightly increased in activity after 650 °C exposure and experienced a slight decay with 900 °C exposure (Table 3.3), we confirmed that small Pt substitution provides some sintering resistance resulting ultimately in increased activity in comparison to monometallic Pd. With further Pt substitution, 0.7 Pd-0.3 Pt, activity losses due to 650 °C and 900 °C exposure were observed. Even further substitution, 0.3 Pd-0.7 Pt, resulted in an further increase in activity loss after the 650 °C exposure, and even more so after 900 °C exposure. Since the 0.3 Pd-0.7 Pt particles grew more in comparison to the other bimetallics (Table 3.3), further Pt substitution beyond 0.9 Pd-0.1 Pt provided less sintering resistance. Therefore, regeneration methods requiring high temperatures are less effective for bimetallic catalysts with less than 90% Pd because benefits associated with sulfur removal could be canceled out by losses associated with sintering.

Since all catalysts were previously exposed to the reference TPO conditions, no additional sintering occurred with the TPO regeneration method, and activity was regained to various degrees for all catalysts containing Pd. SO_2-exposed Pd recovered almost all activity via TPO regeneration and increased in activity via TPR regeneration. The 0.9 Pd-0.1 Pt sample also increased in activity after TPR but did not recover all activity via TPO regeneration. As more Pt was substituted for Pd, the TPO regeneration method became less effective. This is in good agreement with the DRIFTS data (Figures 3.5b and 3.6b) that showed catalysts with little to no Pd cannot completely decompose or oxidize sulfites to form sulfates below 300 °C. This again supports the idea that delayed

sulfite decomposition or sulfate formation means an increased temperature is required for active site regeneration.

The TPD regeneration method resulted in some activity recovery for all bimetallic catalysts except 0.3 Pd-0.7 Pt. Similarly, the TPR regeneration method was the most effective at improving activity for 0.9 Pd-0.1 Pt but negatively impacted the 0.3 Pd-0.7 Pt activity, more than the sulfur exposure. These results again show that substituting some Pt for Pd provides some sinter and sulfur resistance in comparison to monometallic Pd. These aspects also allow SO_2-exposed bimetallics, like 0.9 Pd-0.1 Pt and 0.7 Pd-0.3 Pt, to be regenerated via TPO or TPD while only having a slightly negative impact on activity. The data collected from the 0.3 Pd-0.7 Pt sample show that substituting too much Pt for Pd results in no benefits in terms of sinter or sulfur resistance. Under the conditions tested, for Pt, CH_4 oxidation activity was not impacted by SO_2 exposure or its regeneration methods.

3.4 Conclusions

In this study we examined the effect of SO_2 exposure on CH_4 oxidation reaction with respect to Pd:Pt mole ratio. At 100 °C, all samples physisorbed and chemisorbed molecular SO_2 but only catalysts containing Pd also formed aluminum surface sulfite species. As increasing Pt amounts were substituted for Pd, catalysts were not capable of fully oxidizing alumina surface sulfite species at 300 °C resulting in less sulfates formed at low temperatures. Failure to form sulfates at lower temperatures resulted in the CH_4 oxidation reaction being inhibited over a broader temperature span even after low-

temperature desorbing species, i.e., molecular SO_2 and some aluminum surface sulfite species, were removed. We believe this extended inhibition was due to sulfites being on or nearby active sites thereby influencing the CH_4 oxidation reaction. In contrast, catalysts with little to no Pt substitution were able to completely oxidize sulfites at 300 °C resulting in an abundance of surface and bulk aluminum sulfates. These sulfates have less impact, at the levels formed in this study, possibly due to their migration away from the active sites. In this case, the CH_4 oxidation reaction was inhibited over a narrower temperature span after low-temperature desorbing species were removed or oxidized.

These differences resulted in different relative extents of sulfur inhibition and sulfur regeneration method effectiveness. The catalysts with little to no Pt substitution recovered some activity via TPO regeneration but recovered the most via TPR regeneration due to sulfate removal and optimized activity associated with the reduction-reoxidation process. Although some Pt substitution for Pd provided some sinter and sulfur resistance, substituting too much Pt for Pd resulted in neither. As a result, the $Pd_{0.3}Pt_{0.7}/Al_2O_3$ catalyst experienced the greatest decay in activity due to SO_2 exposure and declined further after high-temperature sulfur regeneration methods such as TPD and TPR. Overall, when SO_2-exposed bimetallic catalysts contain a greater amount of Pt than Pd, TPD and TPR regeneration are not effective. For these bimetallic catalysts, the presence of sulfur was less detrimental to CH_4 oxidation activity than the sintering effects associated with TPD and TPR processes.

Chapter 4 Complete CH_4 Oxidation Kinetic Experiments and Reactor Modeling

4.1 Introduction

Lean-burn natural gas engines typically operate below 550 °C, making complete combustion of its primary component, CH_4, challenging. In addition to uncombusted CH_4, lean-burn natural gas engine exhaust typically contains large relative amounts of H_2O and O_2 as well as low relative amounts of SO_x and NO_x [Gélin and Primet, 2002]. Reviews [Trimm and Lee, 1995; Tahir and Koh, 1997] and many research studies have been conducted on noble metal catalysts to assess their activity in high oxygen [Abbasi et al., 2012; Lampert et al., 1997; Carlsson et al., 2004; Yao, 1980] and water environments [Yamamoto and Uchida, 1998; Kinnunen et al., 2012; Mouaddib et al., 1992].

In general, the complete CH_4 oxidation reaction rate was found to be first order with respect to CH_4 and no dependence on O_2 was observed [Abbasi et al., 2012; Lampert et al., 1997; Carlsson et al., 2004; Yao, 1980]. Yao found similar results for Pd wires but observed an O_2 dependency during CH_4 oxidation experiments with Pt wires [Zhu et al., 2005]. Some researchers concluded that this perceived O_2 dependency was actually O_2 poisoning which can occur under lean-burn CH_4 oxidation conditions [Cullis and Willatt, 1983; Levenspiel, 1998].

Since H_2O and CO_2 are natural-gas engine combustion products and exhaust components, their potential inhibition or enhancement effects on the CH_4 oxidation

reaction needed to be considered. Burch et al. determined that the CH_4 oxidation catalytic activity for Pd/Al_2O_3 catalysts decreased when H_2O or CO_2 was injected into the feed stream. Inhibition solely due to CO_2 was negligible when H_2O was present [Burch et al., 1995]. In regards to product water, the literature contains conflicting notes in regards to whether the product H_2O formed is a sufficient amount to inhibit the CH_4 oxidation reaction for Pd catalysts [Cullis and Willatt, 1984; Giezen et al., 1999]. Although no H_2O inhibition was found during CH_4 oxidation with Pt/Al_2O_3, Abbasi et al. found that it is inhibited by product H_2O over bimetallic Pd:Pt catalysts [Abbasi et al., 2012]. The focus of this work is to establish the baseline kinetics for bimetallic catalysts $Pd:Pt/Al_2O_3$ in complete CH_4 oxidation reactors. Optimization techniques were used to determine the kinetic parameters for the proposed CH_4 oxidation reaction rate equation. A corresponding reactor model, based on the reactor model established by Abbasi et al. [Abbasi et al., 2012], was constructed in MATLAB and utilized to assess how the kinetic parameters and reactor model predicted reactor performance.

4.2 Experimental Methods

4.2.1 Catalyst preparation and reactor experimental set-up

The precursors, $Pd(NO_3)$ and $Pt(NH_3)_4(NO_3)_2$, and Puralox γ-Al_2O_3, were procured from Sigma-Aldrich. Using the incipient wetness impregnation method, the following Pd-Pt/Al_2O_3 powder catalysts were prepared: $Pd_{1.0}Pt_{0.0}/Al_2O_3$, $Pd_{0.9}Pt_{0.1}/Al_2O_3$, $Pd_{0.7}Pt_{0.3}/Al_2O_3$, $Pd_{0.5}Pt_{0.5}/Al_2O_3$, $Pd_{0.3}Pt_{0.7}/Al_2O_3$, $Pd_{0.2}Pt_{0.8}/Al_2O_3$, $Pd_{0.15}Pt_{0.85}/Al_2O_3$, $Pd_{0.1}Pt_{0.9}/Al_2O_3$, $Pd_{0.05}Pt_{0.95}/Al_2O_3$, and $Pd_{0.0}Pt_{1.0}/Al_2O_3$. All catalysts contained the same total number of PM moles used to synthesize a 1 wt. % Pd/Al_2O_3 catalyst. After drying overnight, all samples were calcined in air at 550 °C.

4.2.2 Diffuse reflectance infrared Fourier transform spectroscopy (DRIFTS) characterization

After calcination, unaged catalysts were then transferred to the Harrick Scientific Praying Mantis DRIFTS cell. Background spectra were gathered in 50 ml/min of He only at 35 °C. The background spectra were subtracted from their corresponding spectra obtained at 35 °C during the following experiments.

Prior to CO adsorption experiments, each unaged catalyst underwent an oxidation treatment at 100 °C with 10 vol. % O_2 in He for 5 minutes. The catalyst was then reduced at 400 °C with 5 vol. % H_2 in He for 30 minutes. After reduction, the catalyst was maintained at the 400 °C for an additional 30 minutes while the cell was purged with He to minimize the residual H_2 content within the DRIFTS cell and system lines. The catalyst was then cooled to 35 °C and exposed to 1 vol. % CO and 10 vol. % N_2 in He until CO saturation, which was determined by a lack of change in the collected DRIFTS spectra. The CO adsorption spectrum for each unaged bimetallic sample was analyzed and compared to that of unaged monometallic samples in an effort to assign peaks as well as confirm the catalyst composition and types of PM sites available for participation in the CH_4 oxidation reaction.

4.2.3 Complete CH_4 oxidation experiments

For all reactor pretreatment and experimental conditions, 29.3 mg of active catalyst was used with a flow rate of 200 sccm, to achieve a space velocity of 50,000 hr^{-1}. The active catalyst mass was diluted with inert silica beads to prevent dense packing and hot spots within the catalyst bed. Each sample was installed in a 4 mm diameter quartz tube. Quartz wool was placed at both catalyst bed ends to secure the bed particles,

maintain the catalyst bed position in the quartz tube, and maintain a 20 mm catalyst bed length. Prior to experiments, each catalyst underwent an oxidation pretreatment with 10 vol. % O_2 in N_2 at 500 °C for 1 hour. Each catalyst sample was then pretreated with 2000 ppm CH_4 and 10 vol. % O_2 in N_2 until CH_4 conversion stabilized. For all CH_4 oxidation experiments, the level of conversion was calculated as

$$\%Conversion = 100 * \left[\frac{Initial\ \mathrm{CH_4}\ concentration - Final\ \mathrm{CH_4} concentration}{Initial\ \mathrm{CH_4}\ concentration}\right]. \quad (1)$$

The following catalysts were used for CH_4 oxidation kinetics characterization experiments: $Pd_{1.0}Pt_{0.0}/Al_2O_3$, $Pd_{0.9}Pt_{0.1}/Al_2O_3$, $Pd_{0.7}Pt_{0.3}/Al_2O_3$, $Pd_{0.5}Pt_{0.5}/Al_2O_3$, $Pd_{0.3}Pt_{0.7}/Al_2O_3$, $Pd_{0.1}Pt_{0.9}/Al_2O_3$, and $Pd_{0.0}Pt_{1.0}/Al_2O_3$. Complete CH_4 oxidation experiments were conducted utilizing a minimum of three of the four O_2 concentrations (5, 7, 10, and 12 vol. %) for each CH_4 concentration of interest. At least three of the following four CH_4 concentrations were used: 500, 1000, 1500, and 2000 ppm. Only a subset of these experiments was conducted on the monometallic catalysts to confirm the reported H_2O inhibition for Pd [Burch et al., 1995; Ribeiro et al., 1997] and O_2 inhibition for Pt [Trimm and Lam, 1980; Burch et al., 1996]. For each CH_4/O_2 concentration combination, the furnace temperature was increased at a ramp rate of 5 °C per minute until greater than 20% CH_4 conversion was achieved. In order to focus characterization efforts on the kinetic regime, only data collected up to 20% CH_4 conversion was utilized for kinetic parameter fitting. To simulate steady state conditions, a slow ramp rate of 5 °C per minute was used. The CH_4 concentration at the reactor outlet and the inlet gas temperature was measured throughout the experiment.

4.2.4 Complete CH_4 Oxidation Model Development

A reactor model was developed using a method similar to that of Abbasi et al. [Abbasi et al., 2012]. Per Levenspiel, a one dimensional, plug-flow reactor model can be used if a large number of catalyst particles exist in the catalyst bed. For our reactor, the number of particles [Levenspiel, 1998] was calculated as

$$Number\ of\ catalyst\ particles = \left(\frac{catalytic\ bed\ length}{catalyst\ particle\ diameter}\right). \quad (2)$$

Since the number of particles for our reactor was ~60, a one-dimensional, plug-flow reactor model was used. Levenspiel also found that bypass effects can be neglected if

$$\frac{reactor\ diameter}{catalyst\ particle\ diameter} > 10. \quad (3)$$

Since the ratio of the reactor diameter to the catalyst particle diameters is ~12, bypass effects were neglected. Axial dispersion effects can be neglected if the following Mear's criterion is met [Fogler, 2006],

$$\frac{-R'_{CH_4} Rn}{k_c C_{CH_4} \rho_b} < 0.15\ , \quad (4)$$

where R'_{CH_4} is the rate of CH_4 consumption on a catalyst mass basis, R is the catalyst particle radius, n is the reaction order, k_c is the mass transfer coefficient, C_{CH_4} is the CH_4

concentration, and ρ_b is the bulk catalyst density. Primarily due to the small catalyst particle size, the CH_4 oxidation experiments met the Mear's criterion, so axial dispersion effects were neglected. Since the temperatures for all experiments were well below the adiabatic flame temperature for CH_4, it was assumed that gas phase reactions could be neglected and the main reaction is the reaction at the catalyst surface. A ramp rate of 5 °C per minute was used during ignition experiments. Due to the slow ramp rate, it was assumed that these concentration and temperature measurements could be approximated as steady-state values.

While considering the assumptions above, a mole balance was performed, and the following equation resulted [Abbasi et al., 2012; Yamamoto and Uchida, 1998],

$$\text{Rate of } CH_4 \text{ consumption} = \left(-R_{CH_4}\right) = \frac{U_s C_{CH_{4_0}}}{\eta(1-\varepsilon_b)}\left(\frac{dX}{dz}\right), \tag{5}$$

where U_s is the gas flow velocity, X is the conversion of CH_4, $C_{CH_{4_0}}$ is the inlet CH_4 concentration, ε_b is the catalyst bed porosity, z is the catalyst bed length, and η is the effectiveness factor. In this case, η is defined as

$$\eta = \frac{18*\left(\sqrt{\frac{D_{eff}}{k}}\right)\coth\left(\frac{D_p}{6}\sqrt{\frac{k}{D_{eff}}}\right)}{D_p} - \frac{108*D_{eff}}{k\left({D_p}^2\right)}, \tag{6}$$

where D_{eff} is the effective diffusion coefficient, D_p is the catalysts particle diameter, and k is the CH_4 oxidation reaction rate constant which is defined by the Arrhenius equation

$$k = A * exp^{-(\frac{E_a}{RT_{gas}})} \quad , \tag{7}$$

where the kinetic rate constant parameters, E_a and A, are the activation energy and frequency factor respectively.

Using the equation for $-R_{CH_4}$ to be defined later herein, the above equations were solved iteratively in MATLAB to determine the reaction rate constant for each bimetallic catalyst bed during complete CH_4 oxidation experiments. First an initial guess, based on values for the kinetic rate constant parameters reported in the literature, was entered into the MATLAB code where equations 7 then 6 were solved. The ODE45 solver in MATLAB was utilized to solve equation 5 and calculate the CH_4 conversion based on a given set of experimental conditions. Next, the difference between the calculated conversion and experimental conversion was determined. The fmincon function in MATLAB was used iteratively complete this set of calculations in an effort to minimize the sum of the least squares of the differences between these two values. The estimated parameters, which resulted in the minimal difference between experimental and calculated conversion values, were used as input parameters to the reactor model. The conversion predicted by the model was calculated using the following equation,

$$Calculated\ CH_4\ Conversion = X_{calc} = \int \frac{U_s C_{CH_4{}_0}}{\eta(1-\varepsilon_b)} \left\{1 - \left[exp\left(\frac{-k\eta(1-\varepsilon_b)z}{U_s}\right)\right]\right\}, \tag{8}$$

which was derived from the mole balance for CH_4 consumption. MATLAB and Microsoft Excel were used for all calculations.

4.3 Experimental results and discussion

4.3.1 CO Experimental results

To assist in determining unaged bimetallic catalyst features, unaged monometallic catalysts were characterized using DRIFTS during CO adsorption (Figure 4.1).

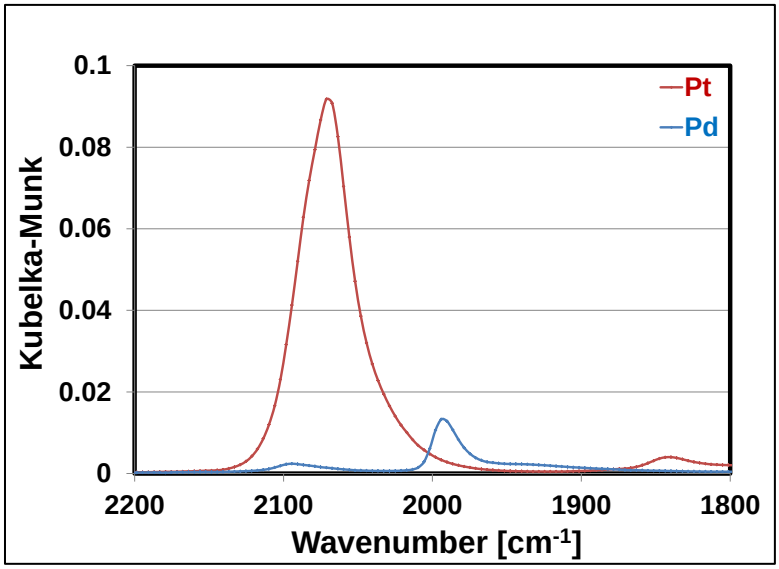

Figure 4.1: DRIFTS spectra obtained after a saturation CO exposure at 35 °C for monometallic Pd and Pt catalysts.

The unaged monometallic Pd sample spectrum (Figure 4.1) displayed peaks at 2091 cm^{-1} and 1991 cm^{-1}. During CO adsorption, linear or bridged carbonyl complexes can form on reduced Pd (Pd^0-CO). The 2091 cm^{-1} band was designated as CO linearly adsorbed on metallic Pd [Zhang et al., 2014; Bensalem et al., 1996; Martinez-Arias et al., 2004], and the 1991 cm^{-1} band as CO bridged across two metallic Pd atoms [Zhang et al., 2014; Martinez-Arias et al., 2004]. The unaged monometallic Pt sample spectrum (Figure 4.1) displayed peaks at 2071 cm^{-1} and 1839 cm^{-1}. The peak at 2071cm^{-1} was assigned to CO linearly adsorbed on Pt sites [Todoroki et al., 2009; Boubnov et al.,

2013]. The peak at 1839 cm^{-1} corresponded to CO adsorbed on metallic Pt in a bridged manner [Todoroki et al., 2009; Toshima et al., 2001; Rades et al., 1996]. These assignments formed the basis for peak assignments of the unaged bimetallic catalysts.

Due to potentials for overlap of Pd and Pt features in 2070 to 2090 cm^{-1} band, a coarse analysis was performed on the unaged bimetallic CO spectra (Figure 4.2a, 4.2b, and 4.2c).

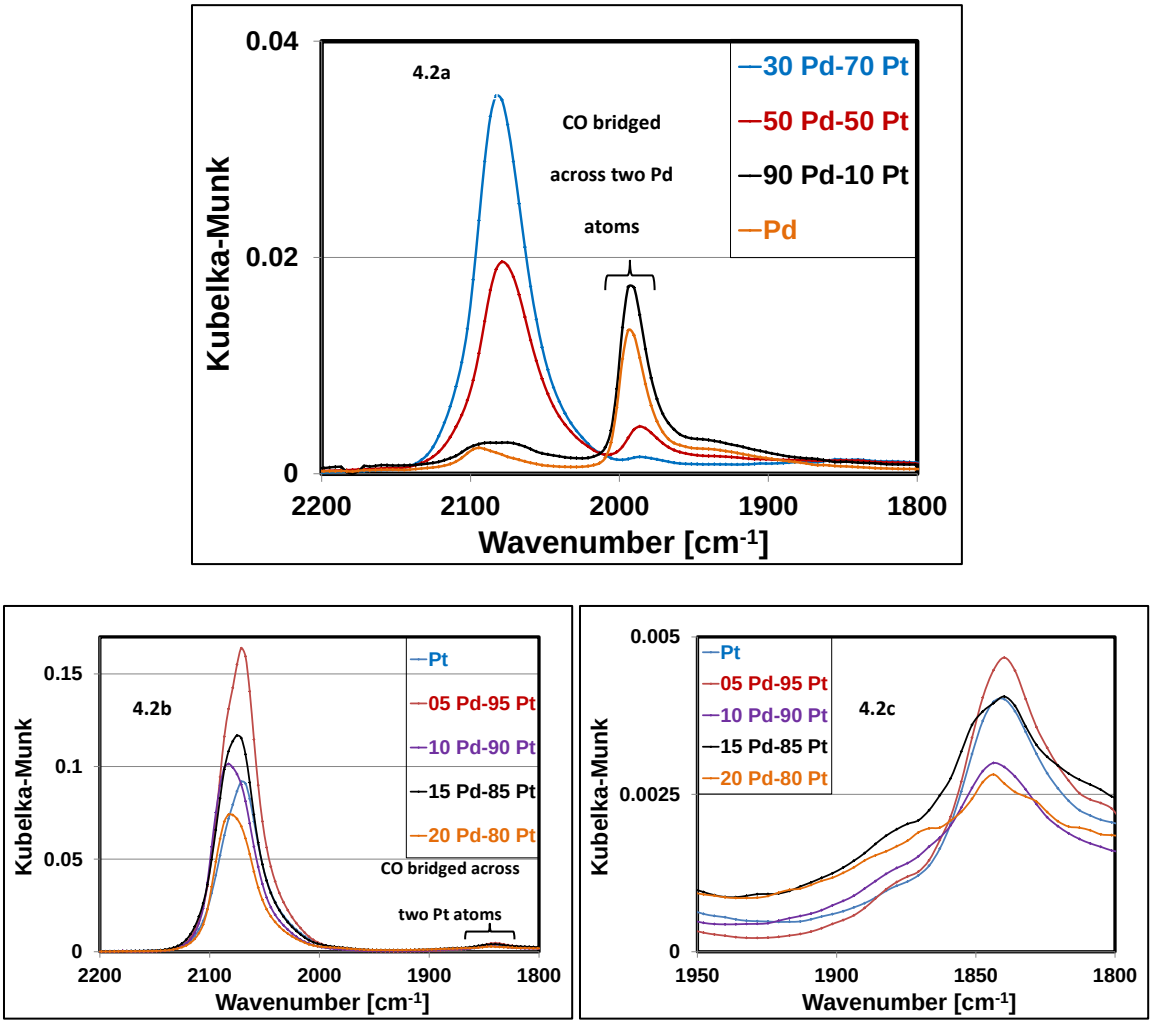

Figure 4.2: CO spectra obtained from unaged samples at 35 °C saturation

This coarse analysis focused on bands for which there were clear and definitive Pd regions or Pt regions which could be used for analysis i.e., CO bridged adsorption sites. The primary objective of this approach was to determine if the CO DRIFTS spectra for unaged bimetallic catalysts contained obvious contributions from both Pd and Pt or primarily portrayed features from one PM.

All spectra collected from unaged bimetallic samples with at least 30% Pd PM moles contained a peak at ~1985 cm^{-1} (Table 4.1 and Figure 4.2a), which was assigned to CO bridged across two metallic Pd atoms [Zhang et al., 2014; Martinez-Arias et al., 2004]. Spectra collected from unaged bimetallic samples with less than or equal to 20% Pd moles contained a peak at ~1935 cm^{-1} (Table 4.1 and Figure 4.2b), which was assigned to CO adsorbed on metallic Pt in a bridged manner [Todoroki et al., 2009; Toshima et al., 2001; Rades et al., 1996]. Although precise interpretations of the catalyst compositions were not possible, the CO saturation results do indicate that (1) bimetallics with at least 30 mol% Pd contain no exposed Pt sites, which typically adsorb CO in a bridged manner and (2) all Pt atoms were not fully covered by Pd for catalysts with up to 20 mol% Pd. Based on these results, we suspected that the bimetallics with at least 30% of the PM moles being Pd would primarily have Pd sites participating in adsorption processes. Due to surface Pt being detected in catalysts with less than or equal to 20% Pd moles, it was suspected that some contributions from Pt may be observed in the flowing experiments with these catalysts.

Table 4.1: DRIFTS spectra obtained after a saturation CO exposure at 35 °C

Pd %	Pt %	Peak 1 [cm^{-1}]	Peak 2 [cm^{-1}]
100	0	2091	1991
90	10	2083	1991
70	30	2075	1987
50	50	2077	1985
30	70	2080	1985
20	80	2077	1844
15	85	2075	1842
10	90	2078	1843
5	95	2072	1835
0	100	2071	1839

4.3.2 Complete CH_4 Oxidation

The ignition profiles obtained during kinetics experiments are compared in Figures 4.3-4.10. Using the temperatures at which 20% CH_4 conversion occurred, T_{20}, as a metric, the catalytic activities were compared for kinetics characterization. When the CH_4 concentration was varied for a set O_2 concentration, the ignition curves were similar for monometallic Pt but varied for Pd (Figures 4.3 and 4.10). For Pt, T_{20} was similar for all Pt ignition curves regardless of CH_4 concentration for a given O_2 concentration (Figure 4.3a), but as the CH_4 concentration increased T_{20} also increased for Pd (Figure 4.4a).

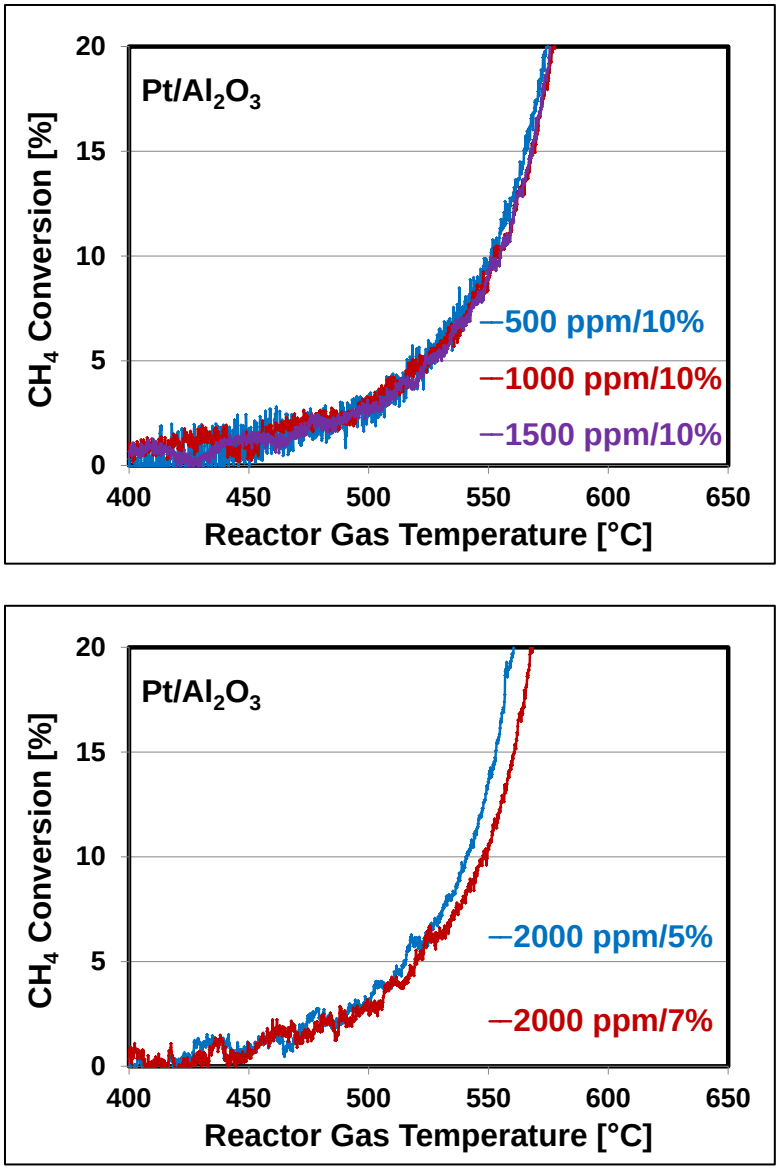

Figure 4.3: TPO in flowing (a) CH_4 and 10 vol. % O_2 in N_2 (b) 2000 ppm CH_4 and O_2 in N_2 with a ramp rate of 5 °C/min for Pt.

In contrast, when the O_2 concentration was varied for a set CH_4 concentration, as the O_2 concentration increased T_{20} also increased for Pt (Figure 4.3b), but T_{20} was similar for all Pd ignition curves regardless of O_2 concentration for a given CH_4 concentration (Figure 4.4b). From these experimental observations, we concluded that CH_4 oxidation reaction rate is not dependent on the O_2 concentration, in the range of 5 vol. % to 12 vol. %, for

Pd. For Pt, we concluded that CH_4 oxidation reaction rate is not dependent on CH_4 oxidation product H_2O, when obtained during complete combustion of 500 ppm to 2000 ppm CH_4. Similar to that suggested in the literature [Burch et al., 1995; Ribeiro et al., 1997; Burch et al., 1996; Trimm and Lee, 1980], we suspected that Pd and Pt exhibited a H_2O and O_2 inhibition respectively.

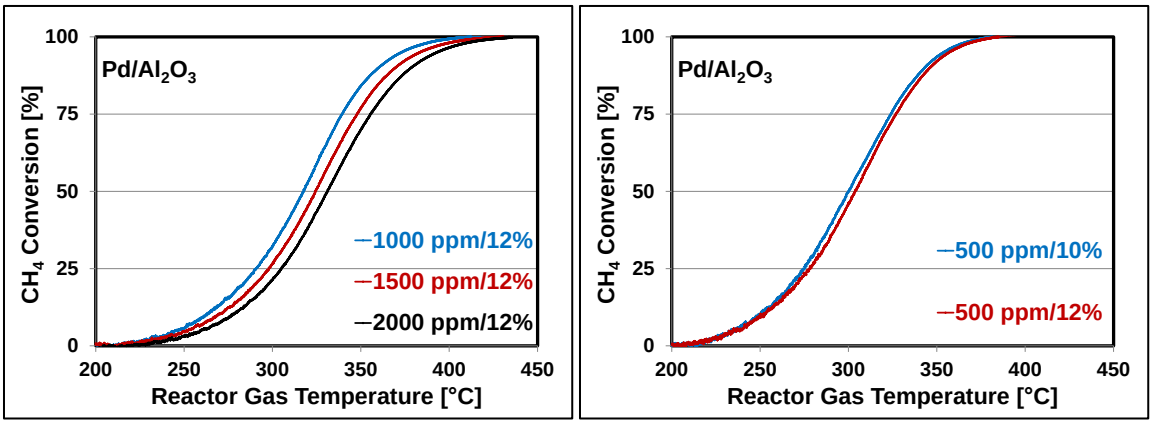

Figure 4.4: TPO in flowing (a) CH_4 and 12 vol. % O_2 in N_2 (b) 500 ppm CH_4 and O_2 in N_2 with a ramp rate of 5 °C/min for Pd.

To investigate how Pd and Pt oxidation characteristics influence bimetallics, complete CH_4 oxidation experiments were performed with $Pd_{0.9}Pt_{0.1}/Al_2O_3$, $Pd_{0.7}Pt_{0.3}/Al_2O_3$, $Pd_{0.5}Pt_{0.5}/Al_2O_3$, $Pd_{0.3}Pt_{0.7}/Al_2O_3$, and $Pd_{0.1}Pt_{0.9}/Al_2O_3$ catalysts. Using the temperature at which 20% CH_4 conversion occurred, T_{20}, as a metric, the catalytic activities were compared in the kinetic regime. When 10 % Pt moles was substituted for Pd, 0.9 Pd-0.1 Pt, a reduction in T_{20} occurred (Figure 4.5). Similar to monometallic Pd, when the CH_4 concentration was varied for a set O_2 concentration, as the CH_4 concentration increased T_{20} also increased for 0.9 Pd-0.1 Pt (Figure 4.6a), but T_{20} remained constant for all 0.9 Pd-0.1 Pt ignition curves regardless of O_2 concentration for

a given CH_4 concentration (Figure 4.6b). When further Pt substitutions were made, T_{20} increased with each subsequent Pt substitution (Figure 4.5).

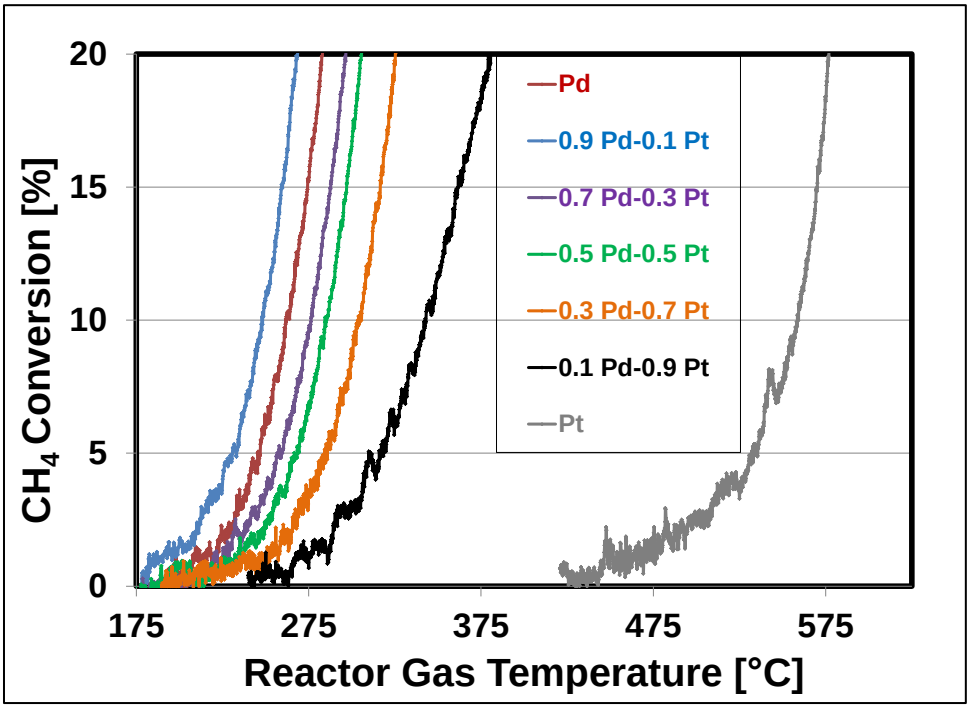

Figure 4.5: TPO in flowing 2000 ppm CH_4 and 10 vol. % O_2 in N_2, with a 5 °C/min ramp rate.

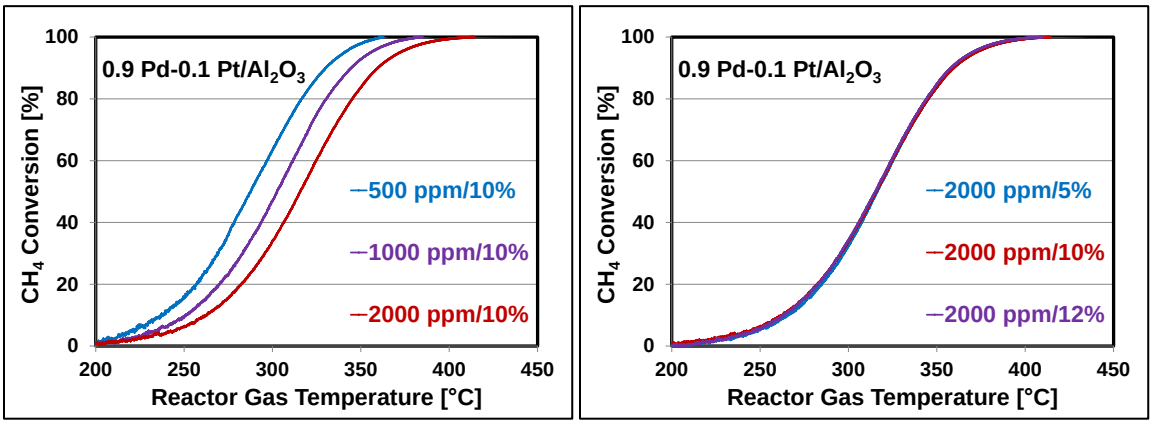

Figure 4.6: TPO in flowing (a) CH_4 and 10 vol. % O_2 in N_2 (b) 2000 ppm CH_4 and O_2 in N_2 with a ramp rate of 5 °C/min for 0.9 Pd-0.1 Pt.

The 0.7 Pd-0.3 Pt and 0.5 Pd-0.5 Pt ignition curves displayed trends (Figures 4.7 and 4.8) similar to that of 0.9 Pd-0.1 Pt. However, as more Pt moles were substituted for Pd moles, a divergence from this theme was observed. A greater increase in T_{20} was observed when reducing the catalyst composition from 30% to 10% Pd moles (Figure 3.5).

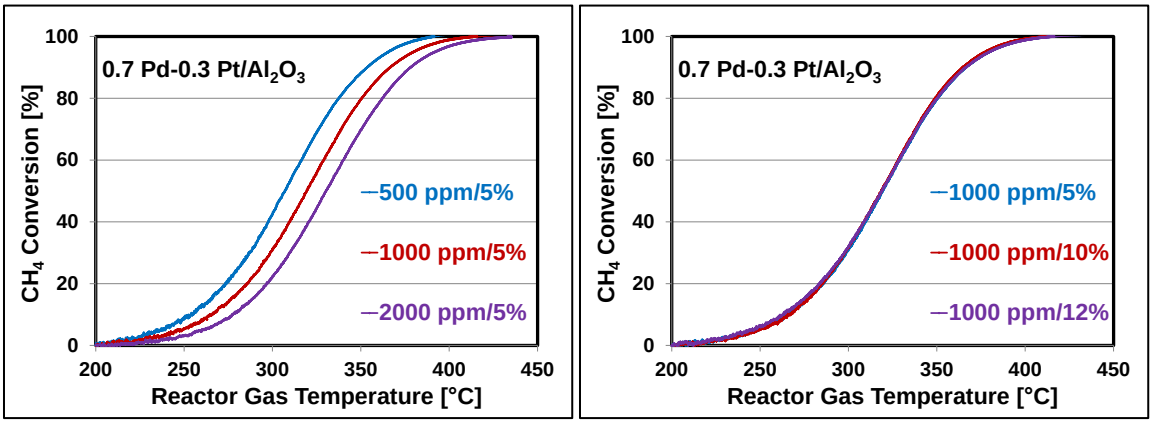

Figure 4.7: TPO with 0.7 Pd-0.3 Pt in flowing (a) CH_4 and 5 vol. % O_2 in N_2 (b) 1000 ppm CH_4 and O_2 in N_2 with a ramp rate of 5 °C/min.

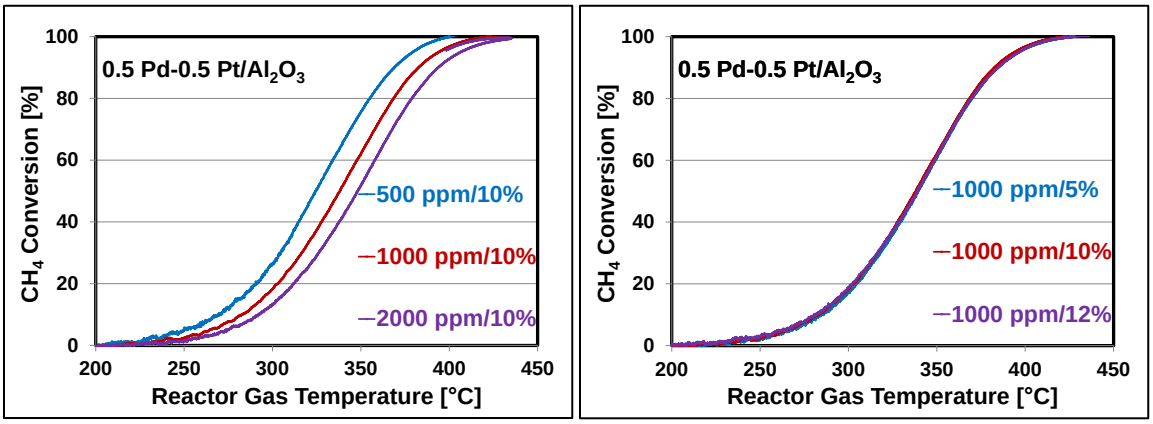

Figure 4.8: TPO in flowing (a) CH_4 and 10 vol. % O_2 in N_2 (b) 1000 ppm CH_4 and O_2 in N_2 with a ramp rate of 5 °C/min for 0.5 Pd-0.5 Pt.

Although no O_2 dependency was observed for this O_2 range, less increase in T_{20} was observed for each increase in CH_4 for a give O_2 concentration (Figures 4.9 and 4.10).

Recalling that Pt (Figure 4.3) ignition curves displayed no dependency on product H_2O and fresh bimetallic samples with 20% or less Pd moles contained exposed Pt surface (Figure 4.2b), we suspected that the reduced H_2O inhibition for the 0.3 Pd-0.7 Pt and 0.1 Pd-0.9 Pt samples was influenced by the increased Pt content and possibly exposed Pt surfaces respectively.

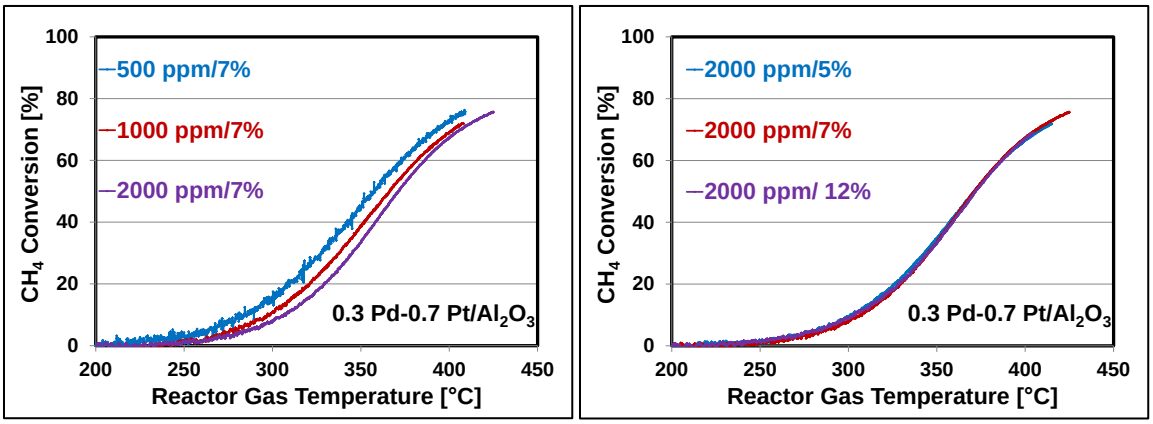

Figure 4.9: TPO in flowing (a) CH_4 and 7 vol. % O_2 in N_2 (b) 2000 ppm CH_4 and O_2 in N_2 with a ramp rate of 5 °C/min for 0.3 Pd-0.7 Pt.

Even when the Pd content was reduced to 10% Pd moles, 0.1 Pd-0.9 Pt, the bimetallic catalysts produced ignition curves more similar to those of Pd than Pt (Figure 4.10).

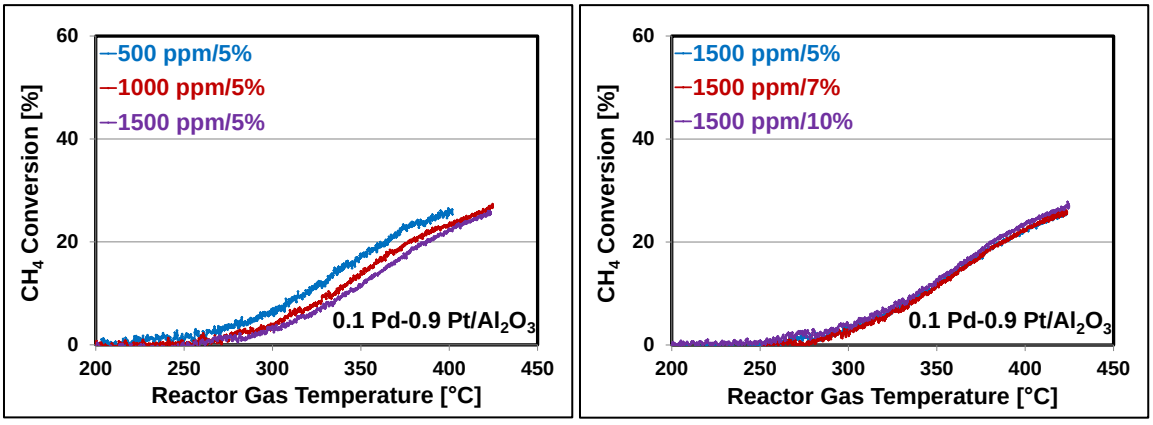

Figure 4.10: TPO in flowing (a) CH_4 and 10 vol. % O_2 in N_2 (b) 1000 ppm CH_4 and O_2 in N_2 with a ramp rate of 5 °C/min for 0.1 Pd-0.9 Pt.

As can be observed in Figures 4.3-4.10, catalyst samples with any Pd content displayed no O_2 dependency on the reaction rate but showed some inhibition to the combustion product, H_2O. In contrast, the pure Pt catalyst displayed an O_2 dependency but no product H_2O inhibition was observed. Based on those observations, the following reaction rate equations were proposed for catalysts containing any Pd (monometallic and bimetallic),

$$\text{Rate of } CH_4 \text{ consumption for catalysts with any Pd} = \left(-\boldsymbol{R_{CH_4}}\right) = \frac{\boldsymbol{kC_{CH_4}}}{\boldsymbol{1+K_{H_2O}C_{H_2O}}} \text{ and Pt, (9)}$$

$$\text{Rate of } CH_4 \text{ consumption for pure Pt catalysts} = \left(-\boldsymbol{R_{CH_4}}\right) = \frac{\boldsymbol{kC_{CH_4}}}{\boldsymbol{1+K_{O_2}C_{O_2}}}. \quad (10)$$

4.3.3 Model Validation

The data obtained from the CH_4 oxidation kinetics experiments was used in order to determine the kinetic rate parameters. The kinetic rate parameters, for $Pd_{1.0}Pt_{0.0}/Al_2O_3$, $Pd_{0.9}Pt_{0.1}/Al_2O_3$, $Pd_{0.7}Pt_{0.3}/Al_2O_3$, and $Pd_{0.5}Pt_{0.5}/Al_2O_3$, are listed in Table 4.3. The determined activation energy values were similar to that found in the literature [Abbasi et al., 2012; Trimm and Lee, 1995; Gélin and Primet, 2002]. The determined parameters were used to predict the conversion achieved at various gas temperatures and inlet concentrations. A comparison of the conversion predicted by the pure Pd model and that obtained from experiments with 1500 ppm CH_4 and 10 % vol. O_2 in N_2 can be viewed in Figure 4.11.

Since a good fit was achieved for the Pd reactor model, the model was adjusted in order to fit parameters from the bimetallic catalyst data sets. In all cases, the data used for fitting the kinetic parameters was collected under conditions where less than 20% CH_4 conversion was observed. Data collected from 1500 ppm CH_4 experiments was omitted

from this group in order to ensure that the goodness of fit between the model and data could be properly assessed with minimal bias. The resultant fit for each bimetallic at 1500 ppm CH_4 and 10 vol. % O_2 in N_2 can be viewed in Figures 4.12, 4.14, and 4.16.

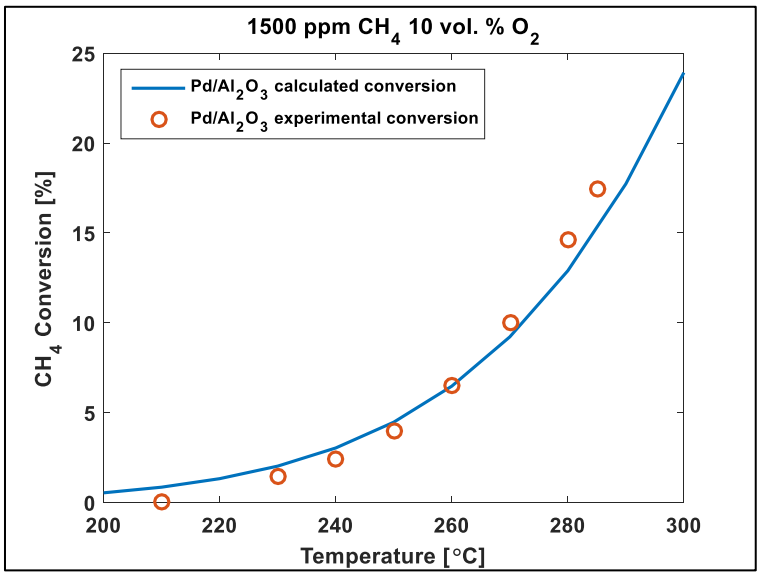

Figure 4.11: Model fit against experimental results obtained during TPO in flowing 1500 ppm CH_4 and 10 vol. % O_2 in N_2 with a ramp rate of 5 °C/min for monometallic Pd.

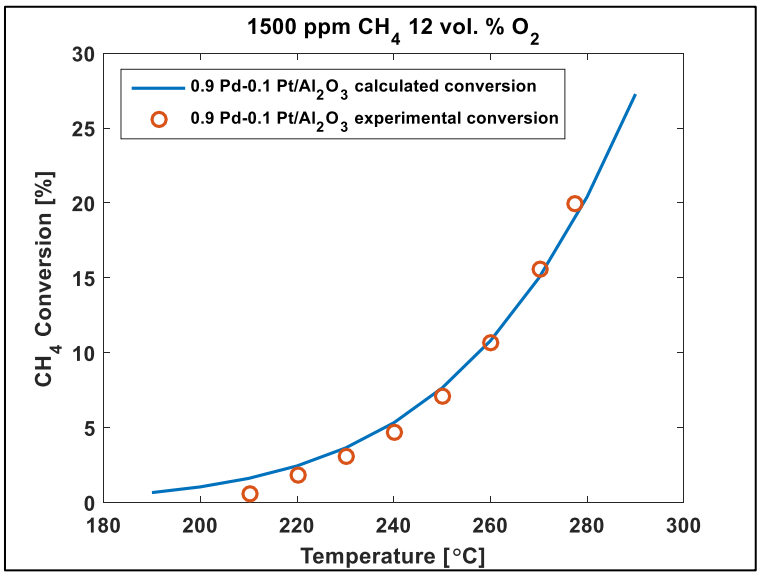

Figure 4.12: Model fit against experimental results obtained during TPO in flowing 1500 ppm CH_4 and 10 vol. % O_2 in N_2 with a ramp rate of 5 °C/min for 0.9 Pd-0.1 Pt.

Similarly, the fit was assessed with the data collected during oxidation of 1500 ppm CH_4 with 5 vol. % O_2 and 12 vol. % O_2 in N_2 to confirm that no O_2 dependency existed. As shown in Figures 4.13, 4.15, and 4.17, a good fit was still achieved at various O_2 concentrations with the 5 vol. % to 12 vol. % O_2 range.

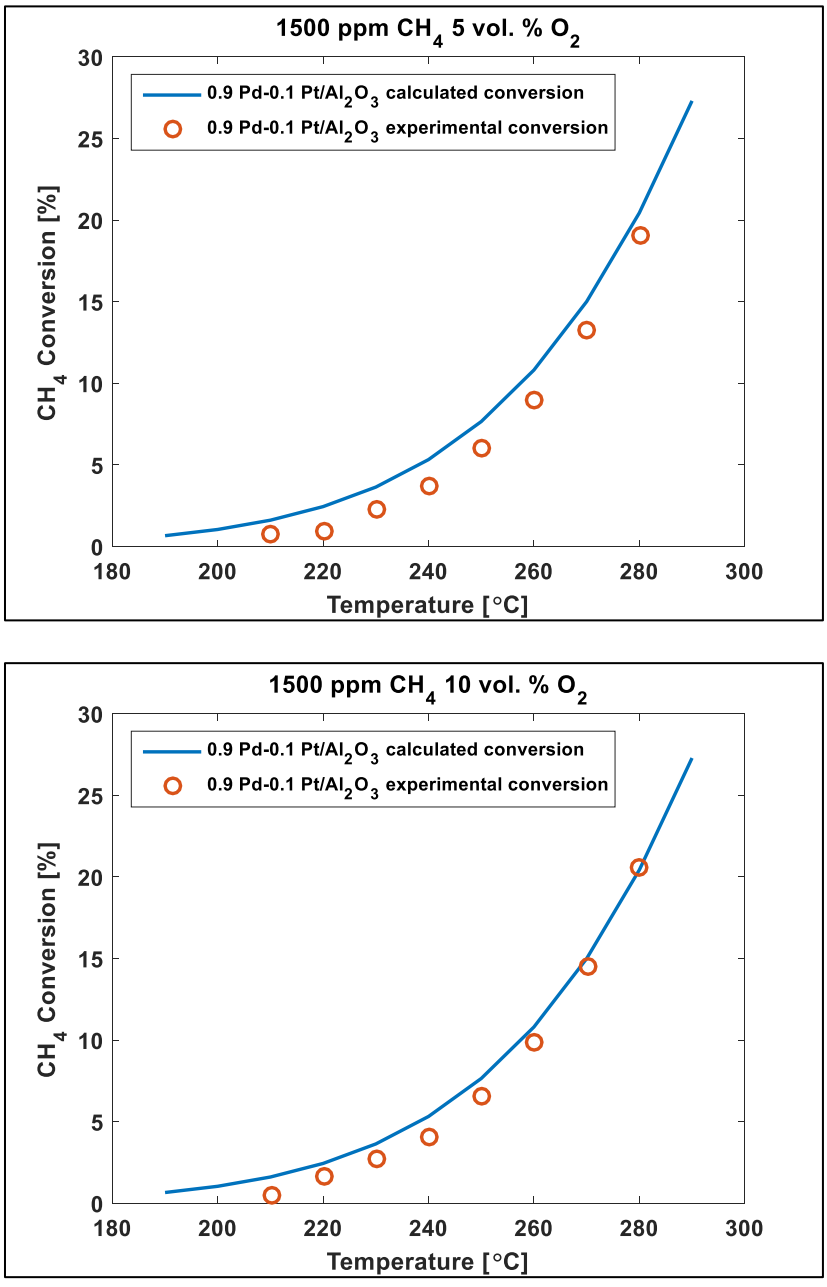

Figure 4.13: Model fit against experimental results obtained during TPO in flowing 1500 ppm CH4 and (a) 5 vol. % O2 (b) 12 vol. % O2 in N2 with a ramp rate of 5 °C/min for 0.9 Pd-0.1 Pt.

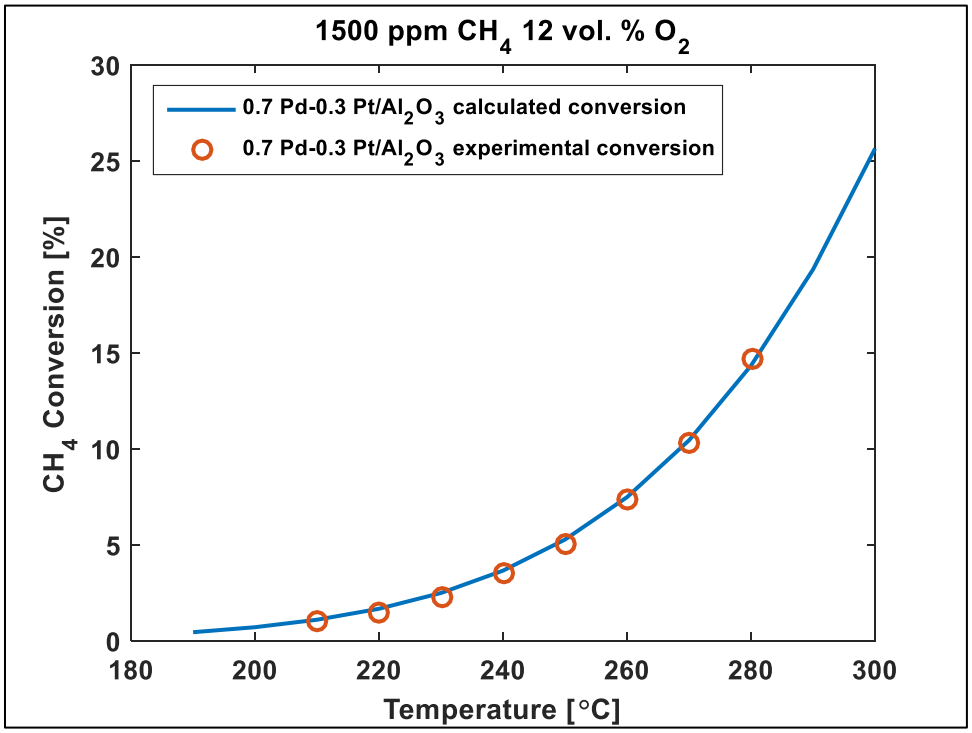

Figure 4.14: Model fit against experimental results obtained during TPO in flowing 1500 ppm CH4 and 10 vol. % O2 in N2 with a ramp rate of 5 °C/min for 0.7 Pd-0.3 Pt.

The fitted kinetic parameters are compared in Table 4.2. In general, the activation energy for CH_4 oxidation was similar for all samples. However, the frequency factor did vary. When accounting for the dispersion of the samples, the turnover rate [TOR],

$$TOR = \frac{X_{CH_4} * \dot{m_{CH_4}}}{D * n_m}, \quad (2)$$

where D is the precious metal dispersion percentage on the catalyst support, n_m is the number of precious metal moles, X_{CH_4} is CH_4 conversion percentage, and m_{CH_4} is the total CH_4 flowrate [Kinnunen et al., 2012]. In this work, n_m, X_{CH_4}, and m_{CH_4} equal 190μmoles, 20%, and $1.5*10^{-8}$ $\frac{moles_{CH_4}}{s}$.

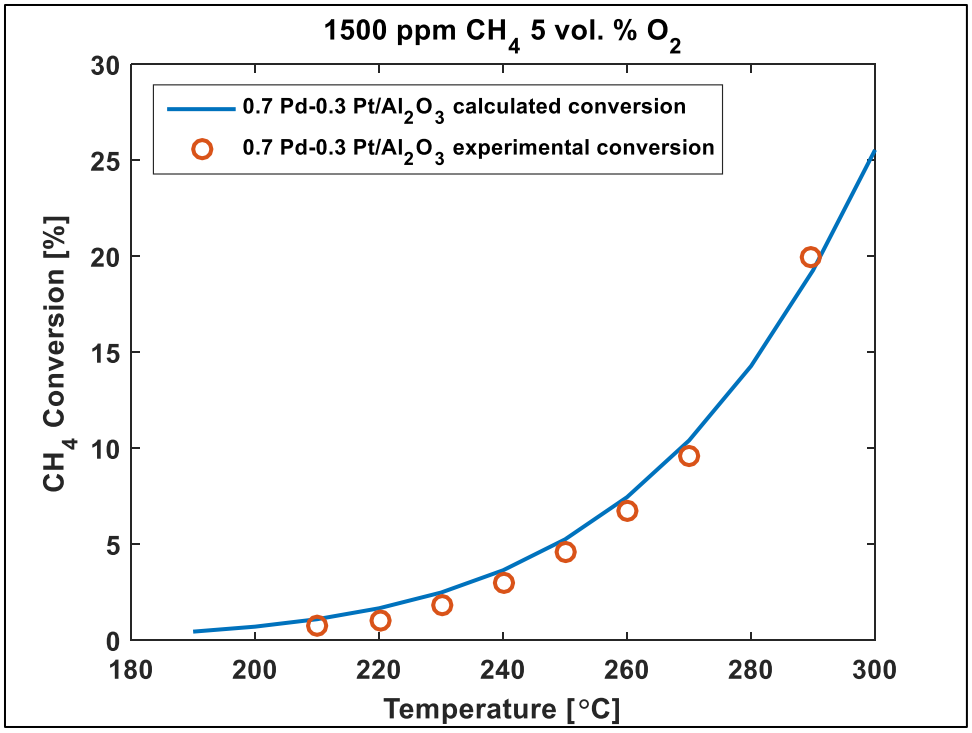

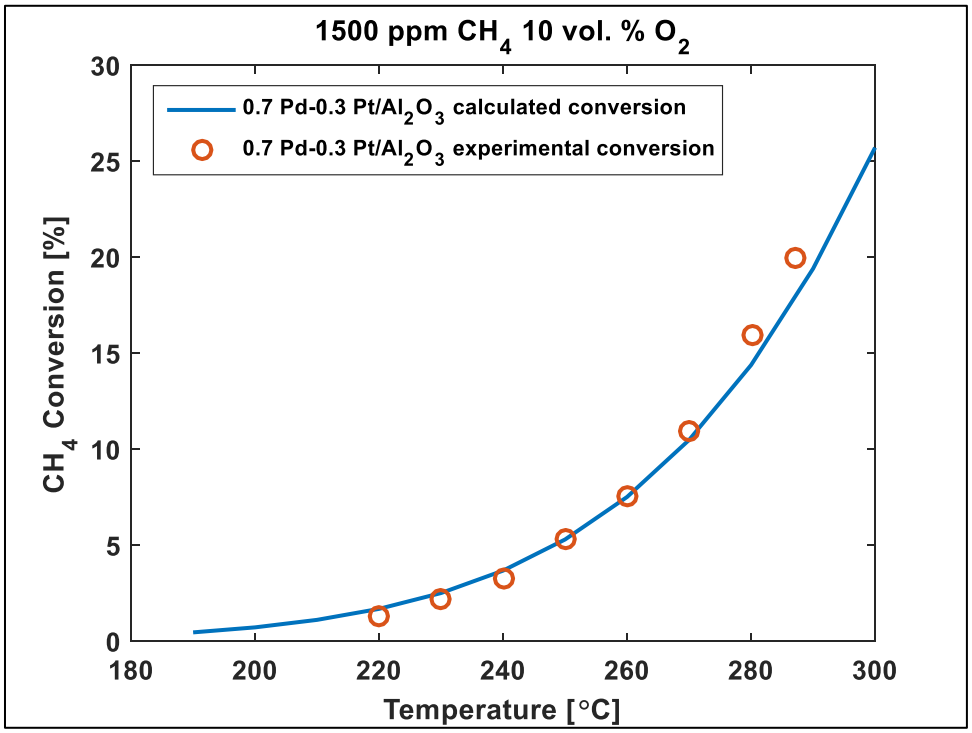

Figure 4.15: Model fit against experimental results obtained during TPO in flowing 1500 ppm CH_4 and (a) 5 vol. % O_2 (b) 12 vol. % O_2 in N_2 with a ramp rate of 5 °C/min for 0.7 Pd-0.3 Pt.

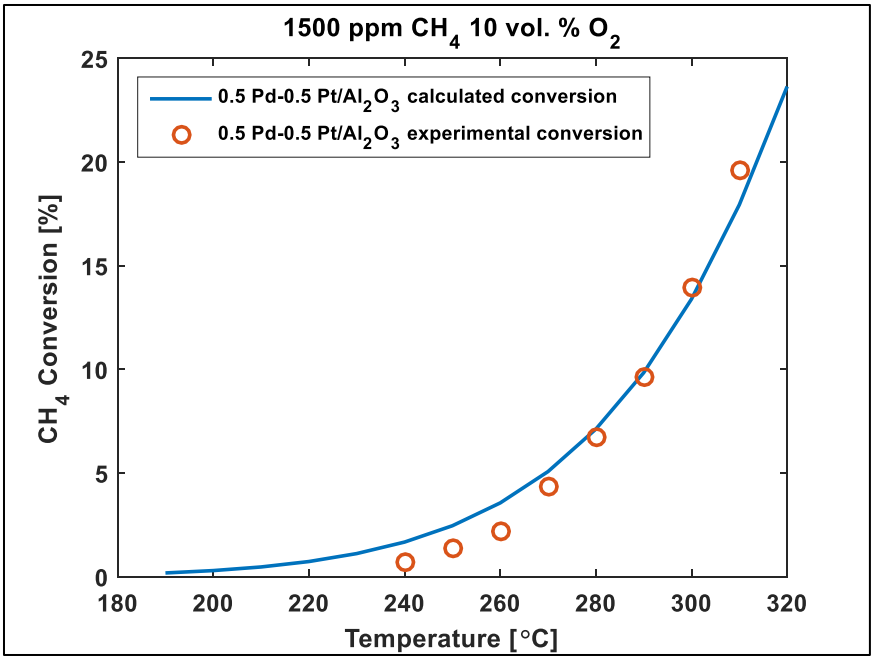

Figure 4.16: Model fit against experimental results obtained during TPO in flowing 1500 ppm CH_4 and 10 vol. % O_2 in N_2 with a ramp rate of 5 °C/min for 0.5 Pd-0.5 Pt.

Table 4.2: Fitted kinetic rate constant parameters and TOR for catalysts containing Pd

Pd Mole %	Pt Mole %	A_CH_4 [s^{-1}]	Ea_CH_4 [kJ/mol]	A_ads_H_2O [cm^3/mol]	ΔH_ads_H_2O [kJ/mol]	PM Dispersion [%]	TOR at 20% CH_4 Conversion [s^{-1}]
100	0	2.79E+12	70.1	0.3	109.2	56.7	2.76E-05
90	10	3.32E+12	69.5	1.1	101.4	64.8	2.42E-05
70	30	3.38E+12	70.3	0.2	99.9	28.5	5.50E-05
50	50	3.08E+12	74.8	0.2	105.5	22.1	7.09E-05

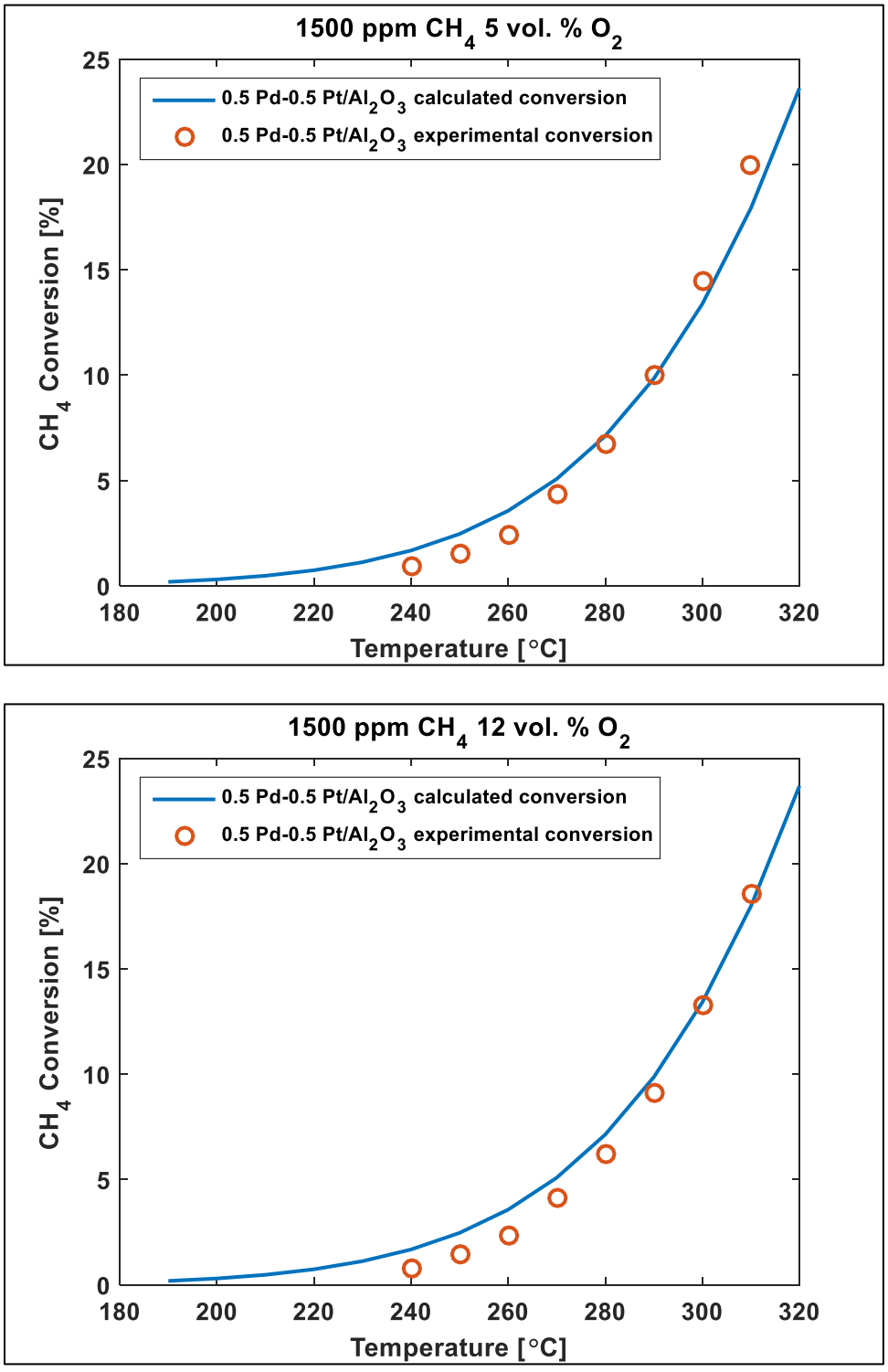

Figure 4.17: Model fit against experimental results obtained during TPO in flowing 1500 ppm CH4 and (a) 5 vol. % O2 (b) 12 vol. % O2 in N2 with a ramp rate of 5 °C/min for 0.5 Pd-0.5 Pt.

4.4 Conclusions

In this study, we examined how Pt substitution in Pd catalysts affects the CH_4 oxidation reaction rate equation and validated these conclusions with a reactor model developed in MATLAB. Similar to Pd, product water inhibited the CH_4 oxidation reaction for all bimetallic samples, but to variable extents. Bimetallics with Pt:Pd ratios of at least 1:1 were inhibited by product water to similar extents. As the Pt content was further increased, product water inhibition was reduced. Since CH_4 oxidation is not inhibited by product water for monometallic Pt, we concluded that the CH_4 oxidation is less inhibited by product water for bimetallics with a large Pt percentage due to their increased Pt content and exposed Pt surfaces. In contrast to Pt, no bimetallics exhibited an O_2 dependency during CH_4 oxidation. We concluded that the reaction rate equation for all catalysts containing some Pd contains an inhibition term for water but none for oxygen.

A kinetic parameter fitting tool and baseline reactor model were established and validated for a reactor utilizing monometallic Pd catalyst. The same tool was used to determine bimetallic kinetic parameters and model CH_4 consumption in the kinetic regime. A good fit between the model predictions and experimental data was achieved in all cases.

Chapter 5 Water Inhibition and Decay Study for Complete CH_4 Oxidation Kinetic Experiments

5.1 Introduction

Natural gas engine aftertreatment systems will be exposed to various engine combustion products [Cullis and Willatt, 1983; Ribeiro et al., 1994; Burch et al., 1995] and a range of exhaust temperatures [Gélin and Primet, 2002; Demoulin et al., 2005] with time on stream. When only CH_4 and air are present in the feed stream, Mowery et al. found that steam aged Pd/Al_2O_3 catalysts were less active than those not previously exposed to water. They concluded that water significantly deactivates Pd catalysts [Mowery et al., 1999]. In another study, when water was injected into the CH_4 oxidation feed stream, CH_4 oxidation activity for monometallic Pd catalysts considerably decayed, but water had less impact on bimetallic activity. Moreover, the activity of these bimetallics appeared to be more stable under these conditions over time on stream [Perrson et al., 2003]. Similarly, other researchers [Lapisardi et al., 2007; Kinnunen et al., 2012] found that addition of Pt to Pd/Al_2O_3 results in increased resistance to decay with time on stream as long as the Pt portion does not exceed 33%. For these reasons, bimetallics are regarded as having greater sinter resistance during high-temperature [Kinnunen et al., 2012] and water [Lapisardi et al., 2007] exposure in comparison to their monometallic counterparts.

Some researchers believe that water injection reduces CH_4 oxidation activity for Pd catalysts because the active sites, i.e., PdO, convert to hydroxyls [$Pd(OH)_2$] that are less active or even inactive in combusting CH_4 [Burch et al., 1999]. Other researchers claim that bimetallics are more tolerant to water exposure because Pt can reduce the rate of particle growth for PdO in bimetallics [Narui et al., 1999] while others attributed this sinter resistance to bimetallic alloy formation [Perrson et al., 2006], probably due to their bimetallics undergoing calcination at ~1000 °C.

In their reviews, Bartholemew reported that Pd is less thermally stable than Pt while Wanke and Flynn reported that noble metals, in general, are more vulnerable to sintering in oxidizing environments than in reducing or inert environments [Bartholemew, 1993; Wanke and Flynn, 1975]. Although some researchers found that Pt does not sinter in oxidizing environments below 500 °C, by simply increasing the oxidizing environment temperature from 600 °C to 700 °C, even in the absence of H_2O, Pt sintering also increases [Yang. 2008]. This part of the thesis work focuses on determining the effect of water injection on the CH_4 oxidation reaction and decay resistance as a function of Pd:Pt ratio.

5.2 Experimental Methods

5.2.1 Catalyst preparation and reactor experimental set-up

Using the incipient wetness impregnation method, the following Pd-Pt/Al_2O_3 powder catalysts were prepared in the manner described in Chapter 4: $Pd_{1.0}Pt_{0.0}/Al_2O_3$, $Pd_{0.9}Pt_{0.1}/Al_2O_3$, $Pd_{0.7}Pt_{0.3}/Al_2O_3$, $Pd_{0.5}Pt_{0.5}/Al_2O_3$, $Pd_{0.3}Pt_{0.7}/Al_2O_3$, $Pd_{0.2}Pt_{0.8}/Al_2O_3$, $Pd_{0.15}Pt_{0.85}/Al_2O_3$, $Pd_{0.1}Pt_{0.9}/Al_2O_3$, $Pd_{0.05}Pt_{0.95}/Al_2O_3$, and $Pd_{0.0}Pt_{1.0}/Al_2O_3$. After drying overnight, all samples were calcined in air at 550 °C.

For all reactor pretreatment and experimental conditions, the MKS FTIR reactor system and oxidation pretreatment conditions described in Chapter 2 were used. Each catalyst sample underwent a pretreatment with 2000 ppm CH_4 and 10 vol. % O_2 in N_2 until CH_4 conversion stabilized. After stabilization, the furnace was cooled to ~ 150 °C. A dry TPO experiment was then performed under the following conditions: flowing 2000 ppm CH_4 and 10 vol. % O_2 in N_2 with a 5 °C/min temperature ramp rate. Gas concentrations were measured with an MKS FTIR 2030. The purpose of the dry TPO was to baseline the fresh catalytic activity for each catalyst.

5.2.2 Complete CH_4 Oxidation with H_2O in the feed

After the dry TPO, the reactor furnace was set to ~ 150 °C while 1.8 vol. % H_2O, 2000 ppm CH_4, and 10 vol. % O_2 were injected into the N_2 feed stream. For this work, these concentrations were referred to as wet TPO flow conditions. After the sample was saturated with H_2O, the furnace temperature was increased using a ramp rate of 5 °C per minute until greater than 50% conversion was achieved. After the wet TPO protocol, a dry TPO was performed again in an effort to compare the initial catalytic activity to that observed following H_2O exposure.

After conducting the final dry TPO experiment, select samples were reduced at 400 °C under a 5 vol. % H_2 in N_2 flow stream. Following reduction pretreatment, the reactor was purged with N_2 to remove residual H_2 then cooled to 35 °C. Using a Valco pulse injection valve, 10 μL CO was injected in regular intervals. When the injection pulse-signature remained constant with each following CO pulse injection, the sample was assumed saturated. After saturation was achieved, the total volume of CO adsorbed was used to determine the sample PM dispersion and corresponding particle size. These

data were used to assess whether the water exposure had any negative effect on CH_4 oxidation activity.

5.2.3 Complete CH_4 Oxidation with extended time on stream

After stabilization and the baseline dry TPO assessment, selected samples were held 500 °C under the following reactants: 2000 ppm CH_4 and 10% O_2 balanced with N_2. After a 24 hour period, the catalysts underwent two dry TPOs up to 500 °C. This process was repeated each 24 hours until a hold period of at least 72 hours was completed. A final dry TPO was performed to determine whether any activity decay occurred over the 72 hour period.

5.2.4 Temperature-programmed desorption (TPD)

Select fresh catalysts were exposed to 1.8 vol. % H_2O in N_2 at 150 °C until saturation. After saturation, the reactor was purged with N_2 at 150 °C for an additional 15 minutes to minimize the residual H_2O content within the reactor system lines and detach weakly adsorbed H_2O from the catalyst surface. TPD was then performed, with a ramp rate of 10 °C /minute to 900 °C followed by a hold at 900 °C for an additional 15 minutes. The purpose of this TPD experiment was to assess how the Pd:Pt mole ratio impacts H_2O adsorption and desorption.

5.3 Experimental results and discussion

Prior to water exposure, the samples underwent a baseline TPO to establish the fresh catalytic activity. The ignition profiles obtained during this experiment are compared in Figure 5.1. Using the temperature at which 20% CH_4 conversion occurred,

T_{20}, as a metric the catalytic activities in the kinetic regime were compared. Substituting Pd moles with Pt moles in small amounts, 0.9 Pd-0.1 Pt, resulted in an increased activity in comparison to Pd. Greater substitutions led to decreased activity, especially for catalysts with a Pd content less than 15%. Lapisardi et al. observed similar trends for 2 wt. % Pd:Pt/Al_2O_3 catalysts [Lapisardi et al., 2007].

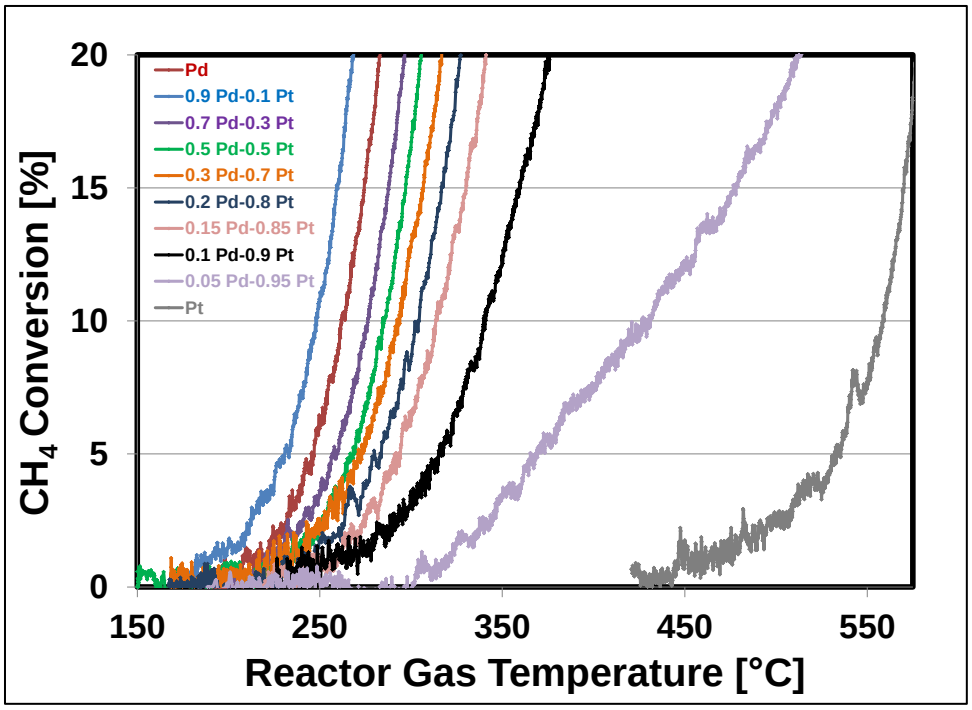

Figure 5.1: TPO in flowing 2000 ppm CH_4 and 10 vol. % O_2 in N_2, with a 5 °C/min ramp rate.

Using the temperature at which 20% CH_4 conversion occurred, T_{20}, as a metric the catalytic activities in wet and dry conditions were compared. As indicated in the literature, the complete CH_4 oxidation reaction is inhibited by water for Pd whereas Pt is unaffected (Figure 5.2).

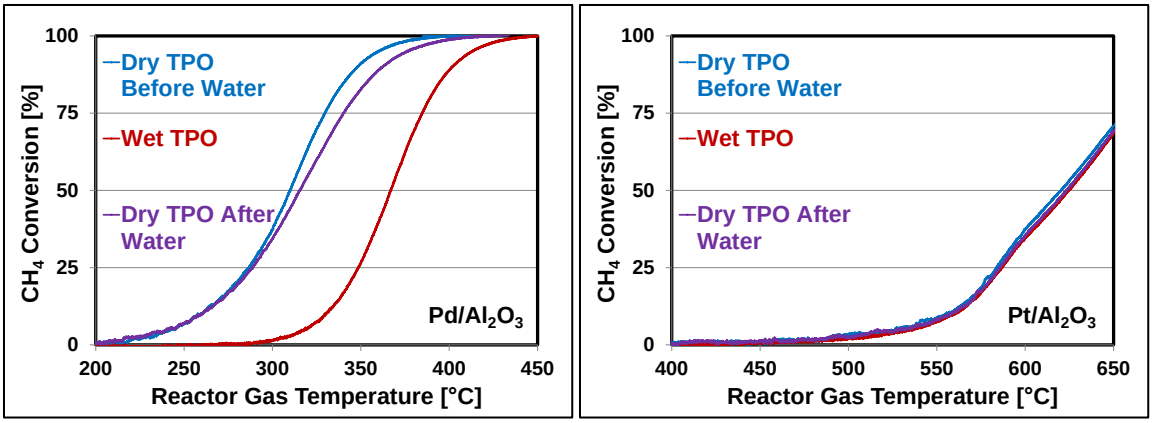

Figure 5.2: TPO in flowing 2000 ppm CH_4 and 10 vol. % O_2 in N_2 with a ramp rate of 5 °C/min for (a) Pd (b) Pt; wet (1.8 vol. % H_2O) and dry (0 vol. % H_2O) conditions were compared.

No change in T_{50} was observed after water was removed from the feed stream during CH_4 oxidation with Pt. Upon removing water from the feed stream, the T_{50} for Pd decreased but was ~5 °C greater than that observed prior to water exposure. We concluded that water exposure resulted in moderate to no permanent decay for Pd and Pt monometallic catalysts respectively.

To investigate how Pd and Pt water tolerance characteristics influence bimetallic tolerance to water exposure, bimetallic catalysts underwent complete CH_4 oxidation experiments with 1.8 vol. % H_2O injected into the feed stream continuously. Similar to monometallic Pd, the CH_4 oxidation reaction was inhibited during water injection for 0.9 Pd-0.1 Pt, 0.7 Pd-0.3 Pt, and 0.5 Pd-0.5 Pt (Figure 5.3). As further Pt substitutions were made, water inhibition continued to be observed until the catalyst composition was less than 10 mol% Pd (Figures 5.4 and 5.5).

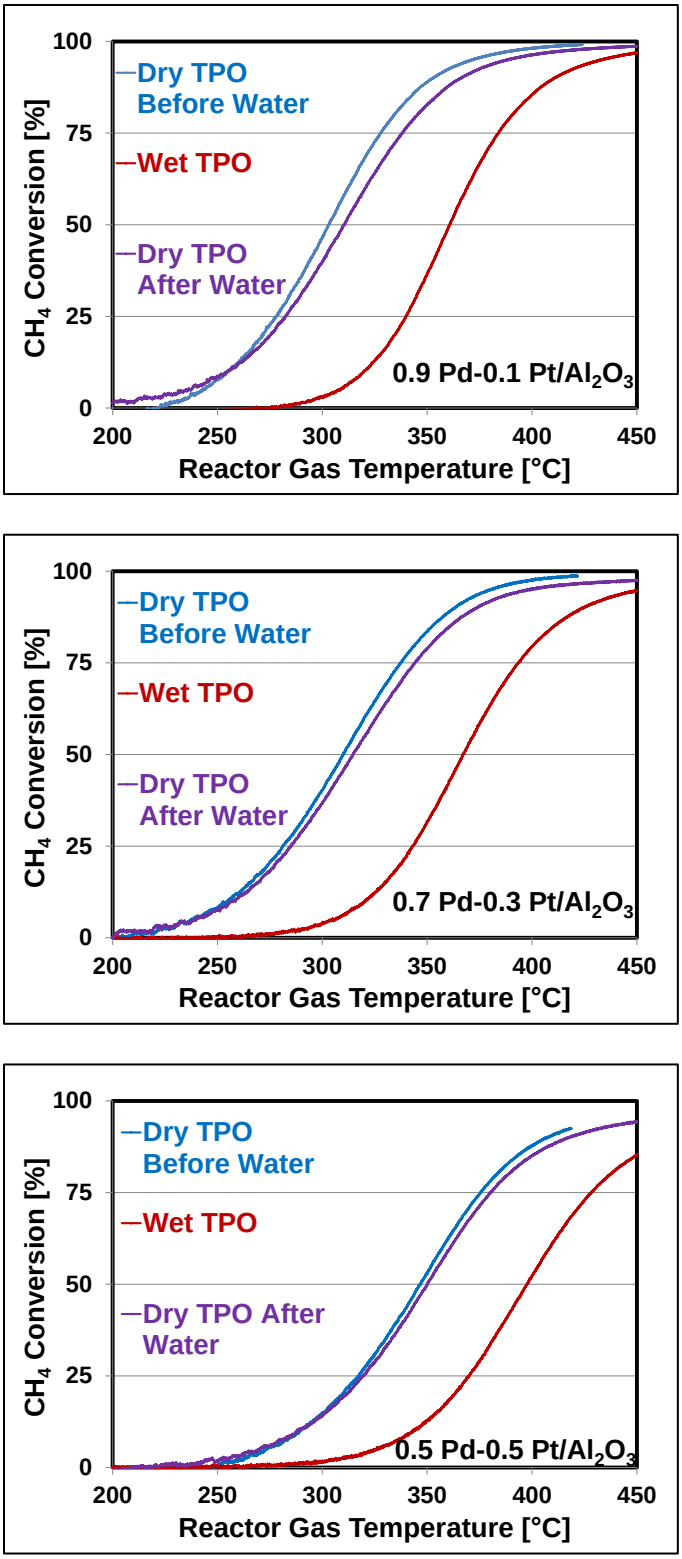

Figure 5.3: TPO in flowing 2000 ppm CH_4 and 10 vol. % O_2 in N_2 with a ramp rate of 5 °C/min for (a) 0.9 Pd-0.1 Pt (b) 0.7 Pd-0.3 Pt (c) 0.5 Pd-0.5 Pt; wet (1.8 vol. % H_2O) and dry (0 vol. % H_2O) conditions were compared.

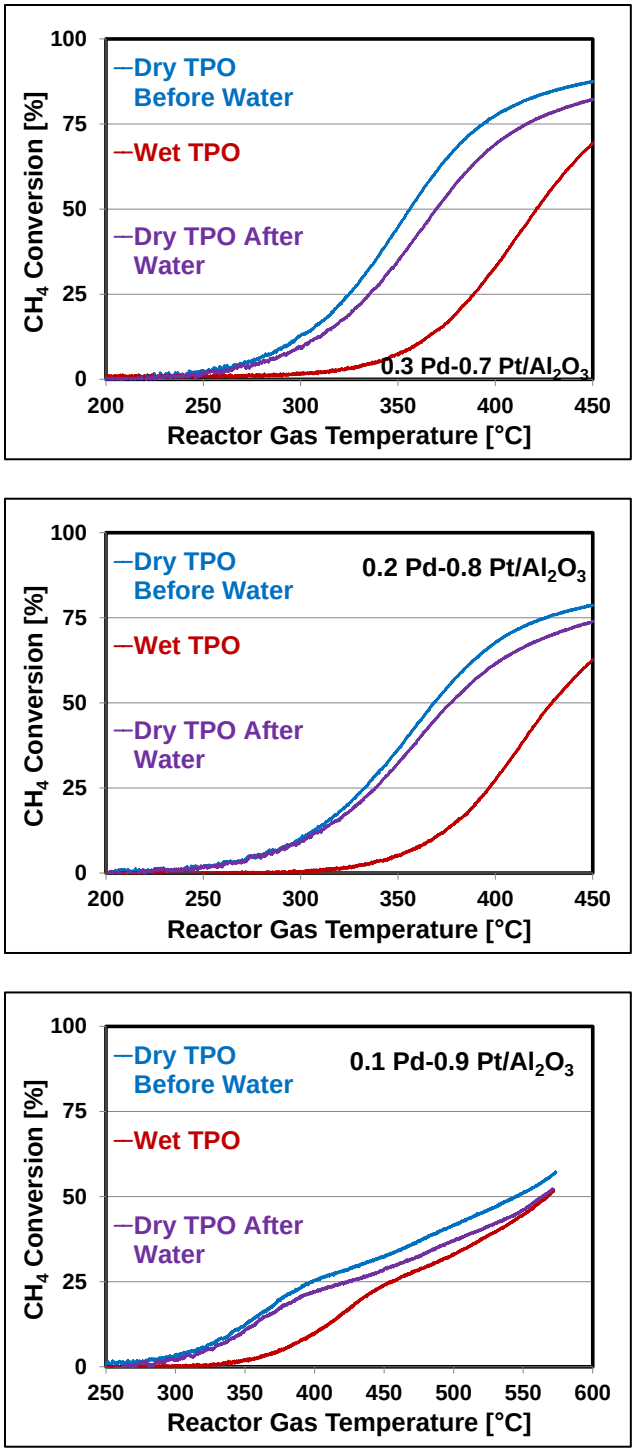

Figure 5.4: TPO in flowing 2000 ppm CH_4 and 10 vol. % O_2 in N_2 with a ramp rate of 5 °C/min for (a) 0.3 Pd-0.7 Pt (b) 0.2 Pd-0.8 Pt (c) 0.1 Pd-0.9 Pt; wet (1.8 vol. % H_2O) and dry (0 vol. % H_2O) conditions were compared.

When water was introduced to the feed stream, T_{50} was less impacted for 0.1 Pd-0.9 Pt when compared to catalysts with 15 mol% Pd or more. Similar to monometallic Pt, T_{50} only slightly increased when water was introduced to the CH_4 oxidation feed stream for the 0.05 Pd-0.95 Pt sample (Figure 5.5).

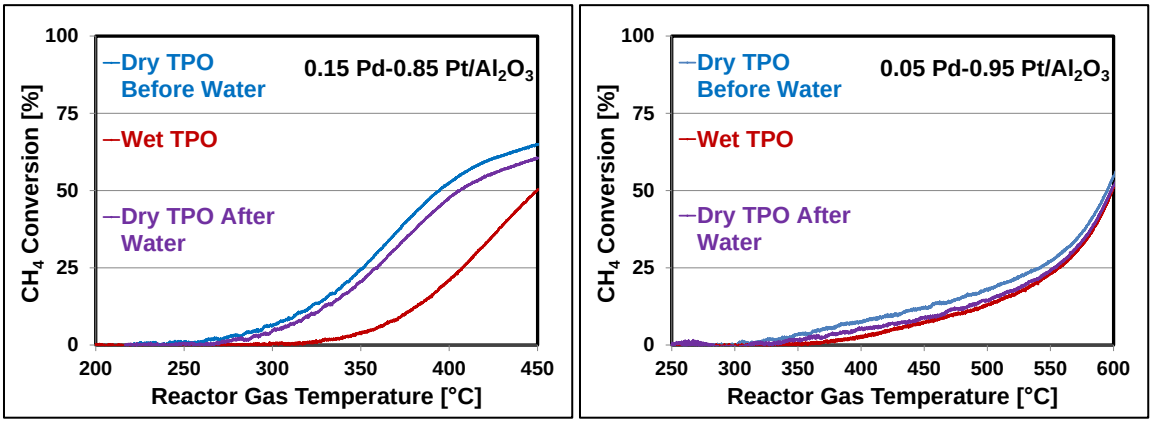

Figure 5.5: TPO in flowing 2000 ppm CH_4 and 10 vol. % O_2 in N_2 with a ramp rate of 5 °C/min for (a) 0.15 Pd-0.85 Pt (b) 0.05 Pd-0.95 Pt; wet (1.8 vol. % H_2O) and dry (0 vol. % H_2O) conditions were compared.

When all samples were compared (Figure 5.6), it became apparent that a transition point occurred at 0.3 Pd-0.7 Pt. The CH_4 oxidation reaction was inhibited by water for all catalysts with at least 50% Pd, and the corresponding impact on T_{50} was an increase of ~57 °C. The maximum water inhibition was observed for 0.3 Pd-0.7 Pt, with a corresponding 65 °C increase in T_{50}. As more Pt was substituted for Pd, the extent of water inhibition decreased approaching the lack of inhibition observed for monometallic Pt.

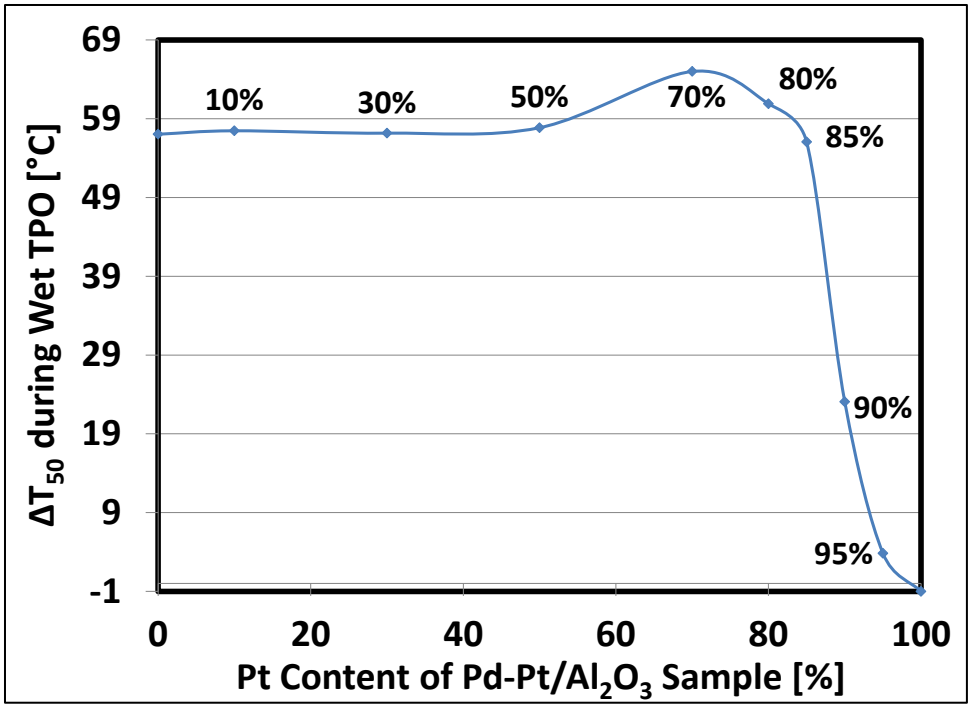

Figure 5.6: Change in T_{50} during complete CH_4 oxidation due to water in the feed.

When the T_{50} for the fresh 0.9 Pd-0.1 Pt was compared to that after water exposure, an increase of ~7 °C was observed. Similar findings were observed when further Pt substitutions were made up to a catalyst composition of 50% Pd (Figure 5.7). For 0.3 Pd-0.7 Pt, in addition to increased water inhibition, ~13 °C increase in T_{50} was observed due to decay resulting from water exposure. As more Pt was substituted for Pd, similar increases of ~12 to 19 °C in T_{50} after exposure to water were observed. In contrast, 0.05 Pd-0.95 Pt displayed the least water inhibition and decay when compared to the other bimetallics. We suspected that either sintering or water adsorption differences were affecting these results on a mole ratio basis.

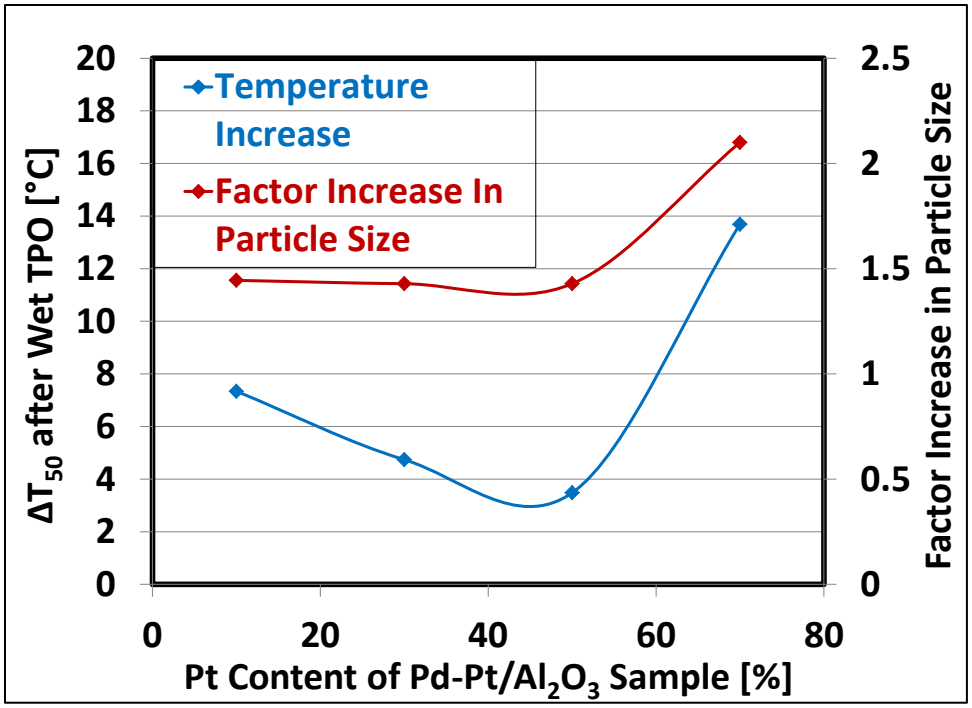

Figure 5.7: Change in T_{50} during complete CH_4 oxidation and PM particle size after water exposure.

To determine whether some samples sintered more during water exposure, CO chemisorption experiments were conducted on a subset of the samples after the final dry TPO. All bimetallic catalysts with at least 50 mol% Pd displayed a 40% increase in PM particle size after water exposure. Similar to the transition in water inhibition and water decay characteristics upon decreasing the Pd content to 30%, the 0.3 Pd-0.7 Pt sample displayed a PM particle size increase by 110% after water exposure.

To examine whether water adsorption and residual variations on a Pd:Pt ratio basis were also influencing the CH_4 oxidation results, H_2O adsorption and TPD experiments were performed. As shown in Figure 5.8, the saturated monometallic Pt and 0.3 Pd-0.7 Pt samples released similar amounts of water over similar temperature spans during the H_2O TPD. We concluded that the Pd:Pt mole ratio does not influence H_2O

uptake in this case. Rather, the H_2O TPD characteristics are due to the common denominator, the alumina support, for this case.

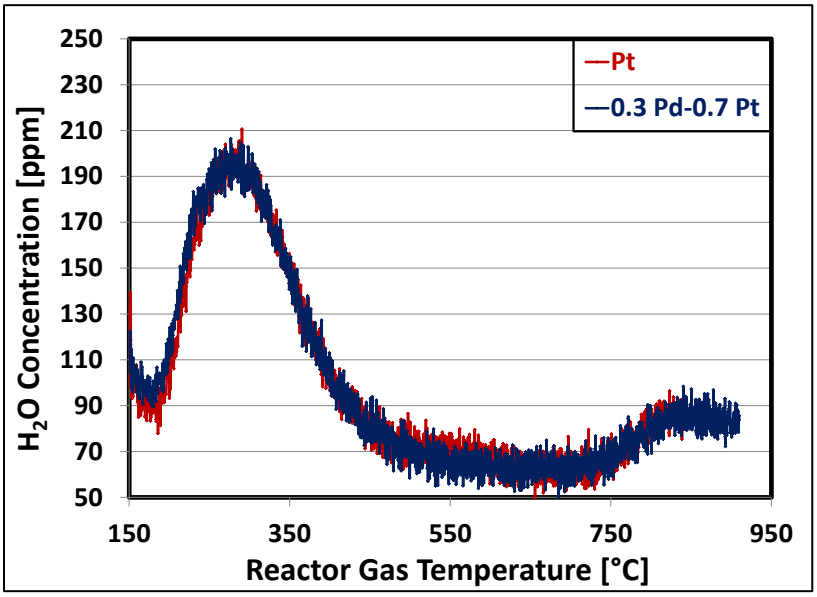

Figure 5.8: H_2O desorption during TPD in flowing N_2, with a ramp rate of 10 °C/min.

Due to increases in T_{50} during water exposure, we concluded that bimetallics with at least 30 mol% Pd exhibit the same CH_4 oxidation reaction inhibition due to water exposure as Pd. As greater Pt substitutions are made, the inhibition effects are reduced approaching the insensitivity of monometallic Pt as shown for bimetallics with 10 mol% Pd or less. Due to the increases in T_{50} after water exposure, we concluded that large substitutions of Pt for Pd in bimetallic catalysts reduce the catalyst tolerance to water exposure and catalyst decay is likely. However, Pd:Pt ratio did not affect H_2O uptake under these conditions.

To assess how the bimetallics decay over time on stream, the 0.7 Pd-0.3 Pt sample was held under CH_4 oxidation reaction conditions for 24 hour intervals followed by two reference TPOs to assess degradation with each 24 hour period. This process was

repeated for a total of 72 hours. In comparing the TPOs after each hold, little decay was observed after each hold period (Figure 5.9a).

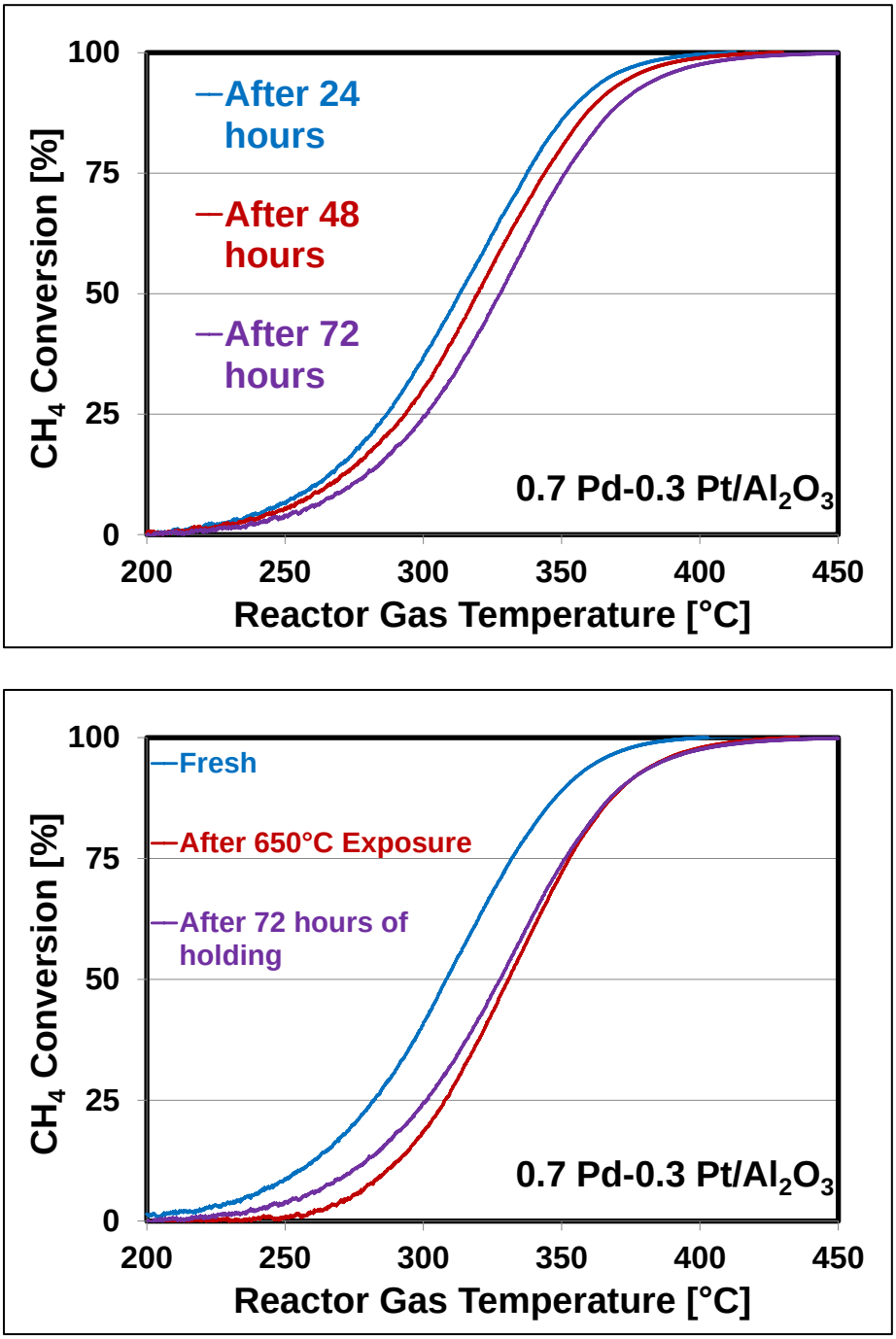

Figure 5.9: TPO in flowing 2000 ppm CH_4 and 10 vol. % O_2 in N_2 with a ramp rate of 5 °C/min. (a) Decay during extended time on stream (b) decay due to accelerated aging at 650 °C for 0.7 Pd-0.3 Pt.

In response to the small amount of decay observed, it was pertinent to develop a way to accelerate aging effects and remove the requirements for an extended hold duration or excessive consumption of reactants. An accelerated aging technique consisting of high temperature exposure in flowing N_2 only was assessed. As shown in Figure 5.9b, similar impacts to T_{50} resulted due to 72 hours of holding under reactants as that of accelerated aging at 650 °C. Although only one bimetallic was assessed, we inferred that the accelerated aging technique was sufficient to perform a rough comparison of the bimetallic samples in an effort to assess whether certain blends are simply more prone to sintering or if water influences the sintering vulnerability.

For the remaining bimetallic catalysts, the accelerated aging technique was used to determine activity decay after 650 °C exposure. After 650 °C exposure, T_{50} for 0.9 Pd-0.1 Pt decreased slightly. However, as further Pt substitutions are made, T_{50} increased with each substitution (Figure 5.10). In general, bimetallics with less than 90% Pd decrease in tolerance to high temperature exposure as the Pt content increases. In the case of water decay, after water was removed from the feed stream, bimetallics with at least 50% Pd demonstrated a similar reduction in activity. For greater Pt substitutions, the extent of reduced activity was increased until a composition of less than 10% Pd was obtained. We concluded that bimetallics with less than 90% Pd are more prone to sintering, but the water decay data show that low Pd content blends are especially vulnerable to sintering resulting from water exposure.

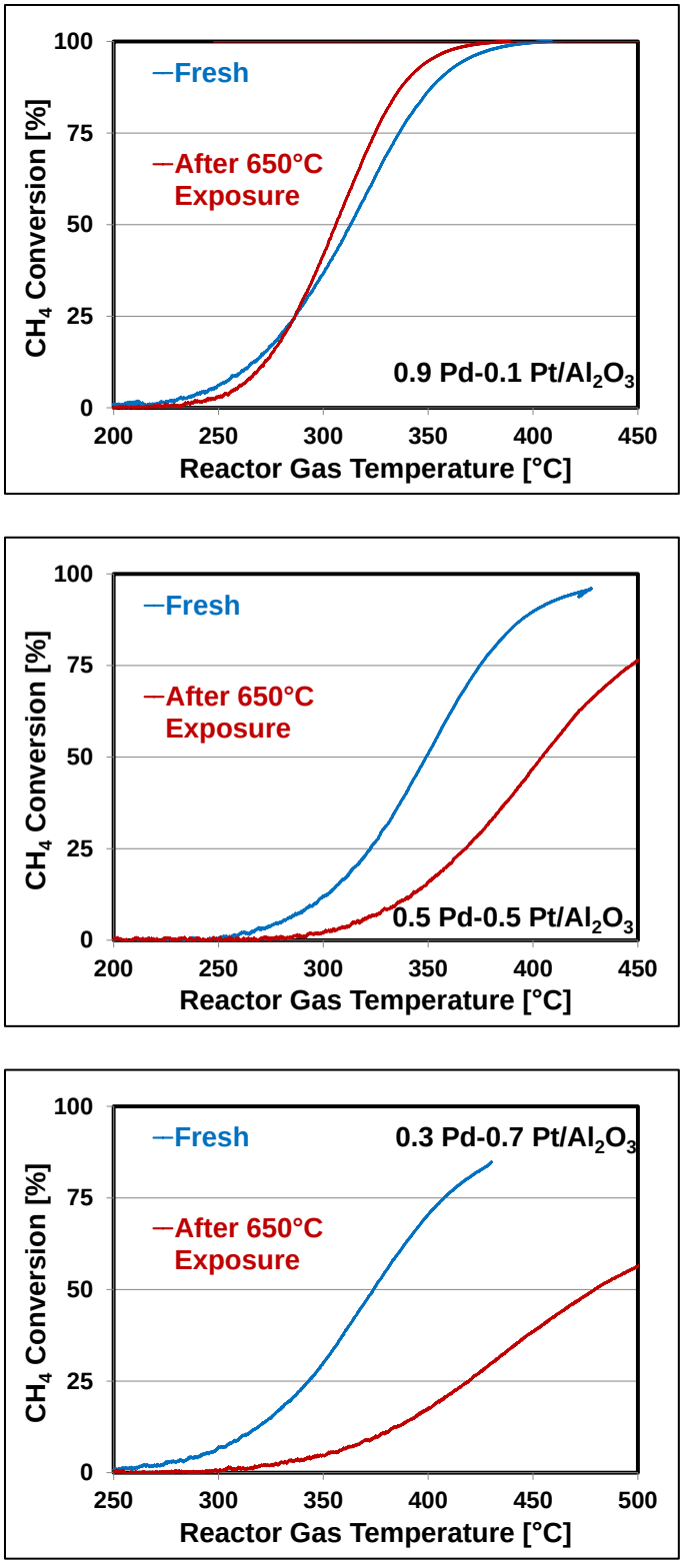

Figure 5.10: TPO in flowing 2000 ppm CH_4 and 10 vol. % O_2 in N_2 with a ramp rate of 5 °C/min. Decay due to accelerated aging at 650 °C for (a) 0.9 Pd-0.1 Pt (b) 0.5 Pd-0.5 Pt (c) 0.3 Pd-0.7 Pt.

5.4 Conclusions

In this study, we examined how CH_4 oxidation activity decays over time on stream and with exposure to water. Using T_{50} as a metric, initially Pt substitution, 0.9 Pd-0.1 Pt, resulted in an increase in activity upon 650 °C exposure. With each additional amount of Pt substituted, T_{50} increased to a greater extent. All bimetallic catalysts with at least 50 mol% Pd exhibit the same CH_4 oxidation reaction inhibition due to water exposure as Pd. As greater Pt substitutions were made, the inhibition effects were initially increased up to 30% Pd but then were reduced with further Pt substitutions, such that activity during water exposure approached the insensitivity observed for monometallic Pt. When water injection ceased, the activity for monometallic Pd returned to its fresh activity with only a minor increase in T_{50} observed. Similarly, bimetallic catalysts with greater than 50 mol% Pd displayed very little decay due to water exposure. As the Pd content further decreased, greater increases in T_{50} after water exposure were observed. We concluded that large substitutions of Pt for Pd in bimetallic catalysts reduced the tolerance to water exposure and catalyst decay is likely. Similarly, we concluded that bimetallic catalysts with greater than 50 mol% Pd are resistant to sintering via water exposure but only small Pt substitutions can be made if high temperature tolerance is desired.

Chapter 6 SO_2 Adsorption and Desorption Characteristics of Bimetallic Pd-Pt catalysts: Pd:Pt ratio dependency

Note: The material in this chapter has been submitted for publication. Therefore the introduction and experimental methodology may appear redundant with other sections. Reference and figure numbers were changed for dissertation consistency.

6.1 Introduction

With vehicle/transportation fuel availability concerns and increasingly stringent vehicular emissions regulations, there has been growing interest in alternative fuels. The relatively newfound abundance of natural gas on a world-wide scale has caused an increased interest in its general use. Under lean-burn conditions specifically, natural gas engine vehicles produce less exhaust nitrogen oxide (NO_x) and particulate emissions in comparison to traditional gasoline- and diesel-fueled engines. Moreover, natural gas has low sulfur content, so sulfur oxide emissions in natural gas engine exhaust are low. These benefits have made lean-burn natural gas engine vehicles a desirable option for use in urban areas [Gélin and Primet, 2002].

On the other hand, natural gas consists of ~90-95% methane and as the combustion process is not perfect, there will be some methane that exits the engine. Unfortunately, methane is the most challenging hydrocarbon to catalytically oxidize,

especially at the low lean-burn natural gas engine exhaust temperatures. Methane being a potent greenhouse gas, its release needs to be mitigated. In addition to the inherent challenge in catalytically oxidizing methane, many methane oxidation catalysts seem to be quite susceptible to catalyst deactivation. Consequently, in an effort to reduce lean-burn natural gas engine emissions, research studies have focused on new methane oxidation catalysts and their potential deactivation sources [Gélin and Primet, 2002].

Pd is considered active in methane oxidation, and there has been significant effort in studying its application for methane oxidation in natural gas engine aftertreatment systems [Cullis and Willatt, 1983; Baldwin and Burch, 1990; Ribeiro et al., 1994; Klingstedt et al., 2001]. For example, Lampert et al. [Lampert et al., 1997] studied methane oxidation with the following Pd/Al_2O_3 catalysts: steam aged, steam and oil aged, aged by exposure to engine inlet conditions, and steam aged with exposure to SO_2 or SO_3. The steam aged catalysts resulted in the highest methane oxidation activity. All other catalysts, which were exposed to some form of sulfur, displayed similar reduced levels of activity. Based on these results, the authors concluded that the presence of sulfur alone was enough to deactivate the catalysts regardless of whether other potential poisons were contained in the engine inlet or oil feed sources. Such an observation has consistently been made – these Pd-based methane oxidation catalysts deactivate in the presence of even trace amounts of sulfur [Corro et al., 2010; Gélin and Primet, 2002;Chaplin et al., 2007; Li-Dun and Quan, 1990; Lee and Rhee, 1998; Xu et al., 2014; Colussi et al., 2010; Badano et al., 2010; Gotterbarm et al., 2012; Ohtsuka, 2011; Jiang et al., 2007; Deng et al., 1993; Li et al., 2013; Balla et al., 2012; Beck et al., 1994; Nasri et al., 1998; Wang et al., 2010; Yu and Shaw, 1998].

Bimetallic Pt/Pd catalysts, known to be sinter-resistant, have been investigated as methane oxidation catalysts. Lapisardi et al. assessed the catalytic activity of Pt/Al_2O_3, Pd/Al_2O_3, and $Pd\text{-}Pt/Al_2O_3$ catalysts during methane oxidation, as well as with exposure to H_2S. Pd/Al_2O_3, $Pd_{0.93}Pt_{0.07}/Al_2O_3$, and $Pd_{0.65}Pt_{0.35}/Al_2O_3$ samples displayed a sharp and rapid decay in activity upon exposure to H_2S. On the other hand, the Pt/Al_2O_3 and $Pd_{0.06}Pt_{0.94}/Al_2O_3$ catalysts resulted in a more gradual decline in activity over time [Lapisardi et al., 2007]. In a study using SO_2 as the sulfur source [Lampert et al., 1997], Pd catalysts oxidized SO_2 to form surface sulfite species, on the Pd, which suppressed methane oxidation reaction. Although Pt catalysts can also form sulfite species during oxidation [Lampert et al., 1997], these species readily spill over to the alumina surface, and were not observed on the Pt surface itself. It was postulated that this was a contributing factor to the resistance of Pt catalysts to sulfur poisoning. Nonetheless, over time with exposure to sulfur, even the Pt catalysts eventually lost activity [Lapisardi et al., 2007]. These examples, and the other literature cited above, clearly show that under relevant methane oxidation conditions, sulfur poisoning is a challenge that must be addressed. Furthermore, as Pt/Pd bimetallics are common oxidation catalysts for diesel engine aftertreatment systems, sulfur poisoning can have an impact on their operation [Li et al., 2014; Wiebenga et al., 2012]. Finally, sulfur poisoning is in general a problem when dealing with catalysis involving hydrocarbons, as sulfur is inherently present.

The work discussed in this paper focuses on what species are formed during Pd:Pt bimetallic catalyst exposure to SO_2 and their stability as a function of temperature. Initial experiments demonstrated that in order to understand why sulfur release characteristics varied with Pd:Pt mole ratio, it was imperative that the precious metal (PM) particle size

contribution be decoupled. For this reason, the sulfur release characteristics due to Pd:Pt mole ratio effects were studied independently by conducting SO_2 adsorption and temperature-programmed desorption (TPD) studies on catalysts with similar precious metal particle sizes.

6.2 Experimental methods

6.2.1 Catalyst preparation and experimental set-up

The $Pd(NO_3)$ and $Pt(NH_3)_4(NO_3)_2$ precursors and Puralox γ-Al_2O_3 were purchased from Sigma-Aldrich. Using the incipient wetness impregnation method, mono- and bimetallic Pd-Pt/Al_2O_3 powder catalysts were prepared, keeping the total number of precious metal moles constant for all catalysts. A 1 wt. % Pd/Al_2O_3 catalyst was used as a basis of reference for precious metal content. All samples were dried overnight and calcined in air at 550 °C. The following Pd-Pt/Al_2O_3 powder catalysts were prepared: $Pd_{1.0}Pt_{0.0}/Al_2O_3$, $Pd_{0.9}Pt_{0.1}/Al_2O_3$, $Pd_{0.7}Pt_{0.3}/Al_2O_3$, $Pd_{0.5}Pt_{0.5}/Al_2O_3$, $Pd_{0.3}Pt_{0.7}/Al_2O_3$, $Pd_{0.2}Pt_{0.8}/Al_2O_3$, $Pd_{0.15}Pt_{0.85}/Al_2O_3$, and $Pd_{0.05}Pt_{0.95}/Al_2O_3$.

Prior to undergoing any experiments, each catalyst was hydrothermally aged under the following flow conditions: 1.8 vol. % H_2O and 10 vol. % O_2 in N_2. To achieve the target PM particle size for a given experiment, the aging duration and temperature were varied from 1 to 12 hours and 700 °C to 750 °C, respectively. After the aging period, the reactor was maintained at the aging temperature for an additional 30 minutes while the reactor was purged with N_2 to reduce residual H_2O and O_2 content within the catalyst bed and reactor system lines. The reactor system lines were maintained at 150 to 180 °C in order to prevent water and sulfur species from depositing on the lines.

6.2.2 Particle size measurements

After aging, a reduction pretreatment was performed using 5 vol. % H_2 in N_2 at 400 °C. Following reduction, the reactor was cooled to 35 °C. Using a Valco pulse injection valve, the sample was periodically dosed with 10 μL of CO. When the injection pulse-signature ceased to change with each additional pulse injection of CO, the sample was considered saturated. After saturation was achieved, the total volume of CO adsorbed was used to determine the sample PM dispersion and corresponding particle size.

6.2.3 Temperature programmed desorption (TPD)

The aged catalysts were exposed to 30 ppm SO_2 in N_2 at 150 °C until saturation, which typically took ~1 hour. After the sulfur exposure, the reactor was maintained at 150 °C for an additional 15 minutes while it was purged with N_2 to reduce residual SO_2 content within the reactor system lines and remove weakly adsorbed SO_2 from the catalyst surface. TPD was then performed, with a ramp rate of 10 °C /minute to 900 °C. The reactor was maintained at 900 °C for an additional 15 minutes.

6.2.4 Diffuse reflectance infrared Fourier transform spectroscopy (DRIFTS)

Background spectra were collected in 50 ml/min of He only at 35 °C, 150 °C, 250 °C, and 400 °C. The background spectrum corresponding to each experimental temperature was subtracted from all spectra collected during the following experiments for that catalyst.

6.2.5 DRIFTS CO chemisorption characterization

After aging was performed in the reactor, catalysts were then transferred to the Harrick Scientific Praying Mantis DRIFTS cell and underwent an oxidation cleaning at 100 °C with 10 vol. % O_2 in He for 5 minutes. The catalyst was then reduced at 400 °C with 5 vol. % H_2 in He for 30 minutes. After the reduction pretreatment, the sample was maintained at 400 °C for an additional 30 minutes while the cell was purged with He to reduce residual H_2 content within the catalyst and DRIFTS system lines. The catalyst was then cooled to approximately 35 °C and exposed to 1 vol. % CO and 10 vol. % N_2 in He until saturation. The CO adsorption spectrum of each bimetallic sample was analyzed and compared to those of monometallic catalysts in an effort to assign peaks as well as to confirm the catalyst composition and types of sites involved in adsorption.

6.2.6 DRIFTS SO_2 adsorption characterization

Each catalyst was exposed to 100 ppm SO_2 and 10 vol. % N_2 in He at 150 °C until saturation as determined by a lack of change in the collected DRIFTS spectra, which typically took ~3 hours. The same procedure was repeated but at 400 °C, based on TPD data to be discussed below.

6.2.7 DRIFTS Sulfur desorption characterization

After saturation was achieved, the system was purged with He, and the sample temperature was increased to 250 °C, where spectra were obtained, followed by an increase to 400 °C where more spectra were obtained. The desorption spectra shown were collected after the DRIFTS spectra ceased to change at each temperature. The desorption

temperatures, 250 °C and 400 °C, were selected based on the cessation of sulfur release observed in the low-temperature range during TPD experiments, to be discussed below.

6.3 Experimental results and discussion

All catalysts characterized were hydrothermally aged to target certain particle sizes and reduced prior to adsorption experiments. This approach helped ensure that the only parameters contributing to the desorption profiles were the mole ratio and particle size. The catalyst Pd:Pt mole ratios and particle sizes, determined by CO chemisorption, are listed in Table 6.1.

6.3.1 CO chemisorption characterization

Table 6.1: Particle sizes determined via pulse-injection, CO chemisorption at 35 °C.

Pd Mole %	Pt Mole %	Particle Size
30	70	1.4 nm
90	10	1.6 nm
100	0	2.0 nm
15	85	3.1 nm
20	80	3.4 nm
70	30	3.2 nm
5	95	12.6 nm
15	85	15.7 nm
50	50	15.2 nm

We first characterized the samples using DRIFTS. In an effort to identify bimetallic catalyst features, the monometallic catalysts were first characterized using CO adsorption (Figures 6.1a and 6.1b).

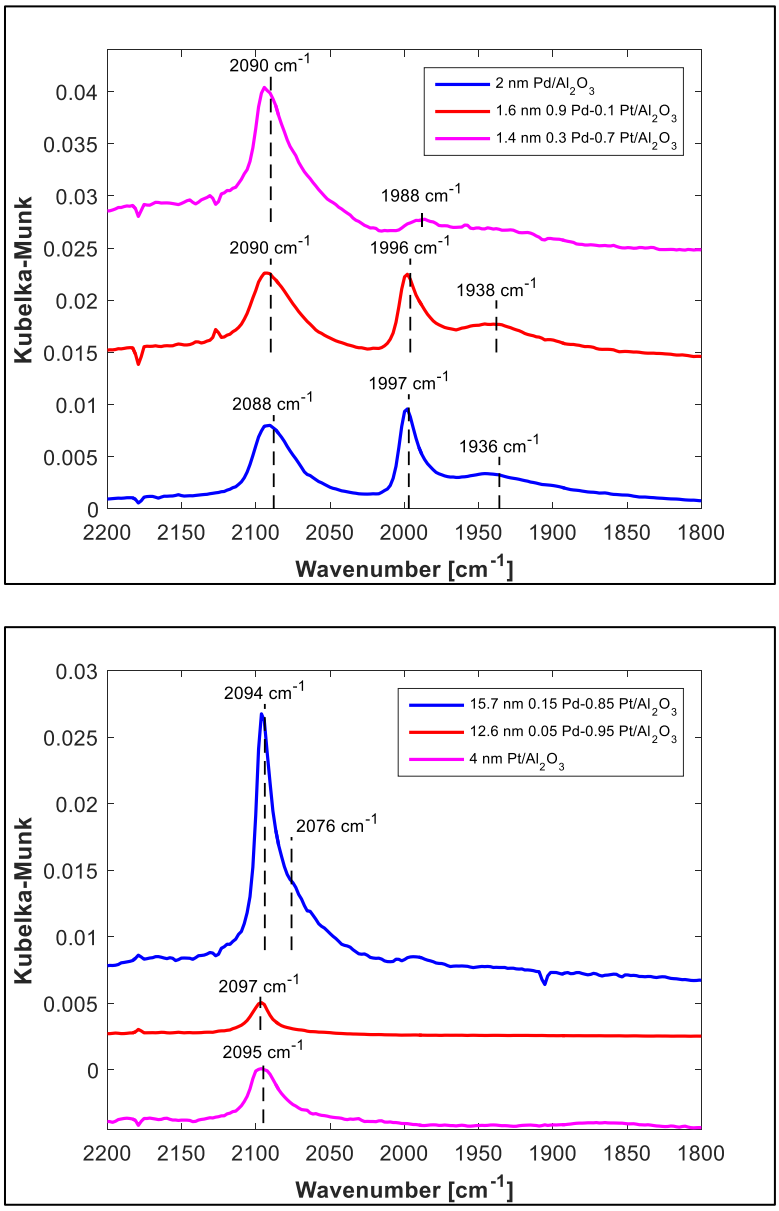

Figure 6.1: CO adsorption DRIFTS spectra obtained after CO exposure saturation at 35 °C for (a) high-Pd content catalysts and (b) low-Pd content catalysts.

The monometallic Pd sample spectrum (Figure 6.1a) displayed peaks at 2088 cm^{-1}, 1997 cm^{-1}, and 1936 cm^{-1}. During CO adsorption, linear or bridged carbonyl complexes can form on reduced Pd (Pd^0-CO). For this reason, the 2088 cm^{-1} band was designated as CO linearly adsorbed on metallic Pd [Zhang et al., 2014; Bensalem et al., 1996; Martinez-Arias et al., 2004], and the 1997 cm^{-1} band as CO bridged across two metallic Pd atoms [Zhang et al., 2014; Martinez-Arias et al., 2004]. The peak at 1936 cm^{-1} was assigned to adsorbed CO bridged across two partially oxidized Pd atoms (Pd^+-CO) [Zhang et al., 2014; Todoroki et al., 2009; Toshima et al., 2001]. The monometallic Pt sample spectrum (Figure 6.1b) displayed peaks at 2095 cm^{-1} and a broad band from 1908 to 1830 cm^{-1}. The peak at 2095 cm^{-1} was assigned to CO linearly adsorbed on Pt sites [Todoroki et al., 2009; Boubnov et al., 2013]. The broad band from 1908 to 1830 cm^{-1} corresponded to CO adsorbed on metallic Pt in a bridged manner [Todoroki et al., 2009; Toshima et al., 2001; Rades et al., 1996]. These assignments formed the basis for peak assignments of the bimetallic catalysts.

Due to bimetallic interactions, Pd:Pt alloys can experience a transfer of electron density between Pd and Pt and this will induce changes in IR peak positions. For example, Rades et al. [Martinez-Arias et al., 2004;] studied CO adsorption on a bimetallic sample and observed lower frequencies, ~2040 cm^{-1}, for CO bound to Pt-Pd alloy samples in comparison to that of monometallic Pt samples, ~2085 cm^{-1}, although Lin et al. [Lin et al., 1995] observed frequencies which were ~20 cm^{-1} higher for Pd:Pt alloy samples in comparison to monometallic Pt samples. Moreover, when Pd:Pt catalysts were exposed to high temperatures it is possible that Pd will diffuse into Pt and form an alloy.

Formation of this alloy can result in a CO adsorption peak shift from ~2090 cm^{-1} for monometallic Pt to ~2070 cm^{-1} for a Pd-Pt alloy [Todoroki et al., 2009].

When the CO adsorption features obtained from the bimetallic catalysts were compared to those of the monometallic catalysts, there was little evidence of shifts in peak wavenumbers. As a result, we deduced that no or little alloying had taken place. As shown in Figure 6.1a, the 0.9 Pd-0.1 Pt spectrum displayed bands at 2090 cm^{-1}, 1996 cm^{-1}, and 1938 cm^{-1}. Similar to monometallic Pd, the bands at 2090 cm^{-1} and 1996 cm^{-1} demonstrate that CO was adsorbed on metallic Pd in a linear and bridged manner respectively while the peak at 1938 cm^{-1} shows that CO linearly adsorbed on partially oxidized Pd. Also shown in Figure 6.1a, 0.3 Pd-0.7 Pt displayed peaks at 2090 cm^{-1} and 1988 cm^{-1} which were assigned to linear and bridged CO adsorption on metallic Pd respectively. Since no Pt features were observed for 0.9 Pd-0.1 Pt or 0.3 Pd-0.7 Pt, we deduced that the Pt atoms were covered with Pd atoms [Todoroki et al., 2009]. However, with different relative IR feature intensities, it is apparent the Pt affects the Pd chemical state.

As shown in Figure 6.1b, 0.05 Pd-0.95 Pt displayed a single peak at 2097 cm^{-1} corresponding to linear CO adsorption on Pt sites. In contrast, 0.15 Pd-0.85 Pt displayed a single peak at 2094 cm^{-1} at ~50 % CO saturation and a peak with a corresponding shoulder, 2094 cm^{-1} and 2076 cm^{-1}, when the sample was completely saturated with CO. The peak at 2095 cm^{-1} was assigned to CO adsorbed linearly on metallic Pt sites. However, the shoulder at 2076 cm^{-1} was associated with bridged CO adsorption on Pd sites [Zhang et al., 2014; Todoroki et al., 2009] near Pt [Lin et al., 1995]. The growth in the Pd-associated feature after the Pt makes sense based on their relative CO poisoning

sensitivities. The saturation results indicate that all of the Pd atoms in 0.15 Pd-0.85 Pt were not fully covered by Pt. Based on these results, it is expected that the bimetallics with at least 30 mol% Pd would display greater similarities to the monometallic Pd catalyst while 0.05 Pd-0.95 Pt would display greater similarity to the monometallic Pt sample. Due to both surface Pd and Pt being detected in 0.15 Pd-0.85 Pt, it was suspected that some contributions from Pd and Pt to the sulfur adsorption and desorption characteristics may be observed. Again, even with similarities in adsorption states, the relative amounts (i.e., bridging, linearly bound) did change with changing Pt or Pd content.

6.3.2 Baseline sulfur desorption assessment

Table 6.2 lists sulfur uptake and release amounts which were measured during the adsorption and subsequent TPD experiments. The following general trends were observed. Larger PM particle size catalysts adsorbed less SO_2 when compared to a broad range of smaller PM particle size catalysts. As the bimetallic catalyst Pt content increased for a particular particle size range, the SO_2 uptake and corresponding release amount decreased. Also, mass balances were nearly closed, with a consistently smaller amount observed desorbing. This could be due to some residual sulfur remaining on the catalyst after the 900 °C TPD exposure. In an effort to determine how Pd:Pt mole ratio specifically affected the type of sulfur species formed and amount of release, TPD profiles of various mole ratio catalysts with similar particle sizes were next compared.

Table 6.2: Adsorbed sulfur amounts with Pd:Pt ratio and particle size

Pd Mole %	Pt Mole %	Particle Size [nm]	Adsorb $[ml_{SO_2}]$	Desorb $[ml_{SO_2}]$	% Adsorbed SO_2 Released During TPD
30	70	1.4	0.156	0.150	96.3
20	80	3.4	0.120	0.113	94.3
50	50	15.2	0.100	0.096	96.6
15	85	15.7	0.084	0.078	92.6
5	95	12.6	0.080	0.077	96.1

The SO_2 TPD profiles of 0.7 Pd-0.3 Pt, 0.2 Pd-0.8 Pt, and 0.15 Pd-0.85 Pt are compared in Figure 6.2.

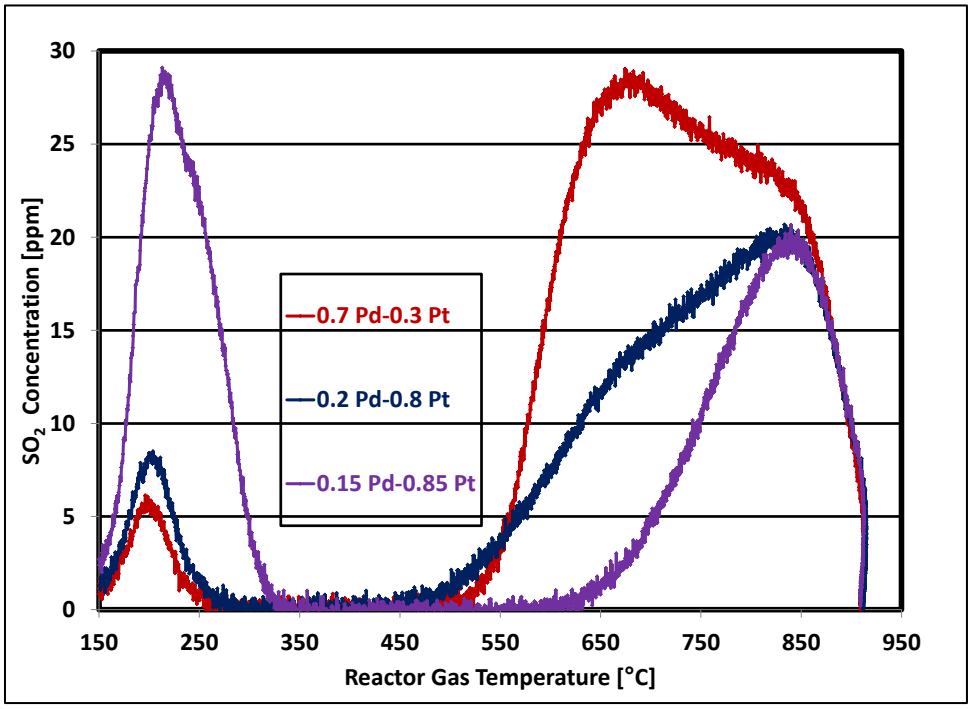

Figure 6.2: SO_2 desorption during TPD in flowing N_2, with a ramp rate of 10 °C/min. The samples had 3 to 4 nm PM particle sizes but different Pd:Pt mole ratios.

The 0.15 Pd-0.85 Pt released the largest amount of low-temperature desorbing species while 0.7 Pd-0.3 Pt released the largest amount of high-temperature desorbing species. In the high-temperature range, the desorption profile of 0.2 Pd-0.8 Pt began at a temperature similar to that of 0.7 Pd-0.3 Pt. On the other hand, the release amount as well as the shape of the desorption profile of this high temperature feature appeared to be an average of the release characteristics associated with 0.7 Pd-0.3 Pt and 0.15 Pd-0.85 Pt. Furthermore, in evaluating the low temperature feature, there is a dramatic change in amount when changing from 0.2 Pd to 0.15 Pd (relative precious metal amount), while there was not much change between 0.7 Pd and 0.2 Pd. These observations identified a potential transition in Pd-dominant release characteristics to Pt-dominant release characteristics. In order to confirm whether the release characteristics of 0.2 Pd-0.8 Pt provided evidence of a transition from general Pd to Pt trends in sulfur release, we studied desorption characteristics of high-Pd content catalysts and low-Pd content catalysts. Here, high-Pd content catalysts were defined as Pd-Pt catalysts containing greater than 0.2 Pd on a precious metal mole basis, and low-Pd content catalysts were defined as Pd-Pt catalysts containing less than 0.2 Pd on a precious metal mole basis.

6.3.3 High-Pd Content Catalyst Sulfur Desorption Assessment

Three SO_2 desorption profiles obtained from high-Pd content catalysts with a 1 to 2 nm particle size range are compared in Figure 6.3. The monometallic Pd catalyst released the largest amount of sulfur species. When compared to Pd, 0.9 Pd-0.1 Pt released the same amount of low-temperature desorbing species but released slightly less high-temperature desorbing species.

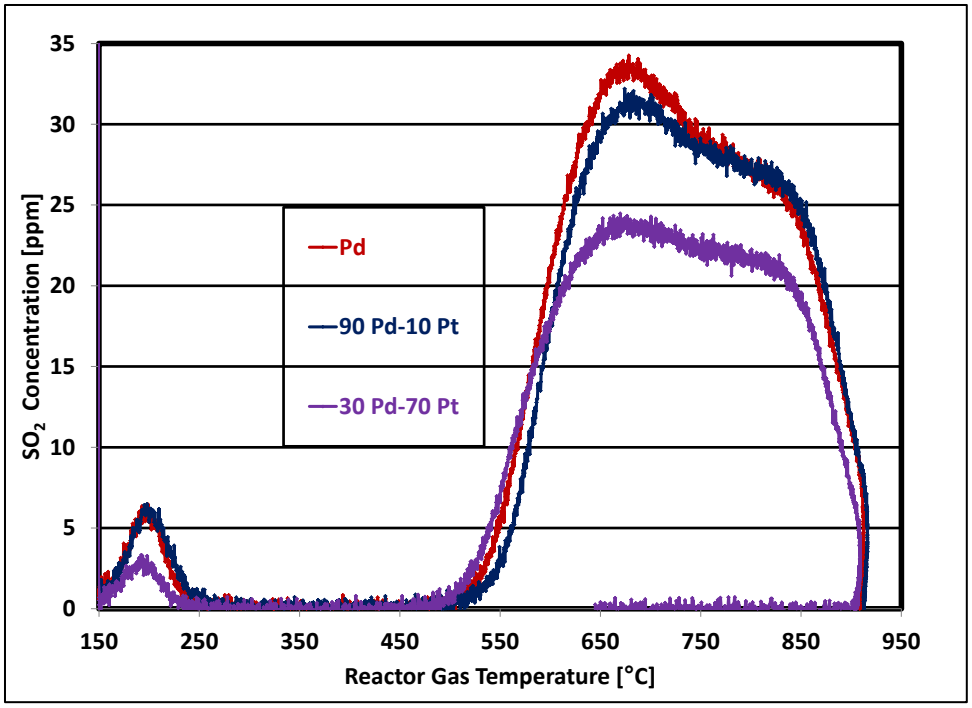

Figure 6.3: SO_2 desorption during TPD in flowing N_2, with a ramp rate of 10 °C/min. The high-Pd content samples had 1 to 2 nm particle sizes.

0.3 Pd-0.7 Pt released slightly less low-temperature desorbing species and significantly less high-temperature desorbing species in comparison to 0.9 Pd-0.1 Pt. The substitution of Pt for Pd in high-Pd-content catalysts resulted in a decrease in the amount of high-temperature desorbing sulfur species and the overall amount of sulfur species released during TPD.

Although the release amounts varied with Pd:Pt mole ratio, the desorption profile of each high-Pd content catalyst contained three distinct desorption peaks. As shown in Table 6.3, via deconvolution, the peak positions associated with the sulfur desorption profile of each high-Pd content catalyst were each located at a similar position. A graphical example of desorption peak locations through deconvolution is shown in Figure 6.4.

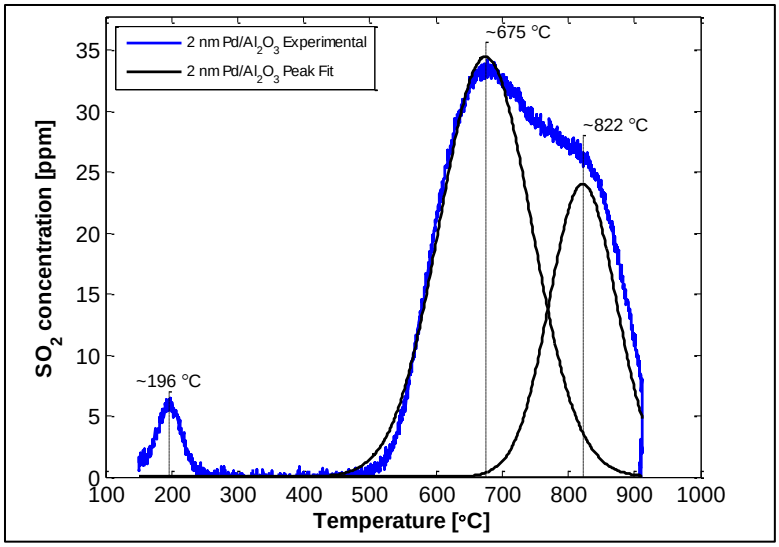

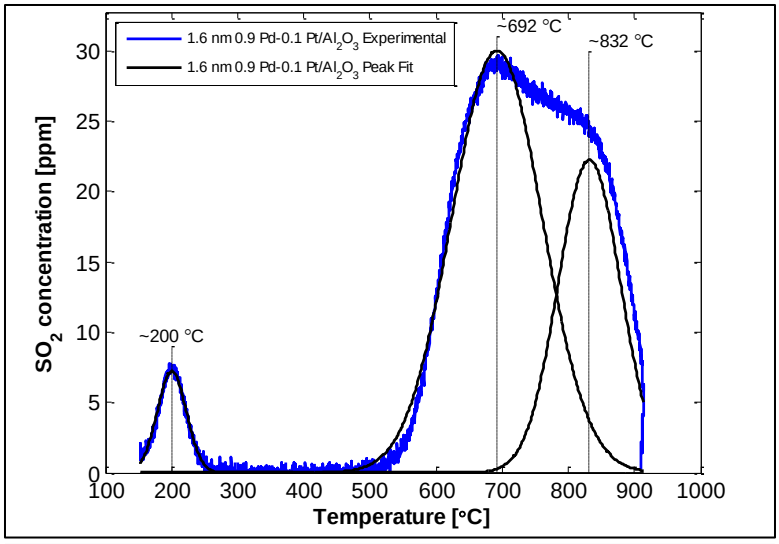

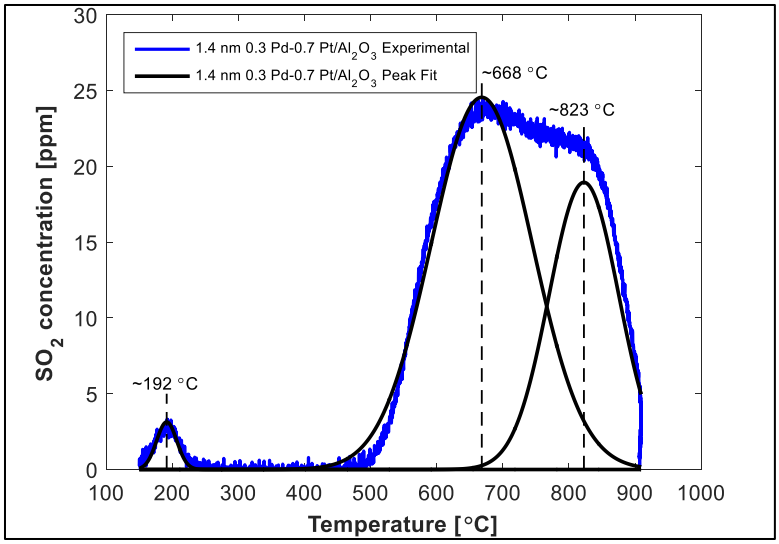

Figure 6.4: Peak deconvolution for 2 nm (a) Pd (b) 0.9 Pd-0.1 Pt (c) 0.3 Pd-0.7 Pt catalysts.

Table 6.3: SO_2 Desorption Peak Positions of High-Pd Content Catalysts

Pd Mole [%]	Pt Mole [%]	Peak 1 [°C]	Peak 2 [°C]	Peak 3 [°C]	Peak 4 [°C]
30	70	192	N/A	668	823
90	10	199	N/A	682	829
100	0	196	N/A	675	822

6.3.4 Low-Pd Content Catalyst Sulfur Desorption Assessment

SO_2 desorption profiles of low-Pd content catalysts, with large, 12 to 15 nm, particle sizes are compared in Figure 6.5. Since higher Pd content samples resulted in smaller particle sizes prior to hydrothermal aging, and were more resistant to sintering during hydrothermal aging, the high-Pd content catalysts in Figure 6.3 contained significantly smaller precious metal particles in comparison to the high Pt content samples. To ensure that any differences in sulfur release characteristics between the high and low-Pd content catalysts were not solely due to precious metal particle size differences, a representative high-Pd content catalyst, 0.5 Pd-0.5 Pt, was included in Figure 6.5 for comparison to low-Pd content catalysts with a similar precious metal particle size. The desorption peak positions are listed in Table 6.4. Upon comparison of Tables 6.3 and 6.4, it is apparent that sulfur did desorb from 0.5 Pd-0.5 Pt at similar temperatures as it did from Pd, 0.9 Pd-0.1 Pt, and 0.3 Pd-0.7 Pt.

As described by the results in Figure 6.5 and Table 6.2, 0.05 Pd-0.95 Pt released slightly more low-temperature desorbing sulfur species, slightly less high-temperature

desorbing species, but a similar overall amount of SO_2 during TPD in comparison to 0.15 Pd-0.85 Pt.

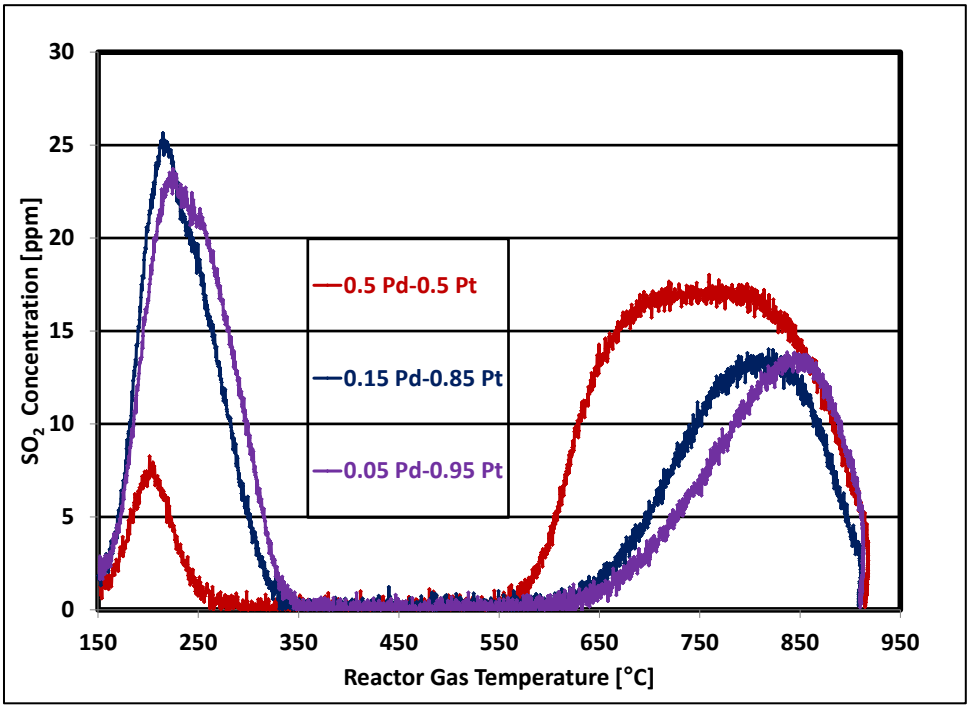

Figure 6.5: SO_2 desorption during TPD in flowing N_2, with a ramp rate of 10 °C/min. The low-Pd content samples and the reference high-Pd content sample had 12 to 15 nm particle sizes.

Table 6.4: Desorption Peak Positions for 12 to 15 nm PM Particle Size Catalysts

Pd Mole [%]	Pt Mole [%]	Peak 1 [°C]	Peak 2 [°C]	Peak 3 [°C]	Peak 4 [°C]
5	95	239	N/A	N/A	823
15	85	215	268	724	817
50	50	203	N/A	694	824

0.5 Pd-0.5 Pt released significantly less low-temperature desorbing sulfur species and significantly more high-temperature desorbing sulfur species when compared to the low-

Pd content catalysts. On the other hand, the overall amount of sulfur release for 0.5 Pd-0.5 Pt was greater than those from the low-Pd content catalysts. Overall, the substitution of Pt for Pd resulted in an increased tendency to form low-temperature desorbing species, a decreased tendency to form high-temperature desorbing species, and reduction in the overall SO_2 sorption when compared to higher Pd content catalysts of a similar precious metal particle size.

6.3.5 Sulfur Adsorption DRIFTS

Similar TPD peak positions obtained with all high-Pd content catalyst samples suggests that high-Pd content catalysts form similar species during SO_2 exposure at 150 °C. However, there was a significant difference in the amount of sulfur species desorbed on a PM mole basis. Similarly, due to the differences in TPD peak positions of 0.15 Pd-0.85 Pt and 0.05 Pd-0.95 Pt, it was unclear whether all low-Pd content catalysts formed the same species during SO_2 exposure. To investigate these differences, representative DRIFTS spectra were collected from SO_2-exposed 0.9 Pd-0.1 Pt, 0.3 Pd-0.7 Pt, 0.15 Pd-0.85 Pt and 0.05 Pd-0.95 Pt catalysts.

DRIFTS spectra obtained from the 0.9 Pd-0.1 Pt and 0.3 Pd-0.7 Pt catalysts after SO_2 exposure at 150 °C are shown in Figure 6.6a. Although both high-Pd content catalysts resulted in similar peaks, 0.3 Pd-0.7 Pt exposure to SO_2 resulted in an additional band near 975 cm^{-1}. At temperatures below 200 °C, when alumina supported catalysts are exposed to SO_2, aluminum surface sulfite species [$Al_2(SO_3)_3$] can form, followed by chemisorption of molecular SO_2 on the alumina surface [Chang, 1978]. After alumina surface saturation with chemisorbed SO_2 and sulfite species, further molecular SO_2 sorption can occur via physisorption on the alumina hydroxyl groups [Datta et al., 1985].

During high-Pd content catalyst exposure to SO_2, aluminum surface sulfite species were formed, which resulted in a wide band from ~1140 cm^{-1} to ~1050 cm^{-1} as well as an additional band at 975 cm^{-1} for 0.3 Pd-0.7 Pt [Datta et al., 1985]. Peaks at ~1272 cm^{-1} and ~1189 cm^{-1} were assigned to chemisorbed molecular SO_2 on alumina [Datta et al., 1985] and peaks at ~1336 cm^{-1} were assigned to physisorbed molecular SO_2 on alumina [Datta et al., 1985; Mitchell et al., 1996].

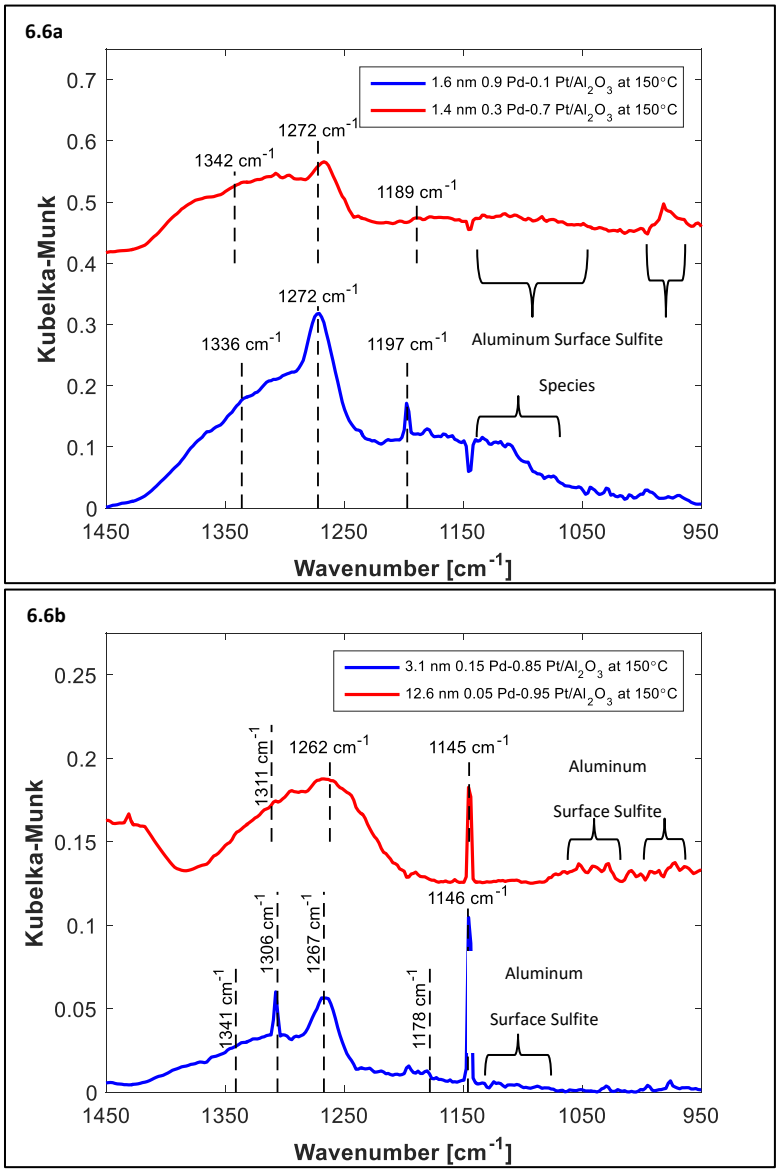

Figure 6.6: SO_2 DRIFTS spectra obtained after exposure to 100 ppm SO_2 and 10 vol. % N_2 in He at 150 °C; (a) high-Pd and (b) low-Pd content catalysts.

With SO_2 exposure at 150 °C, the spectra obtained from the 0.15 Pd-0.85 Pt prior to complete SO_2 saturation, displayed peaks at 1341 cm^{-1}, 1306 cm^{-1}, 1267 cm^{-1}, and 1178 cm^{-1} as well as a low intensity but wide band from ~1140 cm^{-1} to ~1060 cm^{-1}. After these peaks reached steady state in terms of positions and intensity, a narrow peak at 1146 cm^{-1} evolved. Since 0.15 Pd-0.85 Pt appeared to be saturated prior to the evolution of this peak, we deduced that the peak at 1146 cm^{-1} was due to physisorption of molecular SO_2 [Datta et al., 1985; Mitchell et al., 1996]. The wide band from ~1140 cm^{-1} to ~1060 cm^{-1} was assigned to aluminum surface sulfite species [Datta et al., 1985]. The bands at ~1265 cm^{-1} and ~1178 cm^{-1} corresponded to chemisorbed molecular SO_2 on alumina [Datta et al., 1985], and the peaks at 1341 cm^{-1} and 1306 cm^{-1} were assigned to physisorbed molecular SO_2 on alumina [Datta et al., 1985; Mitchell et al., 1996]. The spectrum obtained from the SO_2 exposed 0.05 Pd-0.95 Pt is shown in Figure 6.6b. Similar to 0.15 Pd-0.85 Pt, the peaks at ~1312 cm^{-1} and 1145 cm^{-1} were assigned to physisorbed molecular SO_2 on alumina [Datta et al., 1985; Mitchell et al., 1996], and the peak at ~1265 cm^{-1} was assigned to chemisorbed molecular SO_2 on alumina [Datta et al., 1985]. The wide bands from ~1100 cm^{-1} to ~1000 cm^{-1} [Yu and Shaw, 1998; Datta et al., 1985; Chang, 1978] and ~1000 cm^{-1} to ~950 cm^{-1} [Datta et al., 1985] corresponded to aluminum surface sulfite species.

The spectra collected during 150 °C SO_2 exposure show that both high- and low-Pd content catalysts formed aluminum surface sulfite species in addition to physisorbed and chemisorbed molecular SO_2. On the other hand, when comparing the bands associated with chemisorbed molecular SO_2 and aluminum surface sulfite species, it is visually evident that the high-Pd content catalyst spectra had higher peak intensities in

each of these regions than the low-Pd content catalyst spectra. This observation provides further evidence that the high-Pd content catalysts uptake larger amounts of SO_2 during 150 °C SO_2 exposure.

At temperatures above 300 °C, alumina can oxidize molecular SO_2 or sulfite species to form aluminum sulfate species [$Al_2(SO_4)_3$], including aluminum surface sulfate and bulk aluminum sulfate. Since this oxidation process was possible even in the absence of O2 in the feed stream [Datta et al., 1985], it is possible that the sulfur species adsorbed at 150 °C could be oxidized during the TPD to form sulfate species. Moreover, the presence of the precious metals could catalyze this oxidation at a lower temperature or to a greater extent. To determine if indeed surface transformations occurred during the TPD and to monitor possible decomposition and desorption products, at least to 400 °C, DRIFTS spectra were collected after exposing the samples to SO_2 at 400 °C. Spectra obtained at 400 °C after exposing the 0.9 Pd-0.1 Pt and 0.3 Pd-0.7 Pt samples to SO_2 are shown in Figure 6.7a.

Leading up to saturation of 0.3 Pd-0.7 Pt, the aluminum surface sulfate band position gradually expanded from ~1390 cm^{-1} to ~1413 cm^{-1} along with an increase in peak intensity. Per Waqif et al., as sulfur coverage increases, the band at ~1380 cm^{-1} due to aluminum surface sulfate can broaden, resulting in another peak being detected at ~1410 cm^{-1} [Waqif et al., 1991]. The spectra shown in Figure 6.7 are after saturation and therefore primarily reflect the 1413 cm^{-1} position, assigned to aluminum surface sulfate species [Datta et al., 1995; Waqif et al., 1991; Nam and Gavalas et al., 1989].

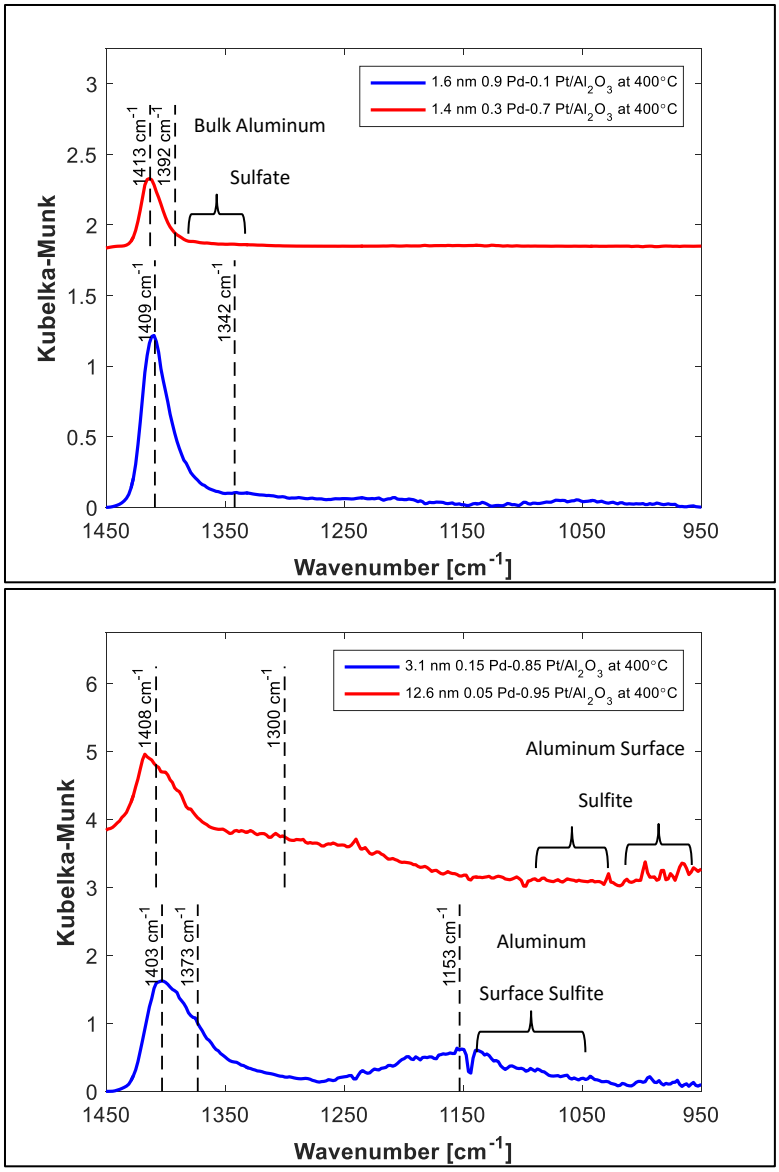

Figure 6.7: SO_2 DRIFTS spectra obtained after exposure to 100 ppm SO_2 and 10 vol. % N_2 in He at 400 °C; (a) high-Pd and (b) low-Pd content catalysts.

Although Bounechada et al. proposed that bands at ~1318 cm^{-1}, 1285 cm^{-1}, and ~1233 cm^{-1} form from bulk aluminum sulfate [Bounechada et al., 2013], some authors have also assigned bands in the 1180 cm^{-1} region [Waqif et al., 1992; Mowery and McCormick, 2001] and 1323 cm^{-1} [Mowery and McCormick, 2001] to bulk-like aluminum sulfate species. During SO_2 oxidation at 500 °C with Pd/Al_2O_3 catalysts, Mowery et al. also

found that palladium sulfate species [$PdSO_4$] were formed and resulted in peaks near ~1240 cm^{-1} and 1100 cm^{-1} [Waqif et al., 1992]. As shown in Figure 6.7a, the 0.9 Pd-0.1 Pt spectrum had a peak 1342 cm^{-1} and the 0.3 Pd-0.7 Pt spectrum had a shoulder band up to ~1300 cm^{-1}, which were both assigned to bulk aluminum sulfate species. It should be noted that no $PdSO_4$ was detected in the spectra collected after SO_2 exposure for high-Pd content catalysts at 400 °C.

In addition to the bands corresponding to aluminum surface sulfite and aluminum surface sulfate species, the spectra obtained from the 0.15 Pd-0.85 Pt and 0.05 Pd-0.95 Pt catalysts exposed to SO_2 at 400 °C displayed peaks at 1153 cm^{-1} and 1300 cm^{-1}. Previous literature [Bounechada et al., 2013; Waqif et al., 1992] has assigned these to bulk aluminum sulfate species.

The spectra collected during 400 °C SO_2 exposure show that both the high- and low-Pd content catalysts formed surface and bulk aluminum sulfate species. However, aluminum surface sulfite species were only detected in the low-Pd content catalysts spectra. This observation provides evidence that the high-Pd content catalysts either a) form aluminum surface sulfite species which completely thermally decompose at temperatures below 400 °C or b) are capable of completely oxidizing aluminum surface sulfite species at 400 °C to form aluminum sulfates.

6.3.6 DRIFTS TPD Characteristics

Although sulfur species formed during SO_2 adsorption at 150 and 400 °C were identified via DRIFTS, this did not provide sufficient evidence to prove whether any oxidation of sulfur species had taken place during the TPD experiments. To help with this aspect, DRIFTS spectra were also collected from a reference catalyst during TPD from

150 °C to 400 °C. Since the 0.15 Pd-0.85 Pt catalyst had two distinct desorption peaks in both the low and high-temperature ranges during the TPD experiments, a SO_2-exposed 0.15 Pd-0.85 Pt catalyst was selected as the reference catalyst for the DRIFTS TPD experiment in an effort to confirm what types of species are being formed and released during the TPD experiments.

After sulfur exposure at 150 °C, the sample temperature was increased to 250 °C and then 400 °C in He, stepwise. Spectra were collected at each temperature and are shown in Figure 6.8.

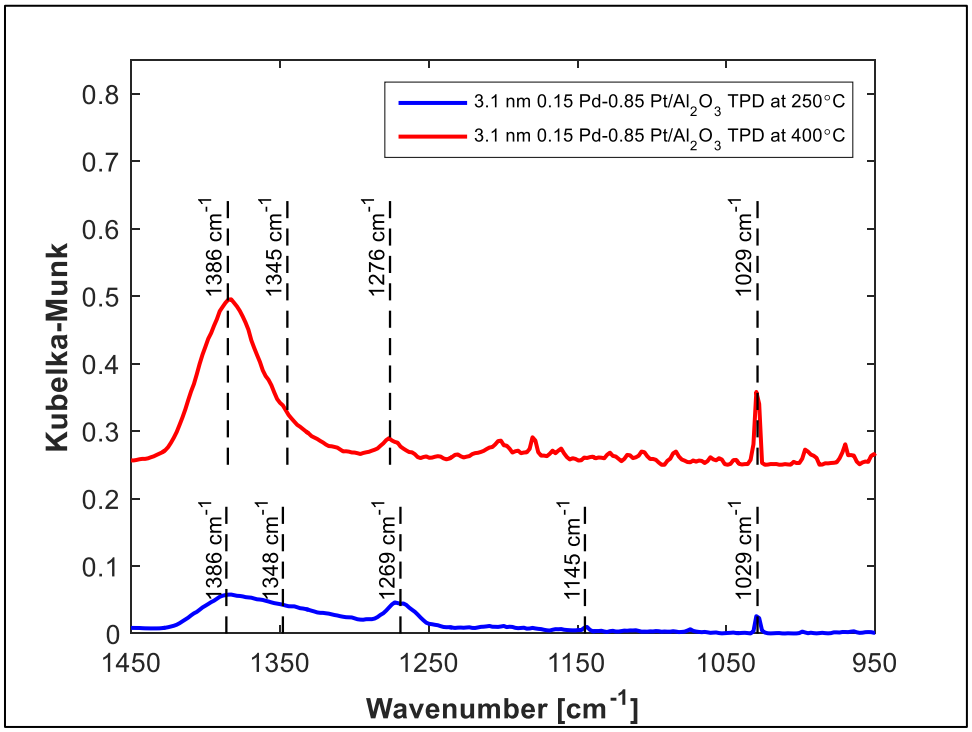

Figure 6.8: SO_2 DRIFTS spectra obtained from the reference bimetallic catalyst during TPD in He at 250 °C and 400 °C.

Per Datta, physisorbed molecular SO_2 is easily removed, and chemisorbed molecular SO_2 is only stable up to ~200 °C [Datta et al., 1985]. For this reason, it was expected that these species would be removed during the TPD from 150 °C to 250 °C. When the

temperature was increased from 150 °C to 250 °C, a peak at 1029 cm^{-1} as well as a wide band from ~1250 to 1150 cm^{-1} appeared and the peak intensities at ~1145 cm^{-1} and 1312 cm^{-1} significantly decreased, due to desorption of physisorbed molecular SO_2 . Also, the peak at 1265 cm^{-1} shifted to 1269 cm^{-1} with a slight decrease in the intensity. Although the intensity of the peak near 1178 cm^{-1} was not significantly reduced, a cumulative view of these decreases in intensity show that weakly and strongly adsorbed molecular SO_2 species were indeed not stable up to 250 °C.

The increase in the band from 1140 cm^{-1} to ~950 cm^{-1} intensity and the new peak at 1029 cm^{-1} provide evidence that some of the molecular SO_2 had been oxidized during the TPD resulting in formation of sulfite and sulfate [Nam and Gavalas et al., 1989; Saur et al., 1986; Piéplu et al., 1998] species on the aluminum surface, respectively. In addition to the evolution of a wide band from ~1250 to 1150 cm^{-1}, an increase in intensity coupled with shifts in peak positions was observed over the ~1400 cm^{-1} to ~1250 cm^{-1} range. The peak at 1345 cm^{-1} demonstrates that oxidation took place due to the formation of surface aluminum sulfate species [Mowery and McCormick, 2001]. Moreover, the broadening of the band near 1200 cm^{-1} corresponded to bulk aluminum sulfate species [Mowery and McCormick, 2001].

Upon increasing the temperature to 400 °C, the intensity of the peak at 1029 cm^{-1} significantly increased, indicating that the aluminum surface sulfite species had been oxidized to form surface sulfate species. While the intensity of the peaks near 1386 cm^{-1} and 1345 cm^{-1} as well as the wide band from ~1250 to 1150 cm^{-1} considerably increased, the peak at 1269 cm^{-1} shifted to 1276 cm^{-1} with a significant decrease in intensity. These data show that the remaining chemisorbed molecular SO_2 was oxidized, resulting in the

decrease in the intensity of the peak at 1276 cm^{-1}. Moreover, an increase in formation of surface sulfate species was evident due to the increase in intensity of the peak at 1386 cm^{-1} and wide band from ~1250 to 1150 cm^{-1}. We postulate that the resultant increase in surface sulfate species coverage facilitated diffusion to the bulk aluminum.

6.3.7 Interpretation of TPD Results from DRIFTS TPD Characteristics

The 0.15 Pd-0.85 Pt DRIFTS TPD data demonstrate that oxidation of sulfur species can occur during TPD and thus during the reactor studies described above. Changes in DRIFTS peak intensities show that chemisorbed molecular SO_2 species were not stable up to 250 °C and aluminum surface sulfate species could be formed below 250 °C. Upon increasing the temperature from 250 °C to 400 °C, the reduction in surface sulfite species and increase in peak intensity of surface and bulk aluminum sulfates showed that sulfite species are primarily decomposed and desorbed or oxidized to form sulfate species above 250 °C.

Although all sulfite and molecular SO_2 species did not completely vanish at 400 °C, there were substantial decreases in surface amounts. In contrast, the sulfate species were still stable. Based on these results, the sulfur species released in the low-temperature range reactor TPD experiments were from molecular SO_2 desorption and decomposition of surface sulfite species. The primary species detected via DRIFTS at 400 °C were sulfate species. Since aluminum surface and bulk sulfates are stable up to 650 °C [Waqif et al., 1991] and 800 °C to 920 °C [Saur et al., 1986] respectively, the sulfur species desorbed in the high- temperature range reactor TPD experiments were due to decomposition of surface and bulk aluminum sulfate species. Per the findings of the 0.15

Pd-0.85 Pt DRIFTS TPD experiment, the peaks for 0.15 Pd-0.85 Pt FTIR TPD experiment were defined as shown in Figure 6.9.

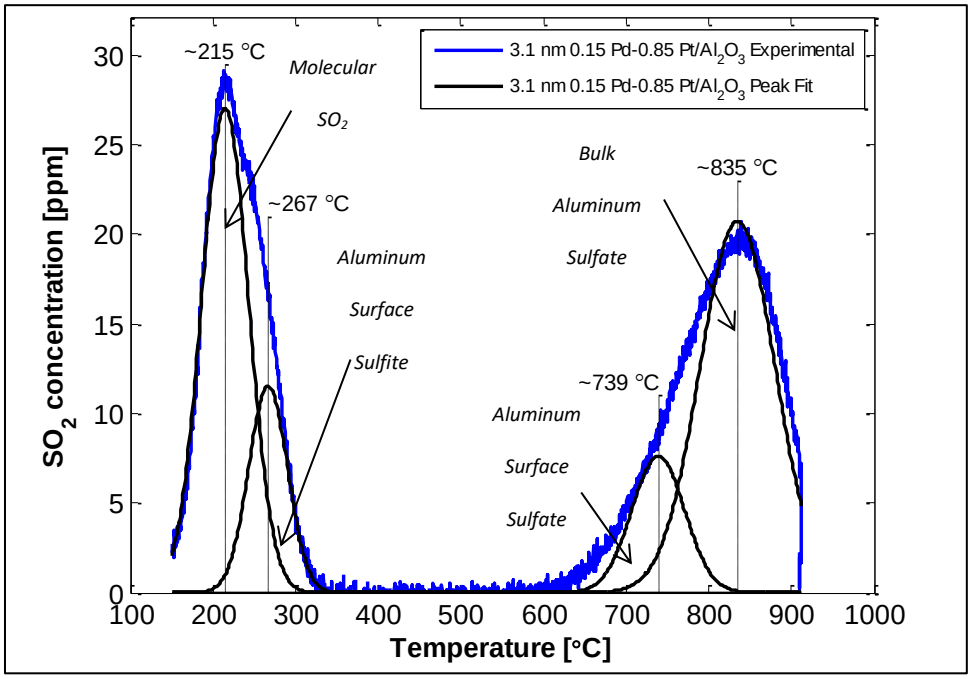

Figure 6.9: SO_2 desorption during TPD in flowing N_2, with a ramp rate of 10 °C/min. TPD Peak Assignment Based on DRIFTS of Reference Bimetallic Catalyst.

The TPD profiles obtained with the high-Pd content catalysts only contained three peaks, thus there were three types of decomposing/desorbing species, whereas low-Pd content catalysts decomposed/released four types of species (Figure 6.5 shows a nice example of the 3 vs 4 peaks). As shown in Figures 6.3 and 6.5, high-Pd content catalysts released a small amount of SO_2 in the low-temperature range, which based on the DRIFTS data shown in Figure 6.6a is molecular SO_2 desorption. It should be noted that the results shown in Figures 6.6a and 6.6b demonstrate that there was molecular SO_2 on alumina and aluminum surface sulfite species formed during SO_2 adsorption at 150 °C. Molecular SO_2 and aluminum surface sulfite species were not detected during SO_2 adsorption at 400 °C, but aluminum surface sulfate species as well as some bulk

aluminum sulfate species were observed. Since the high-Pd content catalysts led to one low temperature TPD feature, they seem capable of completely oxidizing aluminum surface sulfite species at 400 °C to form sulfates.

As shown in Figure 6.5, the low-Pd content catalysts displayed similar sulfur desorption profiles during TPD, although there were definite differences in intensities. Based on the data shown in Figures 6.6b and 6.7b, the low temperature peaks are again associated with molecularly bound SO_2 and surface sulfite species. The DRIFTS data show that the low-Pd content catalysts were not capable of completely oxidizing aluminum surface sulfite species at 400 °C. However, the lack of molecular SO_2 species as well as the increased amount of aluminum surface sulfite detected provided evidence that the low-Pd content catalysts were able to oxidize molecular SO_2 to form stable sulfite species on the aluminum surface at 400 °C. Moreover, when comparing the profiles shown in Figure 6.5 to the peak assignments defined in Figure 6.9, it is evident that more surface sulfite species decomposed below 400 °C on the low-Pd content catalysts during TPD. And less surface sulfate species decomposed during the higher temperature portion of the TPD in comparison to the high-Pd content catalysts. But there was still a significant amount of bulk aluminum sulfate that decomposed over the low Pd content catalysts. Recalling the low activity of low-Pd content catalysts for sulfite oxidation at 400 °C, we inferred that sulfite species on low-Pd content catalysts were more likely to thermally decompose rather than be oxidized during TPD below 400 °C. As a result, less surface sulfate species were formed overall because little sulfite species remained on the surface upon reaching temperatures suitable for oxidation over the low-Pd content catalysts. Considering the evidence of aluminum surface sulfate diffusion to the bulk

aluminum in Figure 6.8, we postulated that as low-Pd content catalysts oxidized some aluminum surface sulfite species to form surface sulfates, which diffused into the bulk aluminum, but did not form a sufficient amount of surface sulfates to thoroughly saturate the bulk aluminum and surface. As a result, primarily bulk aluminum sulfates were decomposed during TPD.

From inspection of Figure 6.2, the 0.2 Pd-0.8 Pt TPD profile appeared to be a combination of the TPD profiles from the high-Pd and low-Pd content catalysts. In comparison to the high-Pd content catalysts, 0.2 Pd-0.8 Pt released a slightly greater amount of low-temperature desorbing species over a similar low-temperature desorption range during the FTIR TPD. Since all high and low-Pd content catalysts were shown to form sulfite species during SO_2 adsorption at 150 °C, 0.2 Pd-0.8 Pt formed aluminum surface sulfite species as well. Due to the lack of SO_2 released in the low-temperature range during FTIR TPD, 0.2 Pd-0.8 Pt was capable of completely oxidizing the sulfite species at low-temperatures, similar to high-Pd content catalysts.

During the reactor TPD experiments, the high-Pd content catalysts released relatively higher levels of SO_2 at high temperatures via surface and bulk aluminum sulfate decomposition. In contrast, the low-Pd content catalysts released a greater amount of low-temperature desorbing species resulting in less species available to undergo oxidation at the higher temperatures. 0.2 Pd-0.8 Pt formed less surface sulfate species in comparison to high-Pd content catalysts but still significantly more than low-Pd content catalysts. Similarly, 0.2 Pd-0.8 Pt formed a similar amount of bulk aluminum sulfate species in comparison to other low-Pd content catalysts. This demonstrates that 0.2 Pd-0.8 Pt had greater proficiency for oxidizing molecular SO_2 and surface sulfite species at

low-temperatures in comparison to the low-Pd content catalysts. However, 0.2 Pd-0.8 Pt did not have the same uptake capability of high-Pd content catalysts resulting in less surface species available to support that oxidation. As a result, the high-temperature region of the reactor TPD profile for 0.2 Pd-0.8 Pt resulted in an averaged high and low-Pd content TPD profiles, which is not surprising based on the CO adsorption characterization data shown in Figures 6.1a and 6.1b.

During CO adsorption, the DRIFTS spectra from catalysts containing 0.3 Pd on a PM mole basis or more, displayed peaks due to CO adsorbed on Pd, none associated with Pt. With the 0.15 Pd-0.85 Pt, minor evidence of Pd was detected, and no Pd was detected for the 0.05 Pd-0.95 Pt catalyst. High-Pd content catalysts should therefore display Pd-dominant characteristics whereas low-Pd content catalysts should display Pt-dominant characteristics and some contribution from Pd. However, it should be noted that the 0.15 Pd-0.85 Pt sulfur release characteristics were quite similar to that of 0.05 Pd-0.95 Pt, i.e., Pt dominant. As a result, the averaged TPD profile of 0.2 Pd-0.8 Pt provides evidence of this transition from Pd-dominant characteristics (0.3 or more Pd on a PM mole basis) to Pt-dominant (0.15 or less Pd on a PM mole basis).

6.4 Conclusions

In order to determine how SO_2 adsorption and release characteristics varied with Pd:Pt mole ratio, it was necessary to categorize and study characteristics of high-Pd content catalysts and low-Pd content catalysts. At 150 °C, all samples formed aluminum surface sulfite species as well as physisorbed and chemisorbed molecular SO_2 on the alumina surface. Low-Pd content catalysts were not only capable of oxidizing molecular

SO_2 species to form aluminum surface sulfite species at 150 °C but these were also still stable at 400 °C. The low-Pd content catalysts were not capable of completely oxidizing sulfite species at temperatures below 400 °C. Failure to form sulfates at lower temperatures resulted in large amounts of SO_2 being released in the low-temperature range of the TPD due to decomposition of some surface sulfite species. In contrast, high-Pd content catalysts were able to completely oxidize sulfites resulting in an abundance of surface and bulk aluminum sulfates. This difference resulted in different relative amounts of low vs high temperature desorbing species. The sulfates being more stable, the high-Pd content catalysts tended to form a great amount of sulfur species which desorbed at high-temperature. In contrast, low-Pd content catalysts tended to form a greater amount of low-temperature desorbing species. In general, it was found that the amount of SO_2 released during TPD decreased with increasing Pt content of Pd:Pt alumina supported catalysts. 0.2 Pd-0.8 Pt marked the transition point from general Pd to Pt trends in sulfur release characteristics.

Chapter 7 SO_2 Adsorption and Desorption Characteristics of Pd and Pt catalysts: Precious metal crystallite size dependence

Note: The material in this chapter has been submitted for publication. Therefore the introduction and experimental methodology may appear redundant with other sections. Reference and figure numbers were changed for dissertation consistency.

7.1 Introduction

Natural gas, which primarily consists of methane, is commonly viewed as a lower emission producing fuel in comparison to gasoline and diesel [Abbasi et al., 2012]. Methane, which is not combusted in the engine, needs to be mitigated and can be combusted over an oxidation catalyst placed in the exhaust stream [Trimm and Lee, 1995; Burch and Loader, 1994; Cullis and Willatt, 1983; Mouaddib et al., 1992]. Natural gas vehicle exhaust temperatures can be as low as 300 °C [Abbasi et al., 2012; Stodolsky and Santini, 1992], making complete conversion challenging. The exhaust can also contain sulfur, a poison to many oxidation catalysts, deactivating the catalyst and reducing the extent of methane conversion [Yamamoto and Uchida, 1998].

Researchers found that alumina-supported bimetallic Pt/Pd catalysts resulted in higher activity with time on stream in comparison to monometallic Pt and Pd catalysts [Yamamoto and Uchida, 1998; Lapisardi et al., 2007]. This improvement was maintained

when exposed to sulfur [Yamamoto and Uchida, 1998] and water [Yamamoto and Uchida, 1998; Lapisardi et al., 2007]. Electron micrographs of fresh $Pd_{0.65}Pt_{0.35}/Al_2O_3$ samples displayed evidence of very small particles in Pt-rich regions and large particles in Pd-rich regions. After these catalyst samples were aged in steam at 600 °C, only large particles were observed. The authors concluded that the Pt-containing catalysts sintered when exposed to steam at high temperatures [Lapisardi et al., 2007].

Researchers also found that smaller Pd particles are more easily oxidized to form PdO in comparison to larger Pd particles [Müller et al., 1997], and for Pt-based catalysts, oxygen adsorbed on larger Pt particles is more reactive than oxygen on smaller Pt particles [Briot et al., 1990]. For these reasons, sintered Pt particles are more active for complete methane oxidation [Briot et al., 1990] whereas the PdO activity decays upon sintering [Lyubovsky et al., 1998] resulting in less methane conversion. In high-Pd content bimetallic catalysts, the interaction between PdO and Pt weakens the Pd-O bond such that PdO forms at higher temperatures and decomposes at lower temperatures in comparison to the PdO in monometallic Pd catalysts. This feature also affects how easily the PdO surface forms oxygen vacancies, which are known to promote PdO activity in the methane oxidation reaction. Lapisardi et al. postulated that bimetallic catalysts are more resistant to sintering because these oxygen vacancies are made with greater ease for bimetallics than those for monometallic Pd [Lapisardi et al., 2007]. These results form some basis in evaluating thermal degradation effects. However, the relationship between sulfur poisoning impact and particle size has not been studied.The work discussed in this paper focuses on what species are formed during Pd and Pt catalyst exposure to SO_2 and their stability as a function of temperature. Initial experiments demonstrated that in order

to understand why sulfur release characteristics varied with precious metal (PM) particle size, it was imperative that the Pd:Pt mole ratio contribution be decoupled. For this reason, the sulfur release characteristics due to particle size effects were studied independently by conducting SO_2 adsorption and temperature-programmed desorption (TPD) studies on catalysts with the same Pd:Pt mole ratios.

7.2 Experimental Methods

7.2.1 Catalyst preparation and experimental set-up

The $Pd(NO_3)$ and $Pt(NH_3)_4(NO_3)_2$ precursors as well as the Puralox γ-Al_2O_3 were purchased from Sigma-Aldrich. The incipient wetness impregnation method was used for mono- and bimetallic Pd-Pt/Al_2O_3 powder catalysts synthesis. The total number of precious metal moles was kept constant for all catalysts using a 1 wt. % Pd/Al_2O_3 catalyst as a basis of reference for precious metal content. All samples were dried overnight and calcined in air at 550 °C. A bimetallic sample, $Pd_{0.5}Pt_{0.5}/Al_2O_3$, was also prepared, using co-impregnation with the same precursors and procedure.

Each catalyst was aged under the following flow conditions: 1.8 vol. % H_2O and 10 vol. % O_2 in N_2. To achieve the target PM particle size for a given experiment, the aging duration and temperature was varied from 8 to 90 hours and 700 °C to 750 °C respectively. After the aging period, the reactor was kept at the aging temperature for an additional 30 minutes while the reactor was purged with N_2 to minimize the residual H_2O and O_2 content within the catalyst bed and reactor system lines. The reactor system lines were kept at 150 °C to 180 °C in order to prevent water and sulfur species deposition on the lines.

7.2.2 Particle size measurements

After aging, all samples were reduced at 400 °C under a 5 vol. % H_2 in N_2 flow stream. Following reduction, the reactor was cooled to 35 °C. Using a Valco pulse injection valve, 10 μL doses of CO were injected into the reactor at regular intervals. When the injection pulse-signature ceased to change with each additional CO pulse injection, the sample was considered saturated. After saturation was achieved, the total volume of CO adsorbed was used to determine the sample PM dispersion, surface area, and corresponding particle size. The CO injection pulse was measured using an MKS FTIR 2030.

7.2.3 Temperature-programmed desorption (TPD)

The aged catalysts were exposed to 30 ppm SO_2 in N_2 at 150 °C until saturation. After saturation, which typically took ~1 hour, the reactor was purged with N_2 at 150 °C for an additional 15 minutes to minimize the residual SO_2 content within the reactor system lines and detach weakly adsorbed SO_2 from the catalyst surface. TPD was then performed, with a ramp rate of 10 °C /minute to 900 °C followed by a hold at 900 °C for an additional 15 minutes. Gas concentration measurements were made with an MKS FTIR 2030.

7.2.4 Diffuse reflectance infrared Fourier transform spectroscopy (DRIFTS) characterization

Background spectra were gathered in 50 ml/min of He only at 35 °C, 150 °C, 250 °C, and 400 °C. The background spectra were subtracted from their corresponding spectra obtained at each temperature in the following experiments.

After aging in the reactor, catalysts were then transferred to the Harrick Scientific Praying Mantis DRIFTS cell for an oxidation cleaning at 100 °C with 10 vol. % O_2 in He for 5 minutes. The catalyst then underwent a reduction pretreatment at 400 °C with 5 vol. % H_2 in He for 30 minutes. After the reduction pretreatment, the sample was maintained at 400 °C for an additional 30 minutes while the cell was purged with He to minimize the residual H_2 content within the catalyst and DRIFTS system lines. The catalyst was then cooled to approximately 35 °C and exposed to 1 vol. % CO and 10 vol. % N_2 in He until CO saturation as determined by a lack of change in the collected DRIFTS spectra. The CO adsorption spectrum of each sample was analyzed and compared to that of a sample with the same catalyst composition but different particle size in an effort to assign peaks as well as confirm types of sites and relative PM particle sizes involved in adsorption.

Each catalyst was exposed to 100 ppm SO_2 and 10 vol. % N_2 in He at 150 °C until saturation, which typically took ~3 hours. The same procedure was repeated but at 400 °C, per the TPD data to be reviewed below. Another set of samples was exposed to 100 ppm SO_2 and 10 vol. % N_2 in He at 150 °C until saturation. The system was then purged with He prior to increasing the sample temperature to 250 °C, where spectra were collected. The sample temperature was further increased to 400 °C where more spectra were collected. The desorption spectra were obtained after the DRIFTS spectra ceased to change at each temperature. The desorption temperatures, 250 °C and 400 °C, were selected based on sulfur release termination in the low-temperature range during TPD experiments, to be discussed below.

7.3 Experimental results and discussion

7.3.1 Baseline sulfur desorption assessment

Table 7.1 lists example sulfur uptake and release amounts which were measured during the adsorption and subsequent TPD experiments for three of the samples examined. Regardless of catalyst Pd:Pt composition and PM particle size, mass balances were nearly closed. Residual sulfur remaining on the catalyst after the 900 °C TPD exposure could have resulted in the consistently smaller amount observed desorbing. The SO_2 uptake amount varied for these three samples, each having a different metal content and particle size. In an effort to determine how particle size specifically affected the type of sulfur species formed and amount of release, adsorption and TPD profiles of catalysts with the same metal content but differing particle sizes were compared.

The SO_2 TPD profiles obtained when evaluating the 0.5 Pd-0.5 Pt sample with 3.6 nm, 15.2 nm, and 34.3 nm metal particle sizes are compared in Figure 7.1.

Table 7.1: Adsorbed sulfur amounts with Pd:Pt ratio and particle size

Pd Mole %	Pt Mole %	Particle Size [nm]	Adsorb $[\mu mol_{SO_2}]$	Desorb $[\mu mol_{SO_2}]$	% Adsorbed SO_2 Released During TPD
0	100	3.9	3.694	3.324	90.0
50	50	15.2	4.444	4.292	96.6
100	0	27.8	2.619	2.418	92.3

The 3.6 nm sample released the largest amount of high-temperature desorbing species while the 15.2 nm and 34.3 nm samples released the largest amounts of low-temperature desorbing species. In the high-temperature range, the desorption profile of the 15.2 nm sample began at a temperature similar to that of the 34.3 nm sample. On the other hand, the release amount as well as the desorption profile shape of this high temperature feature were different. These observations identified a potential transition in small PM particle size release characteristics to large PM particle size release characteristics. In order to confirm whether the release characteristics of 15.2 nm 0.5 Pd-0.5 Pt sample provided evidence of a transition from generally small to large particle size trends in sulfur release, we studied desorption characteristics of monometallic Pd and Pt catalysts with various metal particle sizes.

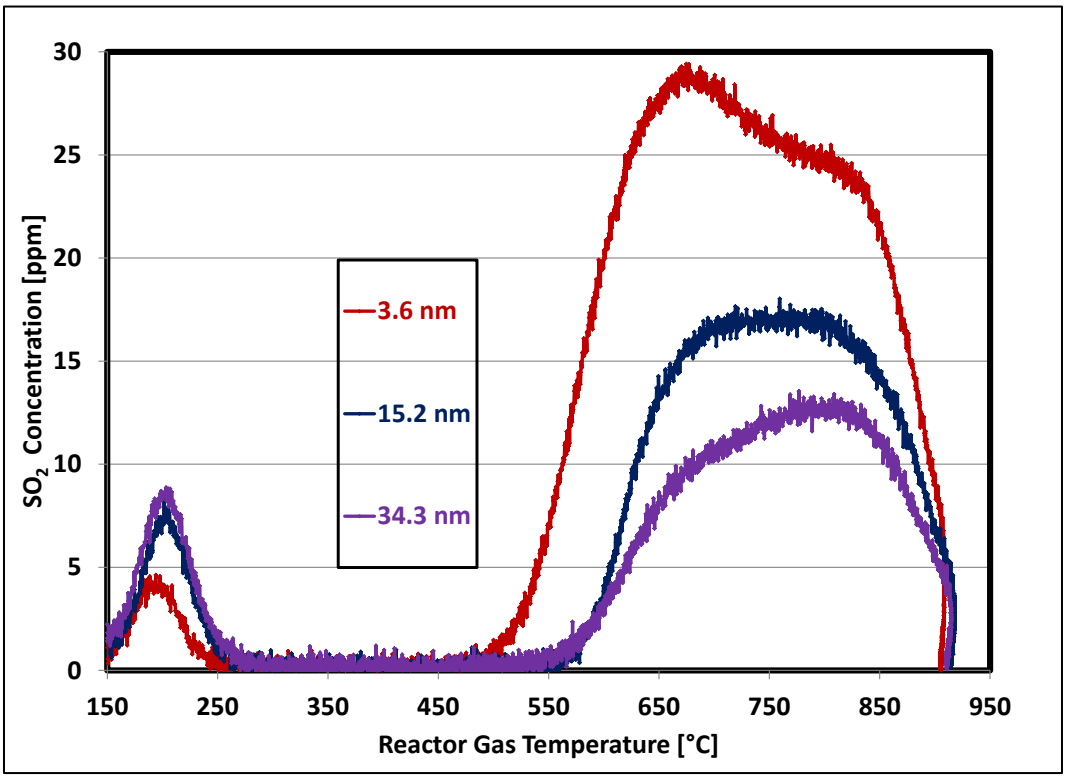

Figure 7.1: SO_2 desorption during TPD in flowing N_2, with a ramp rate of 10 °C/min. The 0.5 Pd-0.5 Pt/Al_2O_3 samples had different PM particle sizes.

7.3.2 CO chemisorption characterization

All catalysts characterized underwent hydrothermal aging for various durations to achieve different particle sizes and a reduction pretreatment prior to adsorption experiments. This approach helped ensure that the only factors influencing the desorption profiles were the mole ratio and particle size. The sample catalyst Pd:Pt mole ratios as well as the metallic surface areas and particle sizes, determined by CO chemisorption, are listed in Table 7.2.

Table 7.2: Particle sizes and surface areas determined via CO chemisorption

Pd Mole %	Pt Mole %	Particle Size	Metal Surface Area [m^2/g Pd-Pt]
100	0	2.0 nm	253.0
100	0	8.0 nm	62.8
100	0	27.8 nm	18.0
50	50	3.4 nm	64.6
50	50	15.2 nm	15.5
50	50	34.2 nm	6.8
0	100	3.9 nm	37.2
0	100	6.4 nm	24.3
0	100	10.4 nm	14.9

Here we first discuss DRIFTS characterization of CO adsorption. The 3.9 nm monometallic Pt sample spectrum (Figure 7.2a) displayed a peak at 2094 cm^{-1} and a broad band from 1908 to 1830 cm^{-1}. The 2 nm monometallic Pd sample spectrum (Figure

7.2b) displayed peaks at 2088 cm^{-1}, 1997 cm^{-1}, and 1936 cm^{-1}. After extended hydrothermal aging, the 27.8 nm monometallic Pd displayed peaks at 2093 cm^{-1}, 2000 cm^{-1}, and 1947 cm^{-1} whereas the 10.4 nm monometallic Pt sample spectrum exhibited a peak at 2097 cm^{-1} and a low intensity band from ~1908 to 1830 cm^{-1}.

Due to the similarities in the CO adsorption features obtained from 3.9 nm and 10.4 nm Pt catalysts, the peaks are related to the same Pt sites and thus generic assignments can be made. The peak near ~2094 cm^{-1} was assigned to CO linearly adsorbed on Pt sites [Todoroki et al., 2009; Boubnov et al., 2013]. The broad band from ~1908 to 1830 cm^{-1} corresponded to CO adsorbed on metallic Pt in a bridged manner [Zhang et al., 2014; Bensalem et al.; 1996; Martinez-Arias et al., 2004]. The 10.4 nm Pt peaks were narrower and less intense in comparison to those observed for 3.9 nm Pt, demonstrating that indeed increasing the Pt particle size resulted in less CO uptake.

When the CO adsorption features obtained from 2 nm and 27.8 nm Pd catalysts were compared, again little evidence of shifts in peak wavenumbers was observed. CO linearly adsorbed on metallic Pd (Pd^0-CO) [Zhang et al., 2014; Bensalem et al., 1996; Martinez-Arias et al., 2004] and CO bridged across two metallic Pd atoms [Zhang et al., 2014; Martinez-Arias et al., 2004] resulted in the ~2088 cm^{-1} and ~1997 cm^{-1} bands respectively. The peak at ~1936 cm^{-1} was designated as CO bridged across two partially oxidized Pd atoms (Pd^+-CO) [Todoroki et al., 2009; Zhang et al., 2014; Toshima et al., 2001]. Since the 27.8 nm Pd had a larger peak intensity near 2000 cm^{-1} but a narrower peak width and smaller peak intensity near 2093 cm^{-1} when compared to the 2 nm Pd, increasing the Pd particle size not only resulted in less CO uptake but also more bridged adsorption sites. As both the Pd and Pt catalysts adsorb less CO as the PM particle size

increased, and there were some differences in relative amounts, we suspected particle size could also influence SO_2 uptake and corresponding TPD release characteristics.

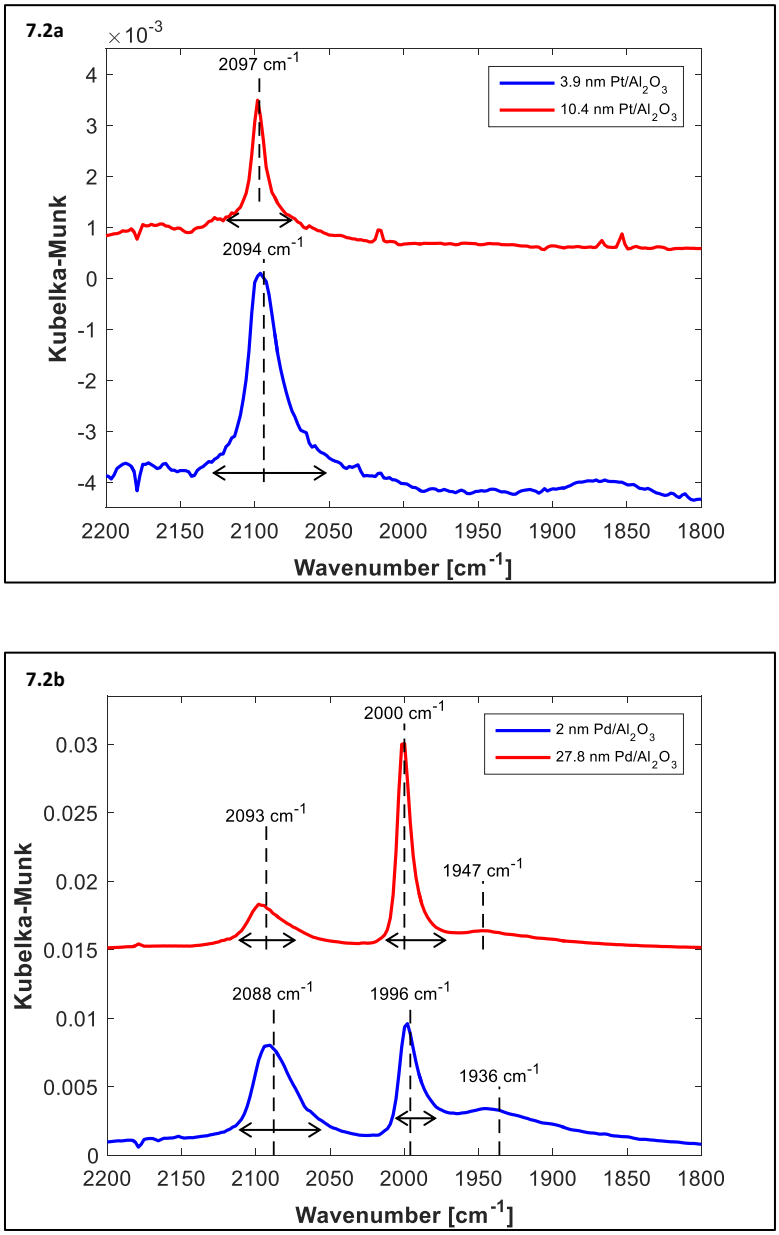

Figure 7.2: DRIFTS spectra obtained after a saturation CO exposure at 35 °C for two PM particle sizes each of (a) Pt/Al_2O_3 catalysts and (b) Pd/Al_2O_3 catalysts.

7.3.3 Pt/Al_2O_3 TPD after SO_2 Exposure

SO_2 desorption profiles and release amounts for 3.9 nm, 6.4 nm, and 10.4 nm Pt/Al_2O_3 catalysts are compared in Figure 7.3 and Table 7.3.

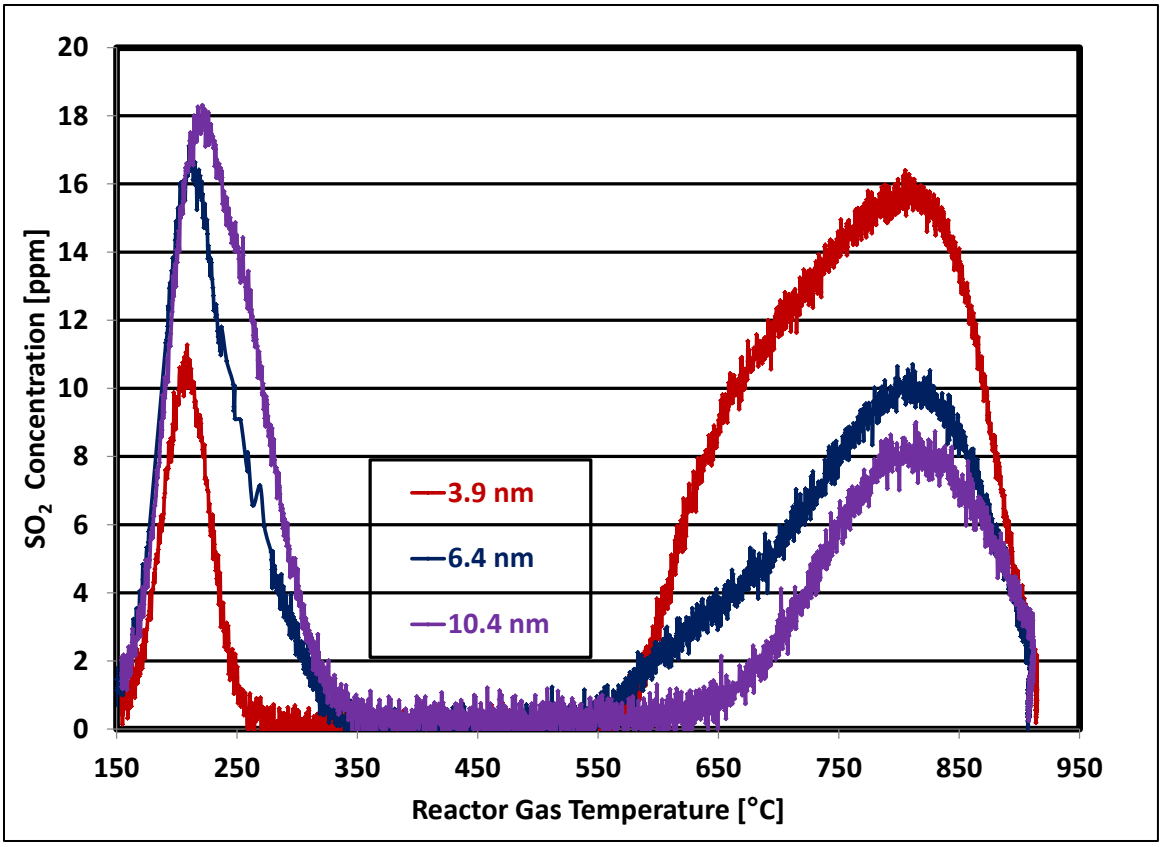

Figure 7.3: SO_2 desorption from three Pt/Al_2O_3 samples during TPD in flowing N_2, with a ramp rate of 10 °C/min. Each was saturated with SO_2 prior to the TPD.

Table 7.3: SO_2 Desorption Amounts and TPD Peak Positions of Pt/Al_2O_3 Catalysts

Pd Mole [%]	Pt Mole [%]	Particle Size [nm]	Desorb [μmol_{SO_2}]	Peak 1 [°C]	Peak 2 [°C]	Peak 3 [°C]	Peak 4 [°C]
0	100	3.9	3.32	207	N/A	707	826
0	100	6.4	2.95	214	281	664	805
0	100	10.4	2.34	231	N/A	N/A	805

The 3.9 nm Pt, having the largest metallic surface area, released the largest total amount of sulfur and the largest amount of high-temperature desorbing species. The 6.4 nm Pt released a greater amount of low-temperature desorbing species but released less total sulfur in comparison to the 3.9 nm Pt. In the high-temperature range, the 3.9 and 6.4 nm Pt desorption profiles contained two distinct peaks, and their release began at a similar temperatures. These desorption profile features suggest that the same species are thermally decomposing at high temperatures. The low-temperature region desorption profiles for 6.4 and 10.4 nm Pt spanned a similar temperature range. However, the 10.4 nm Pt sample, having the smallest metallic surface, released more low-temperature desorbing sulfur species and less high-temperature desorbing species in comparison to the 6.4 nm Pt sample. Overall, an increase in PM particle size for Pt/Al_2O_3 catalysts was accompanied with an increased tendency to form low-temperature desorbing species, a decreased tendency to form high-temperature decomposing species, and a reduction in the overall SO_2 sorption amount. As shown in Table 7.3, these variations in release characteristics also resulted in shifting peak maximum positions for the Pt/Al_2O_3 sulfur desorption profiles, likely due to the combination of different coverage extents and desorption rates.

7.3.4 Pd/Al_2O_3 TPD after SO_2 exposure

SO_2 desorption profiles and release amounts from 2 nm, 8 nm, and 27.8 nm particle size Pd catalysts are compared in Table 7.4 and Figure 7.4. The largest metallic surface area Pd catalyst, possessing a 2 nm particle size, released the largest total amount of sulfur species.

Table 7.4: SO_2 Desorption Amounts and TPD Peak Positions of Pd/Al_2O_3 Catalysts

Pd Mole [%]	Pt Mole [%]	Particle Size [nm]	Desorb [μmol_{SO_2}]	Peak 1 [°C]	Peak 2 [°C]	Peak 3 [°C]	Peak 4 [°C]
100	0	2.0	8.602	196	N/A	675	822
100	0	8.0	4.506	199	N/A	704	820
100	0	27.8	2.418	214	N/A	N/A	793

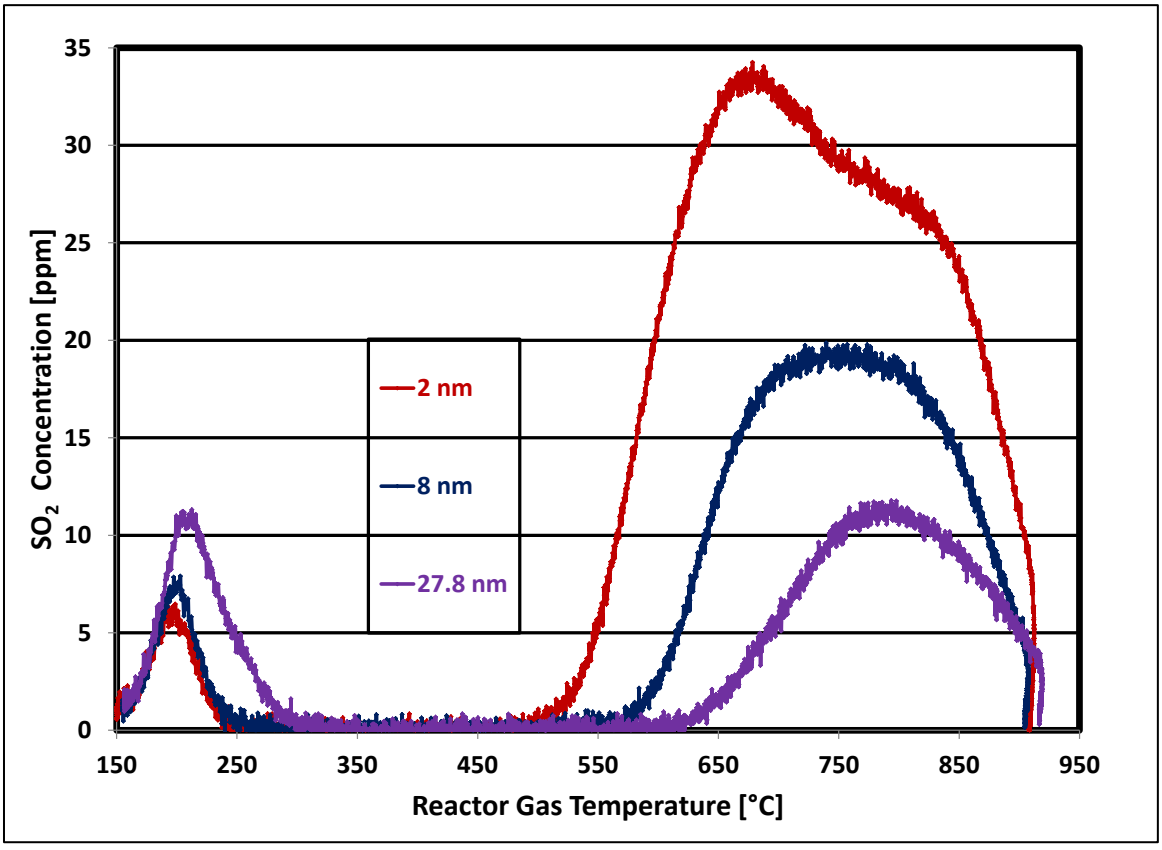

Figure 7.4: SO_2 desorption from three Pd/Al_2O_3 samples during TPD in flowing N_2, with a ramp rate of 10 °C/min. The samples were saturated with SO_2 prior to TPD.

When compared to the 2 nm Pd, the 8 nm Pd released a similar amount of low-temperature desorbing species but released significantly less high-temperature decomposing species. The 27.8 nm Pd released more low-temperature desorbing species and significantly less high-temperature desorbing species in comparison to the 2 and 8 nm Pd catalysts. Like the Pt samples, an increase in Pd/Al_2O_3 catalyst PM particle size resulted in decreased sulfur sorption, a decreased sulfur release amount at high temperatures, and a corresponding change in TPD peak quantity and peak position, as shown in Table 7.4.

7.3.5 Sulfur Adsorption DRIFTS

There were significant differences in the amount of sulfur species desorbed and changes in temperature regions where desorption occurred on a PM particle size basis. To investigate these differences, representative DRIFTS spectra were collected from 3.9 nm and 10.4 nm Pt catalysts as well as 2 nm and 27.8 nm Pd catalysts after exposure to SO_2 (Figures 7.5a and 7.5b respectively).

DRIFTS spectra obtained from the 3.9 nm and 10.4 nm Pt catalysts after SO_2 exposure at 150 °C are shown in Figure 7.5a. At temperatures below 200 °C, when alumina supported catalysts are exposed to SO_2, aluminum surface sulfite species $[Al_2(SO_3)_3]$ form, followed by chemisorption and physisorption of molecular SO_2 on the aluminum surface and hydroxyl groups respectively [Datta et al., 1985]. During Pt catalyst SO_2 exposure, aluminum surface sulfite species were formed, which resulted in wide bands from ~1130 cm^{-1} to ~1060 cm^{-1} and ~1040 to 950 cm^{-1} for 3.9 nm Pt as well as a peak at 1044 cm^{-1} for 10.4 nm Pt [Datta et al., 1985].

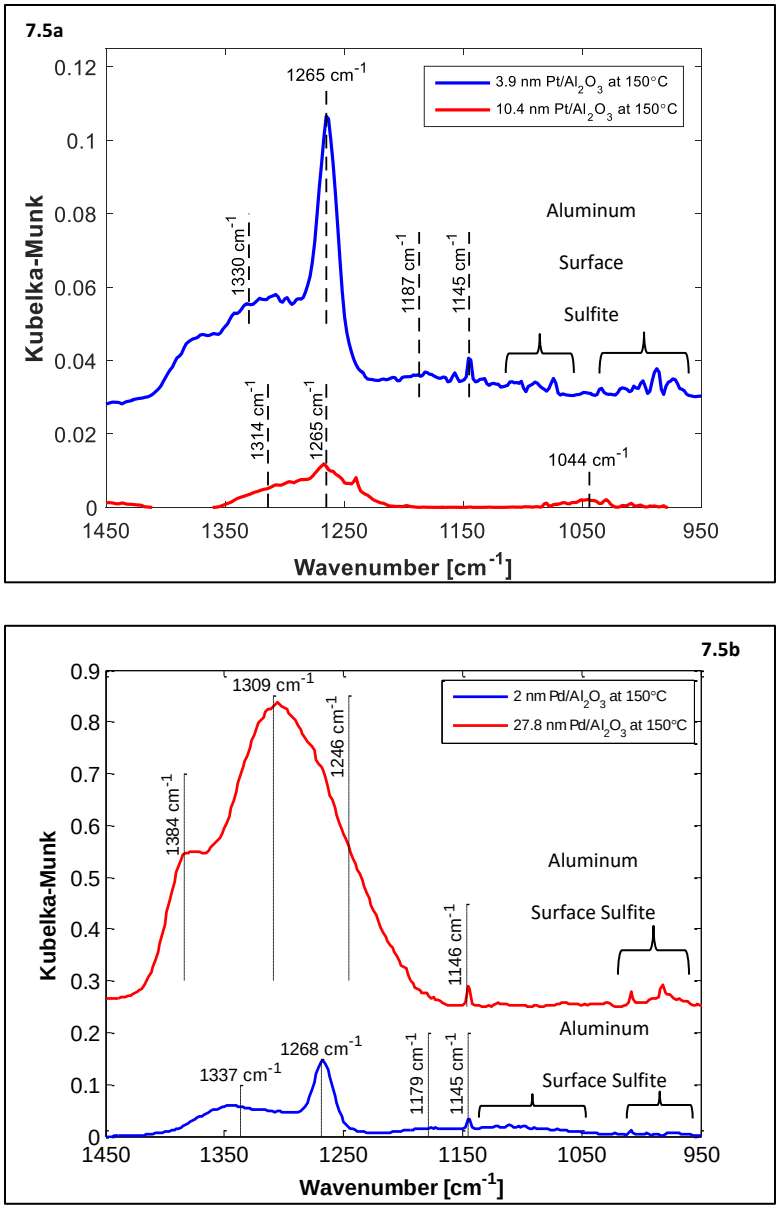

Figure 7.5: DRIFTS spectra obtained after exposure to 100 ppm SO_2 and 10 vol. % N_2 in He at 150 °C; (a) Pt/Al_2O_3 catalysts and (b) Pd/Al_2O_3 catalysts.

For SO_2-exposed 3.9 nm Pt, peaks at 1265 cm^{-1} and 1187 cm^{-1} were assigned to chemisorbed molecular SO_2 on alumina [Datta et al., 1985], and peaks at 1330 cm^{-1} and 1145 cm^{-1} were assigned to physisorbed molecular SO_2 on alumina [Datta et al., 1985,Mitchell et al., 1996]. Spectra obtained from the SO_2 exposed 10.4 nm Pt contained low intensity peaks at 1265 cm^{-1} and 1314 cm^{-1}, which were assigned to chemisorbed

molecular SO_2 on alumina [Datta et al., 1985] and physisorbed molecular SO_2 on alumina [Datta et al., 1985], respectively. After comparing spectra from the 3.9 nm and 10.4 nm Pt catalysts, we confirmed that smaller Pt particle size catalysts adsorbed more SO_2 at 150 °C in comparison to larger Pt particle catalysts and found that Pt catalysts did not form sulfate species at 150 °C.

With 150 °C SO_2 exposure, the spectra obtained from the 2 nm and 27.8 nm Pd samples (Figure 7.5b) displayed wide bands from ~1025 cm^{-1} to ~950 cm^{-1}, and the 2 nm Pd sample spectrum contained an additional band from ~1140 cm^{-1} to ~1050 cm^{-1}. The bands from ~1140 cm^{-1} to ~1050 cm^{-1} and ~1025 cm^{-1} to ~950 cm^{-1} correspond to aluminum surface sulfite species [Datta et al., 1985].

The spectrum from the 2 nm Pd sample also displayed peaks at 1337 cm^{-1}, 1268 cm^{-1}, 1179 cm^{-1}, and 1145 cm^{-1} whereas the 27.8 nm Pd spectrum contained peaks at 1384 cm^{-1}, 1309 cm^{-1}, 1246 cm^{-1}, and 1146 cm^{-1}. For 2 nm Pd, the peaks at 1337 cm^{-1} and 1145 cm^{-1} were assigned to physisorbed molecular SO_2 on alumina [Datta et al., 1985,Mitchell et al., 1996], and the peaks at 1179 cm^{-1} and 1268 cm^{-1} corresponded to chemisorbed molecular SO_2 on alumina [Datta et al., 1985]. For the 27.8 nm Pd sample, the peaks at 1309 cm^{-1} and 1146 cm^{-1} were assigned to physisorbed molecular SO_2 on alumina, but no chemisorbed molecular SO_2 species were observed. Rather, the peak at 1384 cm^{-1} corresponded to aluminum surface sulfate species [Chang, 1978; Waqif et al., 1991; Boubnov et al., 2013] whereas the peak at 1246 cm^{-1} was assigned to palladium sulfate [$PdSO_4$] species [Mowery and McCormick, 2001].

The spectra collected during 150 °C SO_2 exposure show that Pt/Al_2O_3 and Pd/Al_2O_3 catalysts, regardless of PM particle size, formed aluminum surface sulfite

species and physisorbed molecular SO_2. In terms of amounts, when comparing the bands associated with chemisorbed molecular SO_2 and aluminum surface sulfite species in the 3.9 nm Pt and 10.4 nm Pt catalyst spectra, the smaller particle size sample spectrum had larger peak intensities in each of these regions compared to the 10.4 nm Pt catalyst. This observation provides further evidence that the smaller particle size catalysts, for a given Pd:Pt mole ratio, result in more SO_2 uptake during 150 °C SO_2 exposure. When comparing the spectra collected from the SO_2-exposed Pd catalysts, the 27.8 nm Pd spectrum contained bands associated with aluminum surface sulfite, aluminum surface sulfate, and $PdSO_4$ species, but no chemisorbed molecular SO_2 bands were observed. In contrast, no sulfate species were formed during 150 °C SO_2 exposure for the 2 nm Pd catalyst, but chemisorbed molecular SO_2 and aluminum surface sulfite species were detected. Mowery et al. proposed that SO_2 [Mowery and McCormick, 2001] which adsorbs on PdO will be oxidized to form SO_3 and subsequently either a) forms sulfates on PdO or b) spills over to the alumina support. Although we initially reduced our samples, some partially oxidized Pd sites were detected during CO adsorption (Figure 7.2b). We postulate that Pd sites were at least partially reoxidized as a result of increasing the sample temperature, in the presence of the alumina support, in preparation for 150 °C SO_2 exposure, thus allowing Pd sulfate formation.

The 150 °C SO_2 exposure DRIFTS data showed that the larger Pd particle size catalyst was more likely to form aluminum surface sulfite and sulfate species at 150 °C in comparison to smaller Pd particle catalysts. From the increase in SO_2 sorption with decreasing Pd particle size (Figure 7.2b and Table 7.4), we inferred that smaller Pd particle catalysts will uptake more SO_2, which will have more opportunity for spillover to

the support due to the higher dispersion. In contrast, larger Pd particle size catalysts will adsorb less SO_2, and with less interfacial area between the metal and support as well, this results in less opportunity for spillover to the support. Also, per CO DRIFTS data, the larger particles have more bridged sites and thus may provide some stability to the adsorbed S species slowing spillover to the support. As a result, formed SO_3 is either further oxidized to form $PdSO_4$ or spills over to the support when the Pd surface is saturated with sulfur species. As a result, $PdSO_4$ as well as aluminum surface sulfite and sulfate species were observed during 150 °C SO_2 exposure for 27.8 nm Pd.

The presence of oxygen in the feed stream is unnecessary for alumina to oxidize molecular SO_2 or sulfite species to form surface and bulk aluminum sulfate species [$Al_2(SO_4)_3$] at temperatures above 300 °C [Smirnov et al., 2005]. We suspect that the sulfur species adsorbed at 150 °C were oxidized during the TPD to form sulfate species. Moreover, precious metals supported on alumina could facilitate this oxidation process to a higher degree or at a lower temperature, as observed during 150 °C sulfur exposure for 27.8 nm Pd. To determine what products result if surface conversions really occurred during the TPD and to examine possible decomposition and desorption products below 400 °C, DRIFTS spectra were collected after exposing the catalysts to SO_2 at 400 °C (Figures 7.6a and 7.6b).

Spectra obtained at 400 °C after exposing 3.9 and 10.4 nm Pt samples to SO_2 are shown in Figure 7.6a. Upon saturation, spectra from 3.9 nm Pt displayed peaks at 1399 cm^{-1} and 1223 cm^{-1} as well as a broad band from ~1000 cm^{-1} to ~950 cm^{-1}. The peak at 1399 cm^{-1} and the band from ~1000 cm^{-1} to ~950 cm^{-1} were associated with aluminum surface sulfate [Boubnov et al., 2013; Chang, 1978; Waqif et al., 1991] and sulfite [Datta

et al., 1985] species respectively. Per Bounechada et al. [Bounechada et al., 2013], bulk aluminum sulfate species gave rise to the peak at 1223 cm^{-1}. Similarly the 10.4 nm Pt spectrum contained a broad band from ~1200 to 1300 cm^{-1} which we assigned to bulk aluminum sulfate species [Bounechada et al., 2013]. Approaching saturation of 10.4 nm Pt, the aluminum surface sulfate bands gradually grew with associated shift in peaks from ~1373 cm^{-1} to ~1380 cm^{-1} as well as ~1402 cm^{-1} to ~1411 cm^{-1}. Per Waqif et al., as sulfur coverage increases, the band at ~1380 cm^{-1} due to aluminum surface sulfate can stretch and can even result in an another peak being detected at ~1410 cm^{-1} [Waqif et al., 1991]. The spectra shown in Figure 7.6a are after saturation and therefore primarily reflect aluminum surface sulfate species at the ~1411 cm^{-1} site [Boubnov et al., 2013; Chang, 1978; Waqif et al., 1991].

Spectra from the SO_2-exposed 27.8 nm Pd catalyst contained peaks at 1407 cm^{-1}, 1380 cm^{-1}, and 1279 cm^{-1} as well as a broad band from ~1000 to ~950 cm^{-1} whereas the 2 nm Pd spectrum displayed peaks at 1408 cm^{-1}, 1242 cm^{-1}, and 1074 cm^{-1} as well as a broad band from ~1000 to ~950 cm^{-1} (Figure 7.6b). The peaks in the ~1408 to ~1380 cm^{-1} range as well as the band from ~1000 to ~950 cm^{-1} were assigned to aluminum surface sulfate [Boubnov et al., 2013; Chang, 1978; Waqif et al., 1991] and sulfite [Datta et al., 1985] species respectively. The 27.8 nm Pd spectrum also displayed a peak at 1279 cm^{-1}, corresponding to bulk aluminum sulfate species [Bounechada et al., 2013]. Mowery et al. found that $PdSO_4$ species form during SO_2 oxidation at 500 °C, resulting in peaks near ~1240 cm^{-1} and 1100 cm^{-1} [Mowery and McCormick, 2001]. As shown in Figure 7.6b, the 2 nm Pd spectrum displayed a peak at 1242 cm^{-1}, which was assigned to $PdSO_4$

species. Note, no $PdSO_4$ was detected in the 27.8 nm Pd spectrum during SO_2 exposure at 400 °C but was detected during the 150 °C SO_2 exposure.

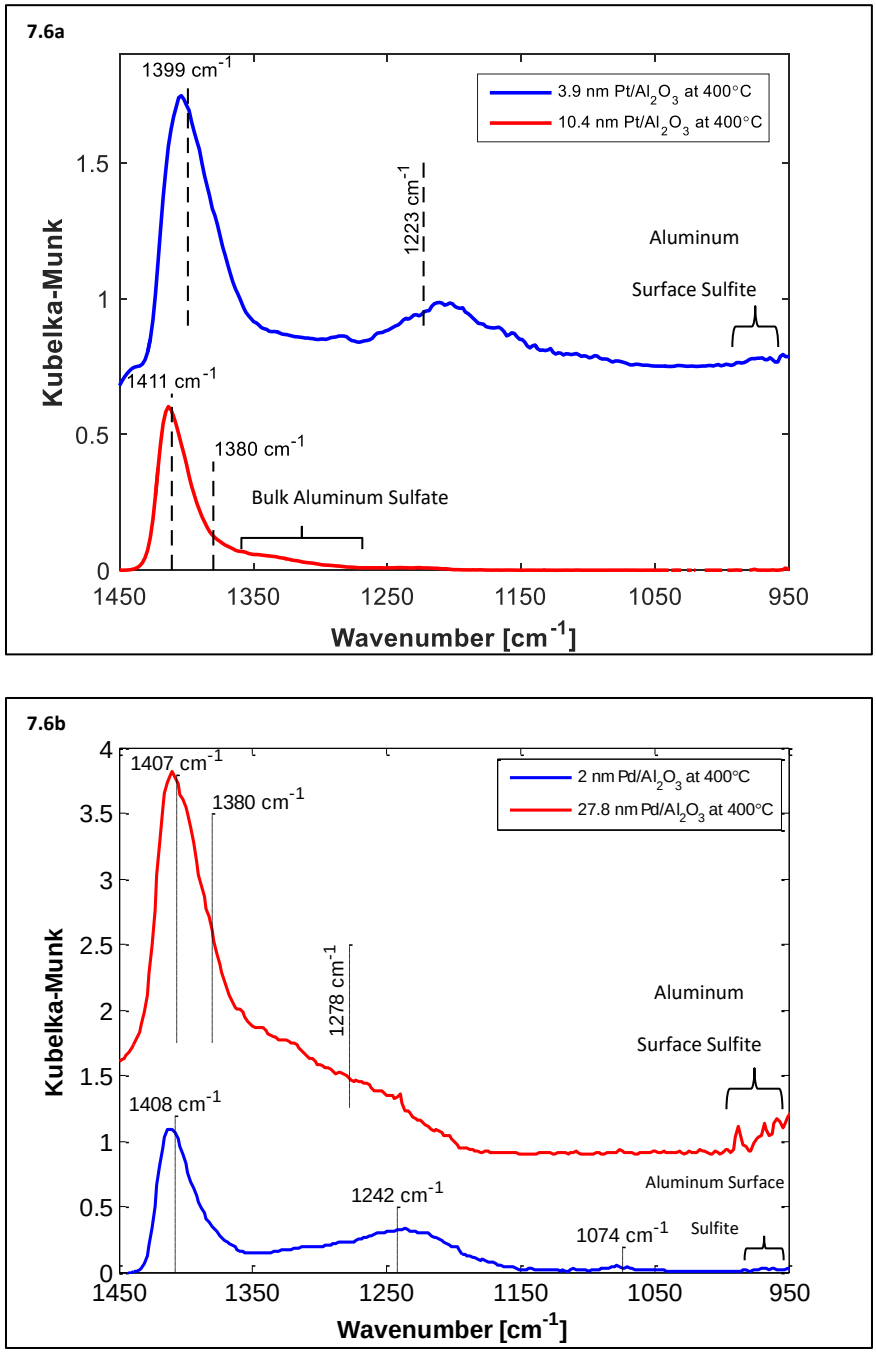

Figure 7.6: DRIFTS spectra obtained after exposure to 100 ppm SO_2 and 10 vol. % N_2 in He at 400 °C; (a) Pt/Al_2O_3 catalysts and (b) Pd/Al_2O_3 catalysts.

The spectra collected during 400 °C SO_2 exposure show that both the 3.9 nm and 10.4 nm Pt/Al_2O_3 catalysts formed surface and bulk aluminum sulfate species. However, aluminum surface sulfite species were not detected in the 10.4 nm Pt spectra. This observation provides evidence that larger particle size Pt catalysts either a) form aluminum surface sulfite species, which completely thermally decompose at temperatures below 400 °C or b) are capable of completely oxidizing aluminum surface sulfite species by 400 °C to form aluminum sulfates.

In contrast, monometallic Pd/Al_2O_3 catalysts are not capable of completely oxidizing or decomposing aluminum surface sulfite species at 400 °C, regardless of particle size. The 400 °C SO_2 exposure spectra show that the 2 nm Pd sample formed aluminum surface sulfates and $PdSO_4$ but no bulk aluminum sulfates, whereas the 27.8 nm Pd formed surface and bulk aluminum sulfates but not $PdSO_4$. It should be noted that the 27.8 nm Pd catalyst formed $PdSO_4$ during 150 °C SO_2 exposure. The lack of $PdSO_4$ on 27.8 nm Pd at 400 °C provides evidence that $PdSO_4$ species formed on larger Pd particle size catalysts either a) are not stable up to 400 °C and sulfur desorbed or b) decomposed and the sulfur migrated to alumina.

7.3.6 DRIFTS TPD Characteristics

Although sulfur species formed during SO_2 adsorption at 150 and 400 °C were identified via DRIFTS, this did not provide direct proof that sulfur species were oxidized during the TPD experiments or what products were formed. Moreover, with spillover of sulfur species from PdO to the alumina support [Mowery and McCormick, 2001] the sulfation rate for PdO should be low. We inferred that the sulfation rate should be especially low and spillover rate should be especially high for small Pd particle size

catalysts, which have greater contact area between the PdO and alumina support. Recalling that 2 nm Pd only formed $PdSO_4$ during exposure to SO_2 at 400 °C but not at 150 °C, it was unclear whether SO_3 formed on both the alumina and PdO during the TPD. If SO_3 did indeed form on small PdO particles, it was still unclear whether any SO_3 diffused to the support prior to being oxidized or formed $PdSO_4$ during TPD. To help resolve these aspects, DRIFTS spectra were also collected from the 3.9 nm Pt and 2 nm Pd samples during TPD from 150 °C to 400 °C.

After SO_2 exposure at 150 °C, the sample temperature was set to 250 °C and then 400 °C in He, stepwise. Figure 7.7a displays the spectra collected at each temperature for 3.9 nm Pt. Since physisorbed molecular SO_2 is easily detached and chemisorbed molecular SO_2 is not stable above ~200 °C [Datta et al., 1985], we expected that these species would be removed during the TPD from 150 °C to 250 °C. When the temperature was increased from 150 °C to 250 °C, the peaks at 1145 cm^{-1} and 1330 cm^{-1} disappeared, due to loss of physisorbed molecular SO_2 desorption. The bands corresponding to aluminum surface sulfite species, ~1130 cm^{-1} to ~1060 cm^{-1} and ~1040 to 950 cm^{-1}, and the peaks assigned to chemisorbed molecular SO_2 on alumina, 1265 cm^{-1} and 1187 cm^{-1}, also disappeared. An overall view of spectral changes shows that weakly and strongly adsorbed molecular SO_2 species were definitely not stable up to 250 °C. The evolution of new peaks at 1391 cm^{-1} and 1107 cm^{-1} with a shoulder at 1255 cm^{-1} provide evidence that some of the molecular SO_2 and aluminum surface sulfite species were oxidized during the TPD resulting in formation of sulfate [Mitchell et al., 1996; Saur et al., 1986; Piéplu et al., 1998] species on the aluminum surface. The low intensity peak at 1391 cm^{-1} corresponded to aluminum surface sulfate species [Bounechada et al., 2013].

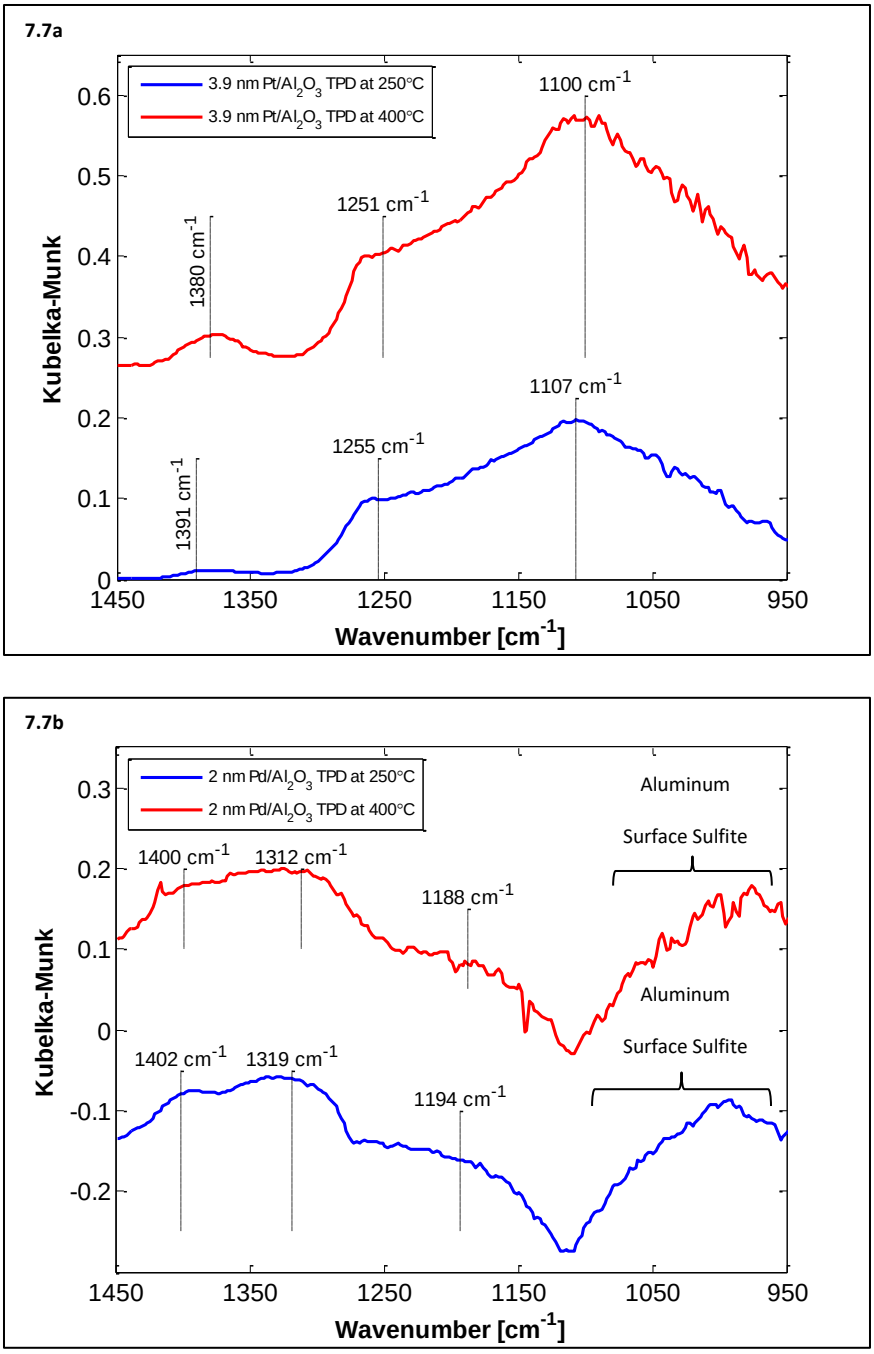

Figure 7.7: DRIFTS spectra obtained from a) 3.9 nm Pt and b) 2 nm Pd catalysts during TPD in He at 250 °C and 400 °C after exposure to SO_2 at 150 °C.

The intense peak at 1107 cm^{-1} was assigned to bulk aluminum sulfate species, due to the shoulder at 1255 cm^{-1} [Mitchell et al., 1996]. Upon increasing the temperature to 400 °C, the peaks at 1391 cm^{-1} and 1107 cm^{-1} as well as the shoulder at 1255 cm^{-1} shifted to 1380

cm^{-1}, 1100 cm^{-1}, and 1251 cm^{-1} respectively. These data show that the sulfate species formed by Pt catalysts are stable and minimal diffusion occurred during the 3.9 nm Pt TPD up to 400 °C.

After the 150 °C SO_2 exposure, the 2 nm Pd sample temperature was increased to 250 °C and then 400 °C in He, stepwise. Figure 7.7b contains spectra corresponding to each temperature. When the temperature was increased from 150 °C to 250 °C, physisorbed molecular SO_2 species were removed resulting in the disappearance of peaks at 1145 cm^{-1} and 1337 cm^{-1}. The peaks assigned to chemisorbed molecular SO_2 on alumina, 1268 cm^{-1} and 1179 cm^{-1}, also disappeared while the bands corresponding to aluminum surface sulfite species, ~1140 cm^{-1} to ~1050 cm^{-1} and ~1025 to 950 cm^{-1}, shifted and combined to form a single, intense broad band from 1100 cm^{-1} to ~950 cm^{-1}. A cumulative view of these changes shows that weakly and strongly adsorbed molecular SO_2 species were again not stable up to 250 °C. The increased intensity in aluminum surface sulfite band as well as the evolution of new peaks at 1402 cm^{-1}, 1319 cm^{-1}, and 1194 cm^{-1} provide evidence that some of the molecular SO_2 and aluminum surface sulfite species had been oxidized during the 2 nm Pd TPD to 250 °C resulting in formation of aluminum surface sulfite and aluminum sulfate [Mitchell et al., 1996; Saur et al., 1986; Piéplu et al., 1998] species correspondingly. The peak at 1402 cm^{-1} as well as the peaks at 1319 cm^{-1} and 1194 cm^{-1} were assigned to surface [Bounechada et al., 2013] and bulk aluminum sulfate species [Mowery and McCormick, 2001; Bounechada et al., 2013] respectively.

Upon increasing the 2 nm Pd sample temperature to 400 °C, the band from 1100 cm^{-1} to ~950 cm^{-1} remained intact while the peaks at 1402 cm^{-1}, 1319 cm^{-1}, and 1194 cm^{-}

[1] shifted to 1400 cm^{-1}, 1312 cm^{-1}, and 1188 cm^{-1} respectively. These data show that the sulfate species were stable and minimal diffusion occurred during 2 nm Pd TPD from 250 °C to 400 °C. Also, these data confirm that the 2 nm Pd is not capable of completely oxidizing the aluminum surface sulfite species to form sulfates at 400 °C. It should also be noted that 2 nm Pd formed aluminum surface sulfates and $PdSO_4$ but no bulk aluminum sulfates during 400 °C SO_2 exposure whereas surface and bulk aluminum sulfates but no $PdSO_4$ species were observed during TPD to 400 °C. Recalling that the 2 nm Pd sample was reduced prior to SO_2 exposure, few PdO sites were present during the 150 °C SO_2 exposure. As a result, less SO_3 could be formed on the Pd particles. Rather, SO_2 was more likely to adsorb on the aluminum surface and be oxidized to form aluminum surface sulfites and later be further oxidized to form surface and bulk aluminum sulfates during the TPD. In this case, no $PdSO_4$ would be detected in the DRIFTS but aluminum sulfates detection would be likely. In contrast, we postulate that the 2 nm Pd sample exposed to SO_2 at 400 °C contained more PdO sites due to sample reoxidation, which occurred during the temperature ramp to 400 °C maybe via the alumina support. More PdO sites being present during 400 °C SO_2 exposure resulted in more SO_3 being produced on the Pd particles with subsequent oxidation to form $PdSO_4$ or spillover to the alumina support to form aluminum surface sulfates.

7.3.7 Interpretation of TPD results from DRIFTS TPD characteristics

Based on the DRIFTS from the 3.9 nm Pt and 2 nm Pd TPD experiments, physisorbed and chemisorbed molecular SO_2 on alumina are not stable up to 250 °C resulting in the low-temperature range SO_2 released during the reactor TPD experiments. TPD DRIFTS up to 250 °C also showed that some of the molecular SO_2 and aluminum

surface sulfite species had been oxidized during the TPD resulting in formation of aluminum sulfates. These sulfate species were stable during DRIFTS TPD up to 400 °C. Since aluminum surface and bulk sulfates are stable up to 650 °C [Waqif et al., 1991] and 800 °C to 920 °C [Saur et al., 1986] respectively, the sulfur species desorbed in the high-temperature range reactor TPD experiments were due surface and bulk aluminum sulfate decomposition. Per the findings of the 3.9 nm Pt and 2 nm Pd DRIFTS TPD experiments, the peaks for 3.9 nm Pt and 2 nm Pd reactor TPD experiments were defined as shown in Figure 7.8a and 7.8b respectively.

As shown in Figure 7.3 and Table 7.3, the Pt catalysts displayed sulfur TPD profiles containing two to four distinct peaks depending on particle size. Based on the data shown in Figure 7.6a, the low temperature peaks are associated with molecularly bound SO_2 and possibly surface sulfite species. Recalling the low activity of Pt catalysts for sulfite oxidation at 150 °C and the large SO_2 release during the low-temperature range reactor TPD experiments for the 6.4 and 10.4 nm Pt, we conclude that aluminum sulfite species formed on larger Pt particles are prone to thermally decompose during TPD rather than be oxidized to form sulfates below 400 °C. As a result, the low-temperature range SO_2 release quantity and temperature span both increased as the Pt particle size increased. Since little sulfite species remained on the surface upon reaching temperatures suitable for oxidation over the Pt catalysts, less sulfates were formed overall resulting in reduced sulfur species decomposition at high temperatures. Considering the lack in evidence of aluminum surface sulfate diffusion to bulk aluminum (Figure 7.7a) and lower total SO_2 uptake on 10.4 Pt in comparison to 3.9 nm Pt (Figure 7.6a), we postulate that Pt catalysts still oxidized some aluminum surface sulfite species to form surface sulfates,

but as the particle size increased Pt catalysts did not form a sufficient amount of surface sulfates to thoroughly saturate the bulk aluminum and surface.

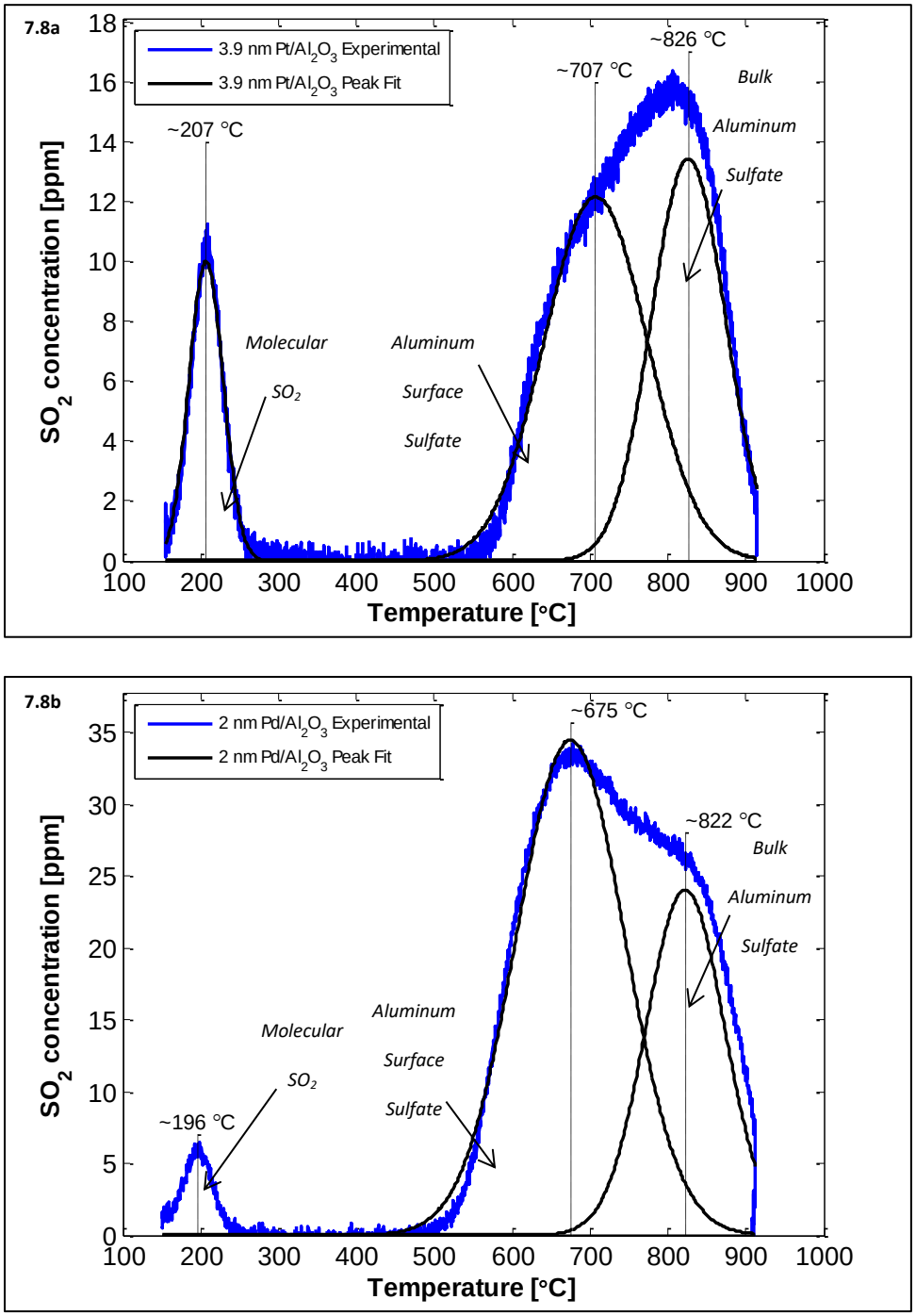

Figure 7.8: SO_2 desorption during TPD in flowing N_2, with a ramp rate of 10 °C/min. a) 3.9 nm Pt and b) 2 nm Pd TPD peak assignments based on DRIFTS analysis.

As a result, primarily bulk aluminum sulfates were decomposed for large particle size Pt samples during the high-temperature range TPD.

Since aluminum surface sulfite species were detected using DRIFTS during the 27.8 nm Pd 400 °C SO_2 exposure, we concluded that larger Pd particles are more likely to form aluminum surface sulfite species which oxidize to form sulfates during TPD above 400 °C rather than thermally decompose during TPD up to 400 °C. As observed in the 2 nm Pd TPD DRIFTS spectrum (Figure 7.7b), there was still evidence for the presence of sulfite species at 400 °C, but there were decreased surface amounts. In contrast, the sulfate species were still stable. Based on these results, the sulfur species released in the low-temperature range reactor TPD experiment for 2 nm Pd were from molecular SO_2 desorption, and the high-temperature range release was due to decomposition of surface and bulk aluminum sulfate species as shown in Figure 7.8b.

The TPD profiles obtained with the Pd catalysts contained three distinct peaks for the 2 nm and 8 nm Pd particles and two distinct peaks for the 27.8 nm Pd particles. As shown in Figure 7.4, the 2 nm and 8nm Pd catalysts released a small amount of SO_2 in the low-temperature range, which based on the DRIFTS data shown in Figure 7.6b was molecular SO_2 desorption. The 27.8 nm Pd released a larger amount of SO_2 in the low-temperature range, which spanned a larger temperature range. We believe that the intense and broad peak in the low-temperature range 27.8 nm Pd TPD contained contributions from two species, the surface sulfites decomposing and the molecularly bound SO_2 desorbing. Since the small Pd particle catalysts led to one low-temperature TPD feature and their aluminum surface sulfite species were still stable at 400 °C during the DRIFTS TPD, they seem more likely to completely oxidize aluminum surface sulfite species to

form sulfates during the TPD. However, the low-temperature TPD feature observed during the 27.8 nm Pd TPD appears to result from mixture of desorbed molecular SO_2 and decomposed aluminum surface sulfite species. Large particle size Pd catalysts seem to decompose some aluminum surface sulfite species as well as be capable of oxidizing some aluminum surface sulfite species to form sulfates during the TPD (Figure 7.5).

Due to the lack in evidence of aluminum surface sulfate diffusion to the bulk aluminum in Figure 7.7b and the reduction in total SO_2 uptake for 27.8 nm Pd in comparison to 2 nm Pd (Figure 7.6b) sample, we postulate that the Pd catalysts, like Pt catalysts, did not form a sufficient amount of surface sulfates to thoroughly saturate the bulk aluminum and surface as the Pd particle size increased. As a result, primarily bulk aluminum sulfates were decomposed for large Pd particles during the high-temperature range TPD. Graphical examples of desorption peak assignments for large Pd and Pt particles are shown in Figures 7.9 and 7.10 respectively.

During the reactor TPD experiments, the following general trends were observed for both Pt and Pd catalysts. Large particle size catalysts released a greater amount of low-temperature desorbing species resulting in a smaller high-temperature release due to a lack of available surface species to undergo oxidation at the higher temperatures. In contrast, the small particle size catalysts released larger amounts of SO_2 at high temperatures via surface and bulk aluminum sulfate decomposition.

Specific to Pt, the 3.9 nm and 6.4 nm particles began sulfur release at similar points in the high-temperature range, providing evidence that the same sulfate types were decomposing. The 6.4 nm and 10.4 nm particles released SO_2 over similar temperature spans in the low-temperature range due to the same molecular SO_2 species desorbing and

aluminum surface sulfites decomposing. It should be noted that no two Pt particles sizes displayed the same sulfur release characteristics at both high and low temperatures (Figure 7.10).

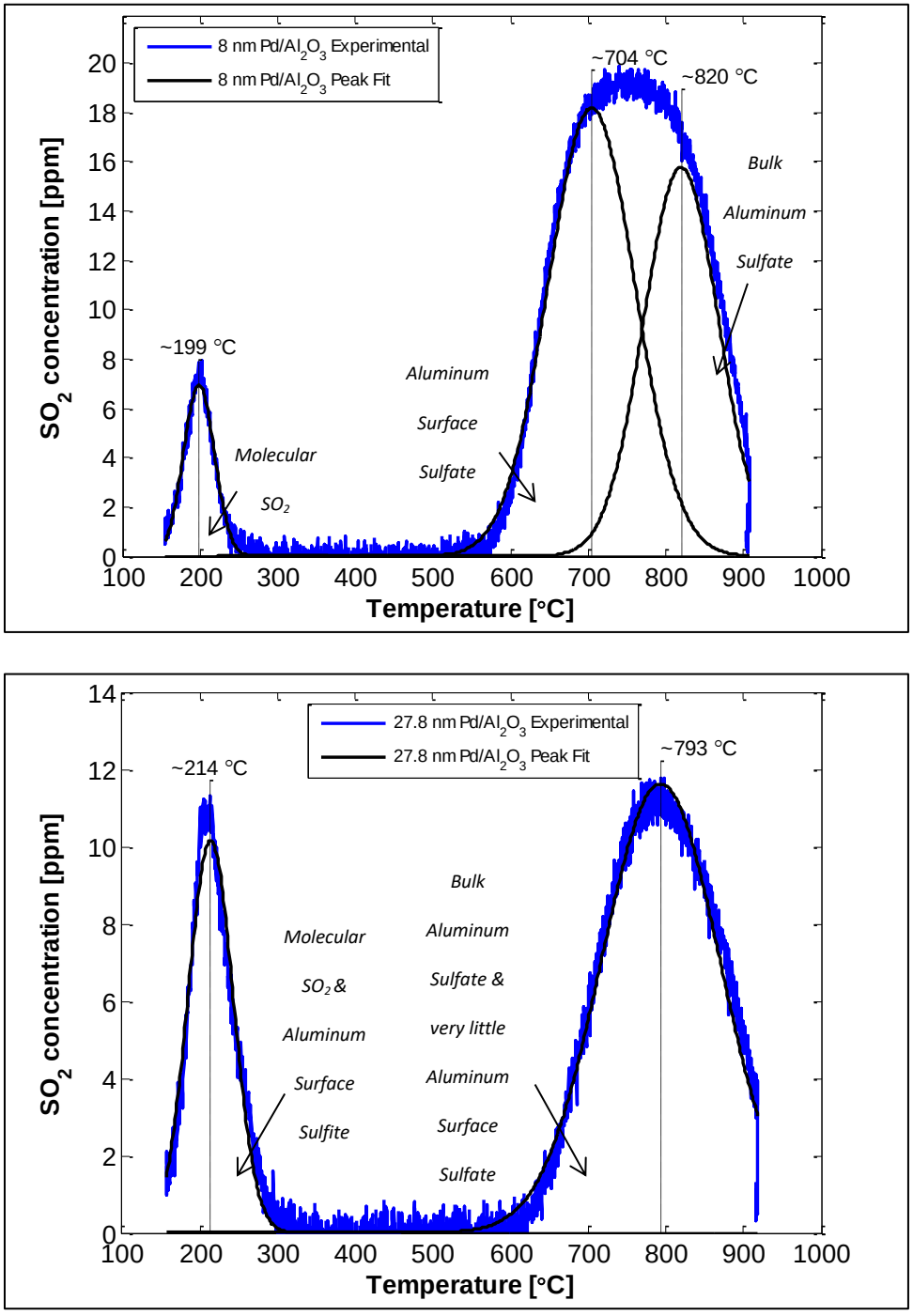

Figure 7.9: SO_2 desorption during TPD in flowing N_2, with a ramp rate of 10 °C/min. a) 8 nm Pd and b) 27.8 nm Pd TPD peak assignments based on DRIFTS analysis.

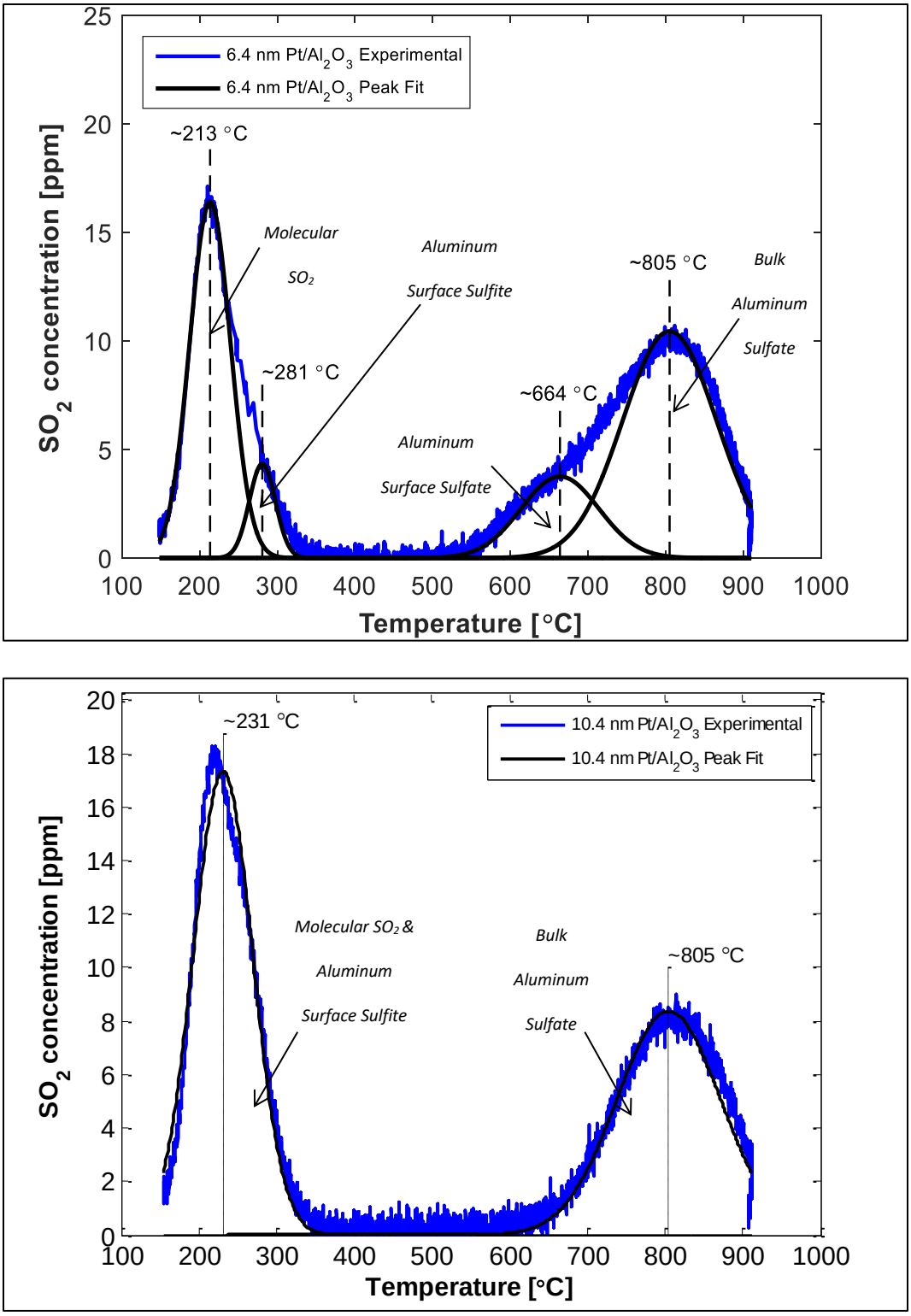

Figure 7.10: SO_2 desorption during TPD in flowing N_2, with a ramp rate of 10 °C/min. a) 6.4 nm Pt and b) 10.4 nm Pt TPD peak assignments based on DRIFTS analysis.

For the three Pd particle sizes assessed, sulfur release was initiated at three different temperatures in the high temperature range. The 2 nm and 8nm Pd released similar peak SO_2 amounts over similar temperature spans in the low temperature range, due to the same molecular SO_2 species desorbing. Similar to Pt, no two Pd particles sizes displayed the same sulfur release characteristics at both high and low temperatures.

In contrast, two of the three particle sizes assessed for 0.5 Pd-0.5 Pt bimetallic sample exhibited similar sulfur release characteristics at both high and low temperatures. The 3.6 nm, 15.2 nm, and 34.3 nm 0.5 Pd-0.5 Pt catalysts released SO_2 over similar temperature spans in the low temperature range, due to the same molecular SO_2 species desorbing, and the 15.2 nm and 34.3 nm 0.5 Pd-0.5 Pt samples released similar amounts at low temperatures. Sulfur release onset from the 15.2 nm and 34.3 nm 0.5 Pd-0.5 Pt samples was observed at similar points in the high-temperature range because the same sulfate types were decomposing. Although the peak release amounts were different at high temperatures, we infer these differences resulted from less SO_2 uptake for 34.3 nm 0.5 Pd-0.5 Pt. Recall that monometallic Pd samples only had similar release characteristics at low temperatures, and all varied at high temperatures; whereas similar sulfur release characteristics were observed for Pt catalysts at low and high temperatures but not for the same combination of particles sizes in both the low and high temperature ranges. Thus, the 0.5 Pd-0.5 Pt desorption profiles appear to have contributions from each of the Pd and Pt trends while also providing evidence of transition points from small to large particle size trends. We conclude that particle size had an impact on sulfur release characteristics, regardless of catalyst metal composition. The particle size at which a transition from

small to large particle release trends occurred was, however, dependent on catalyst metal composition.

7.4 Conclusions

Here we characterized how SO_2 adsorption and release characteristics varied with precious metal particle size for Pt/Al_2O_3, Pd/Al_2O_3 and $Pt/Pd/Al_2O_3$ catalysts. At 150 °C, all samples formed aluminum surface sulfite species as well as physisorbed molecular SO_2 on the aluminum surface. The Pt catalysts and Pd catalysts with small particle sizes contained chemisorbed SO_2 on the aluminum surface. The large particle size Pd catalysts were capable of oxidizing molecular SO_2 species to form aluminum surface sulfite species and subsequently form aluminum surface sulfates even at 150 °C. The larger particle size Pt catalysts were not capable of completely oxidizing sulfite species at temperatures below 400 °C. Failure to form sulfates at lower temperatures resulted in large amounts of SO_2 being released in the low-temperature range of the TPD due to decomposition of surface sulfite species. In contrast, smaller Pd and Pt particle size catalysts were able to thoroughly oxidize sulfites during TPD resulting in an abundance of surface and bulk aluminum sulfates. This difference resulted in different relative amounts of low versus high temperature desorbing species. With sulfates being more stable, the smaller particle size catalysts tended to form a great amount of sulfur species which decomposed at high temperatures. In contrast, larger particle size catalysts tended to form a greater amount of low-temperature desorbing species. In general, it was found

that the amount of SO_2 released during TPD decreased with increasing particle size of Pd:Pt alumina supported catalysts.

Chapter 8 Conclusions and recommendations for future work

8.1 Conclusions

The focus of this dissertation was to study CH_4 oxidation over, and SO_2 interactions with, Pd-Pt/Al_2O_3 bimetallic catalysts for the purpose of lean-burn natural gas engine exhaust emission abatement. I set out to determine the proper amount of Pt that could be substituted for Pd to achieve a minimal reduction in catalytic activity of a Pd-Pt/Al_2O_3 catalyst after exposure to water, high temperatures, or SO_2. To support this effort, ten Pd-Pt/Al_2O_3 powder catalysts were prepared with the following molar compositions: $Pd_{1.0}Pt_{0.0}/Al_2O_3$, $Pd_{0.9}Pt_{0.1}/Al_2O_3$, $Pd_{0.7}Pt_{0.3}/Al_2O_3$, $Pd_{0.5}Pt_{0.5}/Al_2O_3$, $Pd_{0.3}Pt_{0.7}/Al_2O_3$, $Pd_{0.2}Pt_{0.8}/Al_2O_3$, $Pd_{0.15}Pt_{0.85}/Al_2O_3$, $Pd_{0.1}Pt_{0.9}/Al_2O_3$, $Pd_{0.05}Pt_{0.95}/Al_2O_3$, and $Pd_{0.0}Pt_{1.0}/Al_2O_3$.

8.1.1 Sulfur Deactivation and Regeneration of Mono- and Bimetallic Pd-Pt Methane Oxidation Catalysts

During SO_2 exposure at 100 °C, all samples physisorbed and chemisorbed molecular SO_2 on the alumina surface, and catalysts containing Pd also formed alumina surface sulfite species. Only catalysts with high Pd content were capable of fully oxidizing these species to form an abundance of alumina surface sulfates at low temperatures.

The differences in sulfur species formation resulted in different relative extents of sulfur inhibition and sulfur regeneration method effectiveness. Although some Pt substitution for Pd provides some sinter and sulfur resistance, we concluded that, when

the Pt content exceeds that of Pd in SO_2-exposured bimetallic catalysts, TPD and TPR regeneration should be avoided because sulfur inhibition reduces the CH_4 oxidation activity less than sintering which results from the high-temperature regeneration processes.

8.1.2 Complete CH_4 Oxidation Kinetic Experiments and Reactor Modeling

Product water inhibited the CH_4 oxidation reaction for all samples containing any Pd, but to variable extents. After the Pt content exceeded 50%, product water inhibition was reduced. Since CH_4 oxidation is not inhibited by product water for monometallic Pt, we concluded that water inhibition is reduced for bimetallics with a large Pt percentage due to their increased Pt content and exposed Pt surfaces. In contrast to monometallic Pt, no bimetallics exhibited an O_2 dependency during CH_4 oxidation. The resultant CH_4 consumption rate equation is first order with respect to CH_4 for all catalysts and contains an inhibition term for water or oxygen for catalysts containing some Pd or monometallic Pt respectively. A kinetic parameter fitting tool and reactor model were established and validated utilizing CH_4 consumption data collected in the kinetic regime.

8.1.3 Water Inhibition and Decay Study for Complete CH_4 Oxidation Kinetic Experiments

For this study, we examined how Pd:Pt ratio affects CH_4 oxidation activity decay over time on stream and with exposure to water. With increasing Pt substitution for Pd less sinter resistance activity was observed. Catalysts with at least a Pt:Pd ratio of 1:1 exhibited the same CH_4 oxidation reaction inhibition due to water exposure. As Pt went beyond 70% Pt, the inhibition effects decreased, such that activity during water exposure approached the water insensitivity observed for monometallic Pt. When water injection

ceased, the activity for bimetallics with less than 50 mol% Pd was reduced. We concluded that bimetallic catalysts with greater than 50 mol% Pd are resistant to sintering related to water exposure but only small Pt substitutions can be made to maintain high temperature tolerance.

8.1.4 SO_2 Adsorption and Desorption Characteristics of Bimetallic Pd-Pt catalysts:

Pd:Pt ratio dependency

During SO_2 exposure at 150 °C, all samples formed aluminum surface sulfite species as well as physisorbed and chemisorbed molecular SO_2 on the alumina surface, but only high Pd content catalysts were capable of oxidizing these species to sulfates at low temperatures. Failure of the low Pd content catalysts to form sulfates at lower temperatures resulted in larger amounts of SO_2 being released in the low-temperature range of the TPD due to decomposition of some surface sulfite species. Although the 0.2 Pd-0.8 Pt catalyst composition marked the transition point from general Pd to Pt trends in sulfur release characteristics, it was found that the amount of SO_2 released during TPD generally decreased with increasing Pt content of Pd:Pt.

8.1.5 SO_2 Adsorption and Desorption Characteristics of Pd and Pt catalysts:

Precious metal crystallite size dependence

To assess how SO_2 adsorption and release characteristics varied with precious metal particle size, Pt/Al_2O_3, Pd/Al_2O_3 and $Pt/Pd/Al_2O_3$ catalysts were exposed to SO_2 at 150 °C. All samples physisorbed molecular SO_2 on the alumina surface and formed aluminum surface sulfite species. Small particle size catalysts oxidized sulfites during the TPD resulting in an abundance of surface and bulk aluminum sulfates. In contrast, the larger particle size Pd catalysts oxidized some aluminum surface sulfites with ease but

some decomposed during TPD at lower temperatures resulting in less sulfates decomposing at high-temperatures. Failure of large Pd and Pt particle catalysts to form sulfates at lower temperatures resulted in large amounts of SO_2 being released in the low-temperature range of the TPD due to decomposition of surface sulfite species.

These differences resulted in different relative amounts of low versus high temperature desorbing species, and in general the amount of SO_2 released during TPD decreased with increasing particle size for a particular Pd:Pt catalyst composition.

8.2 Recommendations for future work

Based on the findings in this work, the following areas are suggested for future study.

8.2.1 SO_2 adsorption and TPD characteristics as a function of oxidation state

Preliminary studies showed that the oxidation state of Pd, Pt, and bimetallic catalysts influences the SO_2 uptake and desorption characteristics. The PM oxidation state can change over time on stream due to sintering or extended SO_2 exposure, and as shown in this work, depending on the sulfur regeneration method, the oxidation state of the PM particles can change during regeneration as well. It would be beneficial to understand how changes in oxidation state affect sulfur resistance and decay over the life of the catalyst as well as activity after regeneration.

8.2.2 SO_2 adsorption with O_2, SO_3 adsorption, and TPD

In the absence of O_2, the SO_2 sorption studies in this work show that alumina supported catalysts with high-Pd content are more proficient at oxidizing sulfur species

than low-Pd content catalysts. Again, some of my preliminary studies showed that SO_2 adsorption with O_2 vs. SO_2 adsorption without O_2 in the gas stream results in different relative abundances of the types of sulfur species formed. Lean-burn natural gas engine exhaust is a rich O_2 environment, so it is understood that some SO_2 will be oxidized to form SO_3. As seen with SO_2, SO_3 can attack Pd and Pt sites in a different manner. By understanding SO_3 sorption characteristics on a Pd:Pt mole ratio basis, catalysts and sulfur regeneration plans can be optimized to reduce activity loss.

8.2.3 CH_4 oxidation with SO_2 treated catalysts during water injection

Aftertreatment systems for lean-burn natural gas engine exhausts have to oxidize hydrocarbons, primarily CH_4, in the presence of natural gas combustion products such as SO_x, H_2O, and CO_2. As shown in this work, CH_4 oxidation characteristics as well as inhibition and decay due to water and SO_2 exposure vary with Pd:Pt mole ratio. Since SO_x and H_2O have been shown to inhibit CH_4 oxidation and together promote sulfation of PdO and alumina sites, it is pertinent that CH_4 oxidation experiments be performed in the presence of these two deactivation sources. These experimental data will provide a more complete story in regards to how CH_4 oxidation catalysts decay over time on stream in lean-burn natural gas combustion aftertreatment systems. Similarly, these data can be used to support design of aftertreatment systems.

References

1. R. Abbasi, R.E. Hayes, L. Wu, S.E. Wanke, *Chemical Engineering Research and Design* 90 (2012) 1930–1942.
2. K.S. Varde, T. Bohr, *Society of Automotive Engineers Inc.* 931632 (1993).
3. D. L. Trimm, J. H. Lee, *Fuel Processing Technology* 42 (1995) 339-359.
4. F. Stodolsky and D. Santini, *American Chemical Society National Meeting*, Conference 203 ANL/CP-75343 (1992).
5. Elements of Chemical Reaction Engineering, H.S. Fogler. Prentice Hall International 2006.
6. O. Demoulin, B. L. Clef, M. Navez, P. Ruiz, *Applied Catalysis A: General* 344 (2008).
7. H. Yamamoto, H. Uchida, *Catalysis Today* 45 (1998) 147-151.
8. C.S. Weaver, S.H. Turner, M.V. Balam-Almanza, R.Gable, *Society of Automotive Engineers Inc.* 2000-01-3473 (2000).
9. C.A. Sharp, T.L. Ullman, K.R. Stamper, *Society of Automotive Engineers Inc.* 932819 (1993).
10. P. Hupperich and M. Dürnholtz, *Society of Automotive Engineers Inc.* 960857 (1996).
11. M. Ishii, S. Ishizawa, E. Inada, R. Idoguchi, T. Sekiba, *Society of Automotive Engineers Inc.* 942005 (1994).
12. S. Subramanian, R.J. Kudla, M.S. Chattha, *Society of Automotive Engineers Inc.* 930223 (1993).

13. T. Hesterberg, C.A. Lapin, W. B. Bunn, *Environmental Science and Technology* Vol. 42 NO.17 (2008).
14. N.M. Kinnunen, J.T. Hirvi, M. Suvanto, T.A. Pakkanen, *Journal of Molecular Catalysis A: Chemical* 356 (2012).
15. M. Skoglundh, L.O. Löwendahl, J.E. Ottersted, *Applied Catalysis* 77 (1991).
16. G. Lapisardi, P. Gélin, A. Kaddouri, E. Garbowski, S. Da Costa, *Topics in Catalysis* Vols. 42-43 (2007).
17. G. Lapisardi, L. Urfels, P. Gélin, M. Primet, A. Kaddouri, E. Garbowski, S. Toppi, and E. Tena, *Catalysis Today* 117 (2006).
18. XP. Xiang, L-H. Zhao, B-T. Teng, J-J. Lang, X. Hu, T. Li, Y-A. Fang, M-F. Luo, J-J. Lin, *Applied Surface Science* 276 (2013) 328-332.
19. P. Gélin, M. Primet, *Applied Catalysis B: Environmental* 39 (2002) 1-37.
20. S.F. Tahir, C. A. Koh, *Chemosphere* Vol. 34 No. 8, 1997.
21. Y. Wu, L. Luo, *Russian Journal of Chemistry* Vol. 85 No. 13, 2011.
22. B. Kucharczyk, J. Zabrzeski, *Environment Protection Engineering* Vol. 34 No. 4, 2008.
23. W. Wang, C. Xu, C. Li, Y. Liu, B. He, C. Chen, *Journal of Natural Gas Chemistry* 20 (2011).
24. S. Petrović, L. Karanović, P.K. Stefanov, M. Zdujić, A. Terlecki-Baričević, *Applied Catalysis B: Environmental*, 58(1) (2005) 133-141.
25. J. E. Miller, A. G. Sault, D. E. Trudell, T. M. Nenoff, S.G. Thoma, N.B. Jackson, *Applied Catalysis A: General* 201 (2000).
26. D. Klvana, K.S. Song, J. Kirchnerova, *Applied Catalysis A: General* 213 (2001).

27. L. Giebeler, D. KeBling, G. Wendt, *Chemical Engineering & Technology* 30 No. 7 (2007).

28. R. Burch, T.R. Baldwin, *Applied Catalysis* 66 (1990).

29. E. Becker, P. Carlsson, and M. Skoglundh, *Topics in Catalysis* 52 (2009).

30. R. Burch, P.K. Loader, *Applied Catalysis B: Environmental* 5 (1994) 149-164.

31. K. Otto, *Langmuir* 5 (1989).

32. C.F. Cullis, B.M. Willatt, *Journal of Catalysis* 83 (1983).

33. R. Burch, F.J Urbano, P.K. Loader, *Applied Catalysis A: General* 123 (1995).

34. M. Niwa, K. Awano, Y. Murakami, *Applied Catalysis* 7 (1983).

35. Y.Y. Yao, *Industrial & Engineering Chemistry Product Research and Development* Volume 19 Issue 3 (1980).

36. G. Zhu, J. Han, D. Y. Zemlyanov, F. H. Ribeiro, *Journal of Physical Chemistry B* 109 (2005).

37. C.F. Cullis, B.M. Willatt, *Journal of Catalysis* 86 (1984).

38. J.C. van Giezen, F.R. van den Berg, J.L. Kleinen, A.J. van Dillen, J.W. Geus, *Catalysis Today* 47 (1999).

39. L. van de Beld, M.C. van der Ven, K.R. Westerterp, *Chemical Engineering and Processing* 34 (1995).

40. J.K. Lampert, M.S. Kazi, R.J. Farrauto, *Applied Catalysis B: Environmental* 14 (1997).

41. P. Carlsson, S. Mollner, K. Arnby, M. Skoglundh, *Chemical Engineering Science* 59 (2004).

42. P. Briot, M. Primet, *Applied Catalysis* 68 (1991).

43. Chemical Reaction Engineering, O. Levenspiel. Wiley-VCH 1998.

44. H. Ohtsuka, *Catalysis Letters* 141 (2011) 413–419.

45. P. Castellazzi, G. Groppi , P. Forzatti, *Applied Catalysis B: Environmental* 95 (2010) 303–311.

46. K. Persson, A. Ersson, K. Jansson, J.L.G. Fierro, S.G. Järås, *Journal of Catalysis* 243 (2006) 14–24.

47. G. Corro, C. Cano, J.L.G. Fierro, *Journal of Molecular Catalysis A: Chemical* 315 (2010) 35–42.

48. N. Ottinger, R. Veele, Y. Xi, Z Liu, *SAE International Journal of Engines* 8 2015-01-0991.

49. F. Arosio, S. Colussi, G. Groppi, A. Trovarelli, *Catalysis Today* 117 (2006) 569–576.

50. S. Colussi, F. Arosio, T. Montanari, G. Busca, G. Groppi, A. Trovarelli, *Catalysis Today*, *155*(1), 2010, 59-65.

51. M. Waqif, 0. Saur, J. Lavalle, S. Perathoner, C. Centi, *Journal of Physical Chemistry* 95 (1991) 4051-4058.

52. T. Rades, V. Yu. Borovkov, V. B. Kazansky, M. Polisset-Thfoin, J. Fraissard, J. *Physical Chemistry* 100 (1996) 16238-16241.

53. Y. Zhang, Y. Cai, Y. Guo, H. Wang, L. Wang, Y. Lou, Y. Guo, G. Lu, Y. Wang, *Catalysis, Science & Technology* 4 (2014) 3973-3980.

54. Bensalem, J. Muller, D. Tessier, F. Bozon-Verduraz, *Journal of Chemical Society Faraday Transactions* Vol. 92 (17) (1996) 3233-3237.

55. Martinez-Arias, A.B. Hungría, M. Fernández-García, A. Iglesias-Juez, J.A. Anderson, J.C. Conesa, *Journal of Catalysis* 221 (2004) 85-92.

56. N. Toshima, Y. Shiraishi, A. Shiotsuki, D. Ikenaga, Y. Wang, *The European Physical Journal D* 16 (2001) 209-212.

57. Datta, R. Cavell, R. Tower, Z. George, *Journal of Physical Chemistry* 89 (1985) 443-449.

58. M. Mitchell, V. Sheinker, M. White, *Journal of Physical Chemistry* 100 (1996) 7550-7557.

59. C. Chang, *Journal of Catalysis* 53 (1978) 374-385.

60. T. Yu, H. Shaw, *Applied Catalysis B: Environmental* 18 (1998) 105-114.

61. D. Mowery, R. McCormick, *Applied Catalysis B: Environmental* 34 (2001) 287-297.

62. Bounechada, S. Fouladvand, L. Kylhammar, T. Pingel, E. Olsson, M. Skoglundh, J. Gustafson, M. Di Michiel, M. Newton, P. Carlsson, *Physical Chemistry Chemical Physics* 15 (2013) 8648-8661.

63. Piéplu, O. Saur, J. Lavalley, O. Legendre, C. Nedez, *Catalysis Reviews: Science and Engineering* Volume 40 Issue 4 (1998) 409-450.

64. S. Nam, G. Gavalas, *Applied Catalysis* 55 (1989) 193-213.

65. R. Burch, E. Halpin, M. Hayes, K. Ruth, J.A. Sullivan, *Applied Catalysis B: Environmental* 19 (1998) 199-207.

66. J. Li, A. Kumar, X. Chen, N. Currier, A. Yezerets, *SAE International Technical Paper* (2013) 2013-01-0514.

67. C. Müller, M. Maciejewski, R.A. Koeppel, A. Baike, *Journal of Catalysis* 166 (1997) 36.

68. Wilson, R. M. Lambert, C. P. Hubbard, R. G. Hurley, R. W. McCabe, H. S. Gandhi, *Journal of Catalysis* 184 (1999) 491–498.

69. J. M. Jones, V. A. Dupont, R. Brydson, D. J. Fullerton, N. S. Nasri, A. B. Ross, A. V. K. Westwood, *Catalysis Today* 81 (2003) 589–601.

70. F. Ribeiro, M. Chow, and R. Dallabetta, *Journal of Catalysis*, 1994, Volume 146, 537-544.

71. N. Todoroki, H. Osano, T. Maeyama, H. Yoshida, T. Wadayama, *Applied Surface Science* 256 (2009) 943-947.

72. A. Boubnov, A. Ganzler, S. Conrad, M. Casapu, and J. Grunwaldt, *Topics in Catalysis* 56 (2013) 333–338.

73. N. Mouaddib, C. Feumi-Jantou, E. Garbowski, M. Primet, *Applied Catalysis A: General* 87 (1992) 129-144.

74. P. Briot, A. Auroux, D. Jones, M. Primet, *Applied Catalysis* Vol. 59(1) (1990) 141-152.

75. M. Lyubovsky, L. Pfefferle, *Applied Catalysis A: General* 173 (1998) 107-119.

76. M. Smirnov, A. Kalinkin, A. Pashis, A. Sorokin, A. Noskov, K. Kharas, V. Bukhtiyarov, *Journal of Physical Chemistry B* 109 (2005) 11712-11719.

77. O. Saur, M. Bensitiel, A. Mohammed Saad, J. Lavalley, C. Tripp, B. Morrow, *Journal of Catalysis* 9 (1986) 104-110.

78. F. Klingstedt, A. Neyestanaki, R. Byggningsbacka, L. Lindfors, M. Lundén, M. Petersson, P. Tengström, T. Ollonqvist, J. Väyrynen, *Applied Catalysis A: General* 209 (2001) 301-316.

79. B. P. Chaplin, J. R. Shapley, C. J. Werth. *Environmental Science & Technology* 41.15 (2007) 5491-5497.

80. A. Li-Dun, D. Quan, *Applied catalysis* 66.1 (1990) 219-234.

81. J-K. Lee, H-K. Rhee. *Journal of Catalysis* 177.2 (1998) 208-216.

82. T. Xu, Q. Zhang, D. Jiang, Q. Liang, C. Lu, J. Cen, X. Li, *RSC Advances 4*(63) (2014) 33347-33354.

83. J. M. Badano, M. Quiroga, C. Betti, C. Vera, S. Canavese, F. Coloma-Pascual, *Catalysis Letters 137*(1-2) (2010) 35-44.

84. K. Gotterbarm, N. Luckas, O. Höfert, M.P. Lorenz, R. Streber, C. Papp, C., F. Viñes, H-P. Steinrück, A. Görling, *The Journal of Chemical Physics*, *136*(9) (2012) 094702.

85. H. Jiang, H. Yang, R. Hawkins, Z. Ring, *Catalysis Today 125*(3) (2007) 282-290.

86. Y. Deng, T.G. Nevell, R.J. Ewen, C.L. Honeybourne, *Applied Catalysis A: General 101*(1) (1993) 51-62.

87. A. Balla, C. Marcu, D. Axente, G. Borodi, D. Lazăr, *Central European Journal of Chemistry 10*(6) (2012) 1817-1823.

88. D.D. Beck, J.W. Sommers, C.L Dimaggio. *Applied catalysis B: Environmental* 3.2-3 (1994) 205-227.

89. N.S. Nasri, J.M. Jones, V.A. Dupont, A. Williams, *Energy & Fuels*, *12*(6) (1998) 1130-1134.

90. W. Ying, T. Minming, T. Zhang, *Mining Science and Technology (China)* 20.6 (2010) 913-916.

91. M. H. Wiebenga, H.K. Chang, S.J. Schmieg, S. H. Oh, D. B. Brown, D.H. Kim, J-H Lee, C. Peden, *Catalysis Today* 184 No. 1 (2012) 197-204.

92. T. Lin, C. Jan, and J. Chang, *Industrial & Engineering Chemistry Research* Vol. 34 No. 12 (1995) 4284-4289.

93. M. Waqif, J. Bachelier, O. Saur, and J. Lavalley, *Journal of Molecular Catalysis* 72 (1992) 127-138;

94. M. F. M. Zwinkels , S. G. Järås , P. G. Menon, T. A. Griffin, *Catalysis Reviews* 35:3 (1993) 319-358.

95. D. L. Mowery, M.S. Graboski, T. R. Ohno, R. L McCormick, *Applied Catalysis B: Environmental 21*(3) (1999) 157-169.

96. D. L. Trimm, C-W. Lam, *Chemical Engineering Science* 35.6 (1980) 1405-1413.

97. J. Yang, V. Tschamber, D. Habermacher, F. Garin, P. Gilot, *Applied Catalysis B: Environmental* 83 (2008) 229–239.

98. H. Bartholomew, *Applied Catalysis A* 107 (1993) l-57.

99. E. Wanke, P. C. Flynn, *Catalysis Reviews* 12:1 (1975) 93-135.

100. Narui, H. Yata, K. Furuta, A. Nishida, Y. Kohtoku, T. Matsuzaki, *Applied Catalysis A: General 179*(1) (1999) 165-173.

101. R. Burch, D. J. Crittle, M. J. Hayes, *Catalysis Today* 47.1 (1999), 229-234.

102. Y. H. Chin, C. Buda, M. Neurock, E. Iglesia *Journal of the American Chemical Society 135*(41) (2013) 15425-15442.

103. K. I. Fujimoto, F. H. Ribeiro, M. Avalos-Borja, E. Iglesia, *Journal of Catalysis 179*(2) (1998) 431-442.

104. MKS MultiGas 2030 FTIR Datasheet, (2007), MultiGas Online Gas Analysis, Retrieved from https://www.mksinst.com/docs/ur/onlinemultigas2030ds.pdf .

105. Harrick High Temperature Reaction Chamber Datasheet, High Temperature Reaction Chamber For Praying Mantis, Retrieved from www.harricksci.com .

106. Harrick Praying Mantis Datasheet, Harrick The Praying Mantis, Retrieved from www.harricksci.com .

107. Sample Injection Valco 6 Port Valve Overview, Sample Injection Valco 6 Port Valve, Retrieved from http://www.vici.com/support/app/app11j.php .